UC San Diego

UC San Diego Previously Published Works

Title

Broken foreland basins and the influence of subduction dynamics, tectonic inheritance, and mechanical triggers

Permalink

https://escholarship.org/uc/item/3v72t9f3

Authors

Horton, Brian K

Capaldi, Tomas N

Mackaman-Lofland, Chelsea

et al.

Publication Date

2022-11-01

DOI

10.1016/j.earscirev.2022.104193

Copyright Information

This work is made available under the terms of a Creative Commons Attribution License, available at https://creativecommons.org/licenses/by/4.0/

Peer reviewed

eScholarship.org Powered by the California Digital Library

University of California

Earth-Science Reviews 234 (2022) 104193

Contents lists available at ScienceDirect

Earth-Science Reviews

journal homepage: www.elsevier.com/locate/earscirev

Invited Review

Broken foreland basins and the influence of subduction dynamics, tectonic inheritance, and mechanical triggers

Brian K. Horton [a,b,*], Tomas N. Capaldi [c], Chelsea Mackaman-Lofland [d], Nicholas D. Perez [e], Meredith A. Bush [a], Facundo Fuentes [f], Kurt N. Constenius [g]

[a] Department of Geological Sciences, Jackson School of Geosciences, University of Texas at Austin, Austin, TX 78712, USA
[b] Institute for Geophysics, Jackson School of Geosciences, University of Texas at Austin, Austin, TX 78712, USA
[c] Department of Geoscience, University of Nevada, Las Vegas, Las Vegas, NV 89154, USA
[d] Department of Earth and Environmental Sciences, Denison University, Granville, OH 43032, USA
[e] Department of Geology and Geophysics, College of Arts and Sciences, Texas A&M University, College Station, TX 77843, USA
[f] Gerencia de Exploración, YPF, 515 Macacha Güemes, Buenos Aires, Argentina
[g] Department of Geosciences, University of Arizona, Tucson, AZ 85721, USA

ARTICLE INFO

Keywords:
Andes
Andean Orogeny
Basin
Broken Foreland
Compression
Cordillera
Faults
Flat slab subduction
Fold-thrust belts
Foreland basins
Inheritance
Intraplate deformation
Laramide Orogeny
North America
Orogeny
Reverse faults
Rocky Mountains
Shortening
South America
Subduction
Tectonics
Thrust faults

ABSTRACT

Broken foreland basins are caused by crustal-scale contractional basement structures that compartmentalize (or break) a contiguous retroarc or collisional foreland basin into smaller disconnected basins. Broken foreland basins differ from their unbroken counterparts in their deformational, depositional, and geodynamic framework. Whereas contiguous (unbroken) foreland basins are generated mainly by regional flexural loading due to shortening of supracrustal cover strata and uppermost basement in organized ramp-flat thrust systems, broken foreland basins are governed principally by isolated topographic loads and structural tilting associated with widely spaced crustal-scale reverse faults that accommodate intraplate basement shortening. These structural contrasts foster either décollement-style fold-thrust belts (orogenic wedges) with large integrated erosional drainage systems (watersheds) spanning diverse sediment source regions (including thin-skinned fold-thrust belts, elevated hinterland zones, accreted terranes, and magmatic arcs) or independent foreland block uplifts with local drainage systems dominated by basement sources. Although the genesis of broken foreland basins has been uniquely attributed to flat slab subduction, these basins are also sensitive to inherited structural, stratigraphic, thermal, and rheological configurations, as well as synorogenic mass redistribution in relationship to climate, erosion, sediment transport efficiency, and sediment accumulation.

Despite the many modern and ancient examples, questions persist over the underlying geodynamic processes that promote development of a broken or compartmentalized foreland basin instead of a single regionally unified flexural foreland basin. Additional uncertainties and misconceptions surround the criteria used to define broken foreland basins and their linkages to subduction dynamics (chiefly slab geometry), strain magnitude, and structural reactivation. Here we review the tectonic framework of broken foreland basins—with emphasis on South and North America (Pampean and Laramide provinces)—and propose that their genesis can be ascribed to a combination of: (i) underlying conditions in the form of tectonic inheritance, including precursor structural, stratigraphic, thermal, and rheological heterogeneities and anisotropies; and (ii) mechanical triggers, such as increased stress, enhanced horizontal stress transmission, and/or selective crustal strengthening or weakening.

1. Introduction

Broken foreland basins are a fundamental but commonly overlooked component of contractional orogenic systems. Along with subduction-related retroarc foreland basins and collision-related peripheral foreland basins, broken foreland basins were originally recognized by Dickinson (1976) as an endmember type of sedimentary basin in zones of continental crustal shortening (Fig. 1). He defined broken foreland

* Corresponding author at: Department of Geological Sciences and Institute for Geophysics, Jackson School of Geosciences, University of Texas at Austin, Austin, TX 78712, USA.
E-mail address: horton@jsg.utexas.edu (B.K. Horton).

https://doi.org/10.1016/j.earscirev.2022.104193
Received 30 May 2022; Received in revised form 12 September 2022; Accepted 14 September 2022
Available online 21 September 2022
0012-8252/© 2022 The Authors. Published by Elsevier B.V. This is an open access article under the CC BY license (http://creativecommons.org/licenses/by/4.0/).

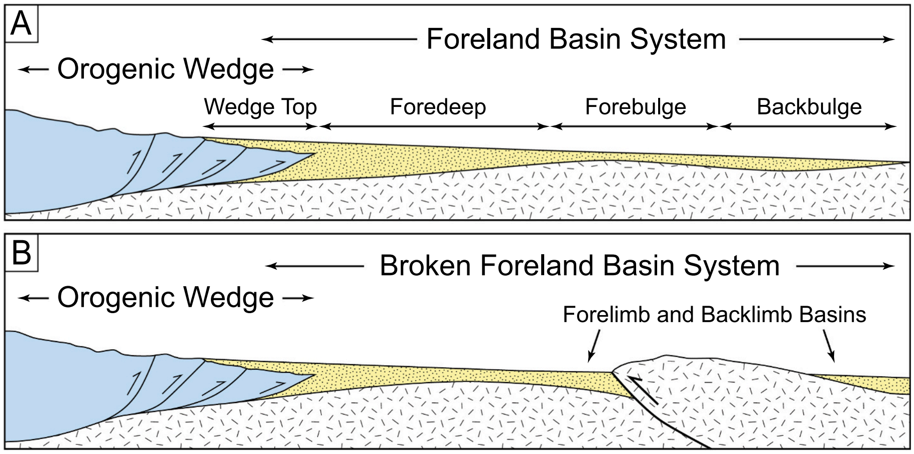

Fig. 1. Schematic cross sections comparing (A) a contiguous (unbroken) foreland basin (after DeCelles and Giles, 1996) with (B) a broken foreland basin. Note that both nonmarine and marine conditions are possible.

basins as zones of subsidence "*formed where basement is involved in foreland deformation to cause block uplifts and basement-cored folds separating isolated basinal depressions; this style of deformation may occur in either peripheral or retroarc settings.*" Broken foreland basins form in continental interior regions in response to isostatic and dynamic forces, including flexural subsidence during intraplate reverse faulting and long-wavelength dynamic subsidence induced by mantle flow and mechanical interactions with a subducting or underthrusting plate (Cross, 1986; Dickinson et al., 1988; Mitrovica et al., 1989; Liu et al., 2014). Further accommodation space may be generated by local footwall tilting adjacent to crustal-scale reverse faults and by drainage closure dictated by topographic barriers (McQueen and Beaumont, 1989; Jordan, 1995; Horton, 2012; Simpson, 2014). Broken foreland provinces are compartmentalized by positive topographic features developed above basement-cored block uplifts (generally fault-bounded structural highs or arches) that deform the adjacent basin margins. Broken foreland basins are readily identified in modern systems and have been proposed for ancient systems involving continental collision or subduction-related Andean-type (Cordilleran) orogenesis (e.g., Suttner et al., 1981; Kluth and Coney, 1981; Schwartz, 1982; DeCelles, 1986; Hendrix, 2000; Ramos et al., 2002; Li and Li, 2007; Liu et al., 2007; Ramos and Folguera, 2009; Hain et al., 2011; Martín-González and Heredia, 2011; Strecker et al., 2012; Coutand et al., 2016; Fang et al., 2016; Kusky et al., 2016; Leary et al., 2017).

Many broken foreland basins result from the structural partitioning (or breaking) of a larger predecessor basin that developed adjacent to an orogenic wedge, including not only antecedent retroarc and peripheral foreland basins along ocean-continent and continent-continent convergent plate boundaries, respectively, but also pro- and retro-wedge basins flanking doubly vergent thrust wedges in continental collision zones (Dickinson, 1974, 1976; Naylor and Sinclair, 2008; Ingersoll, 2012, 2019). Contiguous (unbroken) foreland basins exhibit regional depositional continuity over hundreds of kilometers and are generally coupled with a tapered orogenic wedge containing a thin-skinned fold-thrust belt characterized by organized ramp-flat fault systems above a regional décollement (Fig. 1A). In contrast, the development of broken foreland basins as smaller features with limited depositional continuity is more often affiliated with thick-skinned deformation involving independent faults with a single major ramp that penetrates to middle or lower crustal levels (Fig. 1B). In retroarc systems, basin compartmentalization and intraforeland deformational processes have been linked to shifts in subduction geodynamics, including shallowing of a subducting slab to a subhorizontal (flat) orientation (e.g., Bird, 1984; Gutscher et al., 2000; Liu et al., 2008; Martinod et al., 2010; Eakin et al., 2014; Wagner et al., 2017; Axen et al., 2018; Bishop et al., 2018; Horton, 2018a). Flat slab subduction is widely recognized as an important tectonic process that shaped the modern Andes of South America and the U.S. Rocky Mountains during the Late Cretaceous–Paleogene Laramide orogeny of western North America (Coney and Reynolds, 1977; Dickinson and Snyder, 1978; Constenius, 1996; Bird, 1998; Ramos et al., 2002; Dickinson, 2004; Ramos, 2009; Ramos and Folguera, 2009; Carlotto, 2013; Yonkee and Weil, 2015; Horton et al., 2022). However, because other precursor conditions or discrete catalysts may induce intraplate deformation within continental interiors (Lacombe and Bellahsen, 2016; Giambiagi et al., 2022; Horton and Folguera, 2022), flat slab subduction is not singularly required for the genesis of broken foreland basins. Additional influences on the formation of broken foreland basins include inherited structural, stratigraphic, rheological, and thermal properties as well as operative surface processes that regulate erosion and deposition in response to variations in climate, sediment transport efficiency, and accommodation.

The purpose of this paper is to review the tectonic framework of broken foreland basins and explore the underlying structural, geodynamic, and surface processes that govern their development. We outline the plate tectonic, structural, stratigraphic, accommodation, and sediment routing configuration for broken foreland basins, with emphasis on retroarc systems in North and South America (Fig. 2), noting that many features are shared by collision-related peripheral systems. In our assessment, we propose two sets of circumstances conducive to the development of broken foreland basins: first, favorable *conditions* inherited from the preceding geologic history; and second, specific *catalysts* during orogenesis that trigger distributed intraforeland shortening. We postulate that basin genesis can be attributed to the net effects of: (i) tectonic inheritance in the form of preexisting structural, stratigraphic, rheological, and thermal conditions; and (ii) mechanical triggers that may include elevated stress, long-distance stress transmission, and/or crustal strengthening or weakening within the intraplate regions that host broken foreland basins.

2. Definition of broken foreland basins

A broken foreland basin (Fig. 1) is defined here as: (a) region of sediment accommodation that forms in an intraplate continental setting inboard of a retroarc or collisional orogenic belt; (b) the basin is compartmentalized (partitioned or fragmented) by positive topographic features produced by discrete basement-involved contractional structures; (c) accommodation is regulated by flexural loading and fault-block tilting with subordinate dynamic subsidence and sediment infilling (ponding) within internally drained areas. Multiple criteria differentiate broken foreland basins from their unbroken counterparts (Table 1).

Contiguous (unbroken) foreland basins display considerable regional

Table 1
Key elements of contiguous (unbroken) and broken foreland basins.

Basin type:	Contiguous foreland basin	Broken foreland basin
Basin dimensions	Long wavelength: ~100–300 km wide × >500–1000 km long.	Short wavelength: <50–100 km wide × 100–300 km long; commonly associated with a series of similar basins.
Basin fill architecture	Asymmetric, with a single depocenter 3–10 km thick.	Variably symmetric or asymmetric, with one or more depocenters <1–3 km thick.
Basin margin configuration	Contractional structures along proximal margin; sedimentary pinchout/onlap onto distal margin (forebulge or craton).	Contractional structures along most basin margins, either forelimb or backlimb settings.
Bounding fault geometries	Ramp-flat fold-thrust structures above decollements within sedimentary cover or at basement-cover interface.	Solitary basement-involved uplifts bound by reverse faults, including emergent and non-emergent (blind) geometries.
Shortening magnitude	>20–50% shortening in thin-skinned fold-thrust belt flanking the basin.	<10–20% shortening along basement-involved structures within broken foreland province.
Accommodation mechanisms	Flexure due to thrust loading during regional shortening in the fold-thrust belt and crustal thickening; dynamic subsidence relate to interactions with subducting/underthrusting plate.	Distant flexural loading by fold-thrust belt; flexural loading and local footwall (block) tilting by basement-involved reverse faulting; dynamic subsidence related to interactions with subducting/underthrusting plate; sediment ponding due to endorheic conditions imparted by topographic barriers.
Accumulation rates	>100–500 m/Myr (>0.1–0.5 mm/yr)	Generally <200 m/Myr (<0.2 mm/yr), except near proximal tilted basin margins.
Depositional environments	Marine: shallow marine, coastal, delta. Nonmarine: fluvial megafan, fluvial.	Principally nonmarine: alluvial fan, fluvial, lacustrine.
Stratigraphic patterns	Common upsection stratigraphic shift from distal to proximal facies.	Variable stratigraphic trends related to intermittent closed versus open drainage.
Drainage systems and sediment routing	Large integrated erosional drainage networks spanning diverse sediment source regions.	Small drainage networks restricted to basement sources from intraforeland, basement-cored block uplifts.
Sediment source regions	Fold-thrust belt, magmatic arc, accreted terranes, suture zones.	Distant fold-thrust belt, magmatic arc, accreted terranes, suture zones. Local basement-cored uplifts.
Provenance evolution	Early-stage: chiefly magmatic arc, accreted terranes, suture zones. Late-stage: fold-thrust belt.	Early-stage: fold-thrust belt and hinterland sources. Late-stage: stratigraphic cover and basement of local intraforeland uplifts.
Precursor basin conditions	Retroarc: extensional basin or post-extensional thermal sag. Collisional: subduction trench or passive margin.	Commonly a predecessor contiguous (unbroken) foreland basin, or erosional intraplate (cratonic) setting.
Basin evolution	Continuous basin development and cratonward advance throughout contractional orogenesis (>50–100 Myr).	Commonly restricted to late-stage contractional orogenesis and post-orogenic erosion (<50 Myr).
Examples	North American Cordilleran foreland; Himalayan foreland (India-Asia collision); Zagros foreland (Arabia-Eurasia collision); Appalachian foreland; pre-late Miocene Alpine (broader European) foreland.	Sierras Pampeanas (Pampean), northern Patagonia, and Peru foreland basement provinces of South America; Laramide and Ancestral Rocky Mountains, North America; Variscan foreland, Europe; North China Craton and other central Asian basin systems.

continuity (commonly >100–300 km across strike and > 1000 km along strike) without structural or topographic disruption (DeCelles and Giles, 1996). In contrast, broken foreland basins are spatially restricted entities confined by crustal-scale contractional structures that may collectively form a continuous or discontinuous network of topographic barriers (Fig. 2). Although many systems contain basin-margin and intrabasinal structures, broken foreland regions are distinguished by intrabasinal structures with sufficient structural relief to generate positive topographic features at the Earth's surface, including topographic or bathymetric barriers (in nonmarine or marine systems, respectively) that segregate individual broken foreland basins.

Within a single orogenic system, a broken foreland province may constitute a family of compartmentalized basins with shared structural arrangements and possible episodic depositional connectivity among adjacent basins (Fig. 2). Broken foreland basins often follow a common temporal transition that involves breaking a retroarc or collisional foreland by crustal-scale basement deformation that structurally partitions a contiguous basin into a series of disconnected smaller basins. Many broken foreland basins succeed a predecessor unbroken foreland basin and are ultimately incorporated into an expanding orogenic system during late-stage deformation, and thus susceptible to erosional removal during post-orogenic rebound and erosion. These final phases of orogenesis and post-orogenic erosion may explain why few ancient foreland basins remain intact, including basins associated with Phanerozoic orogens and Precambrian mobile belts (e.g., North American Cordilleran foreland, Appalachian foreland, Variscan foreland, Alpine foreland, North China Craton, and basins generated during Precambrian supercontinent assembly) (Dickinson, 1974; Coney, 1976; Rodgers, 1987; Kuhlemann and Kempf, 2002; Willett and Schlunegger, 2010; Cather et al., 2012; Allen et al., 2015; Kusky et al., 2016; Cawood et al., 2018; Howell et al., 2020).

The best-known examples of broken foreland basins include modern and ancient components of the retroarc regions of western North America and South America (Figs. 2 and 3) (Dickinson, 1976; Jordan et al., 1983; Dickinson et al., 1988; Ramos et al., 2002; Ingersoll, 2012, 2019). The following text considers selected aspects of these systems, including: the plate tectonic, structural, and topographic configurations (in map view and cross section); sediment accumulation histories; time-stratigraphic patterns; depositional environments and facies; sediment routing and provenance; and the ultimate tectonic drivers and mechanics of broken foreland basins.

3. Pampean and Laramide broken foreland provinces

3.1. Structural framework

3.1.1. Pampean broken foreland, South America

The Sierras Pampeanas province represents a modern broken foreland province inboard of the Andean orogenic belt (Fig. 2A). Situated in the retroarc region of west-central Argentina at 27°–33°S, the Pampean broken foreland spans ~750 km along strike (N-S) and ~ 500 km across strike (E-W). Deformation has penetrated ~800 km inboard of the modern trench, reaching halfway across the South American continent at these latitudes (Ramos et al., 2002). This intraforeland province comprises a series of topographically distinct late Cenozoic basins bordered by a network of ~12 NNW- to NNE-trending ranges that constitute the Sierras Pampeanas (Jordan et al., 1983; Fielding and Jordan, 1988; Jordan, 1995; Ramos, 1999a). These basement ranges are the product of W- and E-directed contractional structures that are geometrically and kinematically distinct from the east-directed thin-skinned structures involving Phanerozoic cover strata in the Precordillera fold-thrust belt to the west (Fig. 2A).

Most of the basement-cored uplifts are controlled by solitary faults, with some exhibiting strike lengths of 200–400 km. These range-

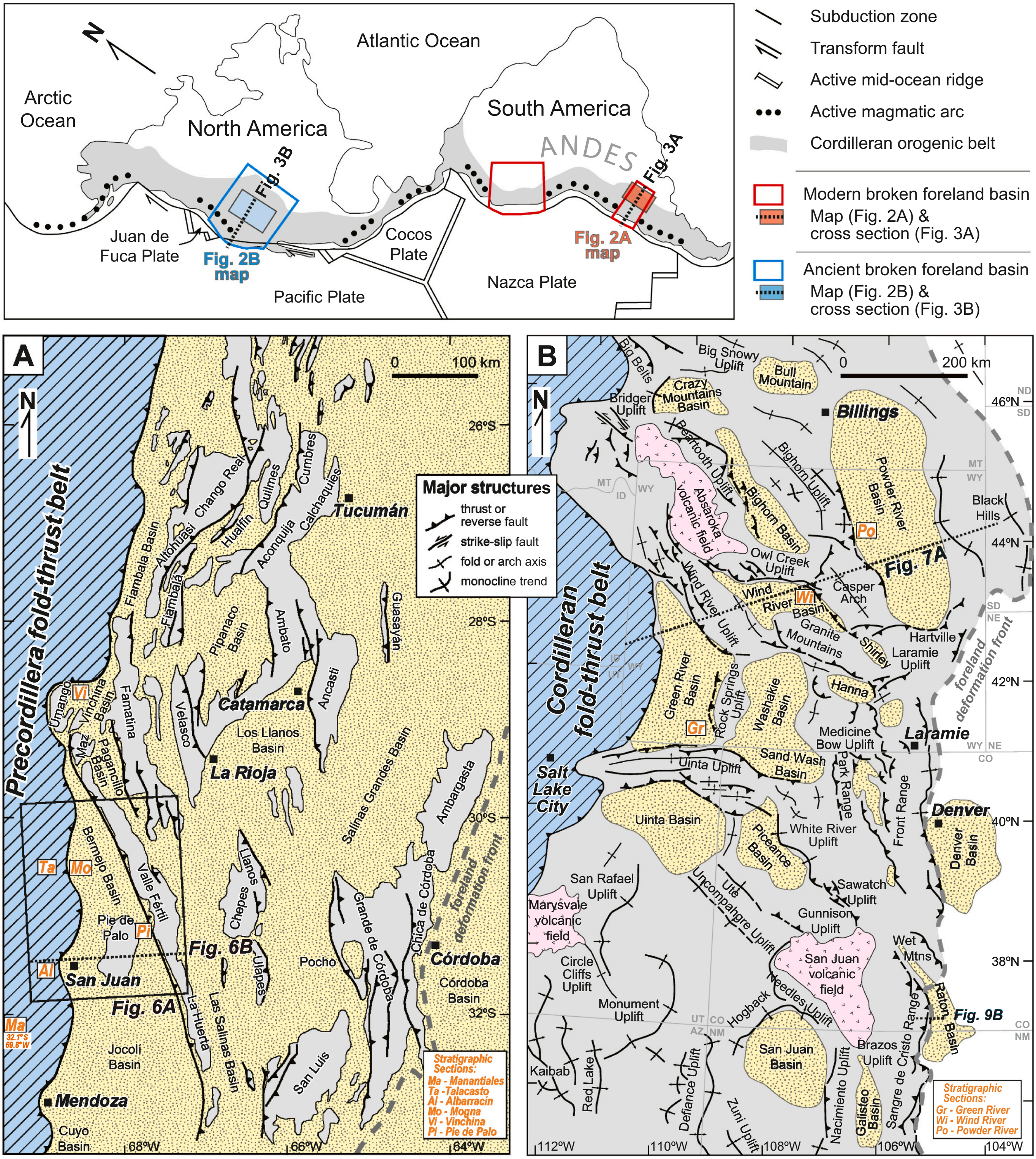

Fig. 2. (Top) Map of the Circum-Pacific orogenic system (after Dickinson, 2004) showing locations of broken foreland basin systems in South America and North America, and corresponding maps (Figs. 2A and 2B) and cross sections (Fig. 3). (A) Geologic map of the Pampean broken foreland partitioned by contractional structures and individual ranges of the Sierras Pampeanas adjacent to the Precordillera fold-thrust belt of the southern central Andes, South America (after Ramos et al., 2002). (B) Map of the Laramide province in the western U.S.A. showing major structures, basement-cored block uplifts, basins, and post-orogenic volcanic fields of the Late Cretaceous–Paleogene broken foreland of the Cordilleran fold-thrust belt, North America (after Dickinson et al., 1988). Locations of map (Fig. 6A) and cross sections (Figs. 6B, 7A, and 9B) and stratigraphic sections with sediment accumulation records (Fig. 8) are indicated.

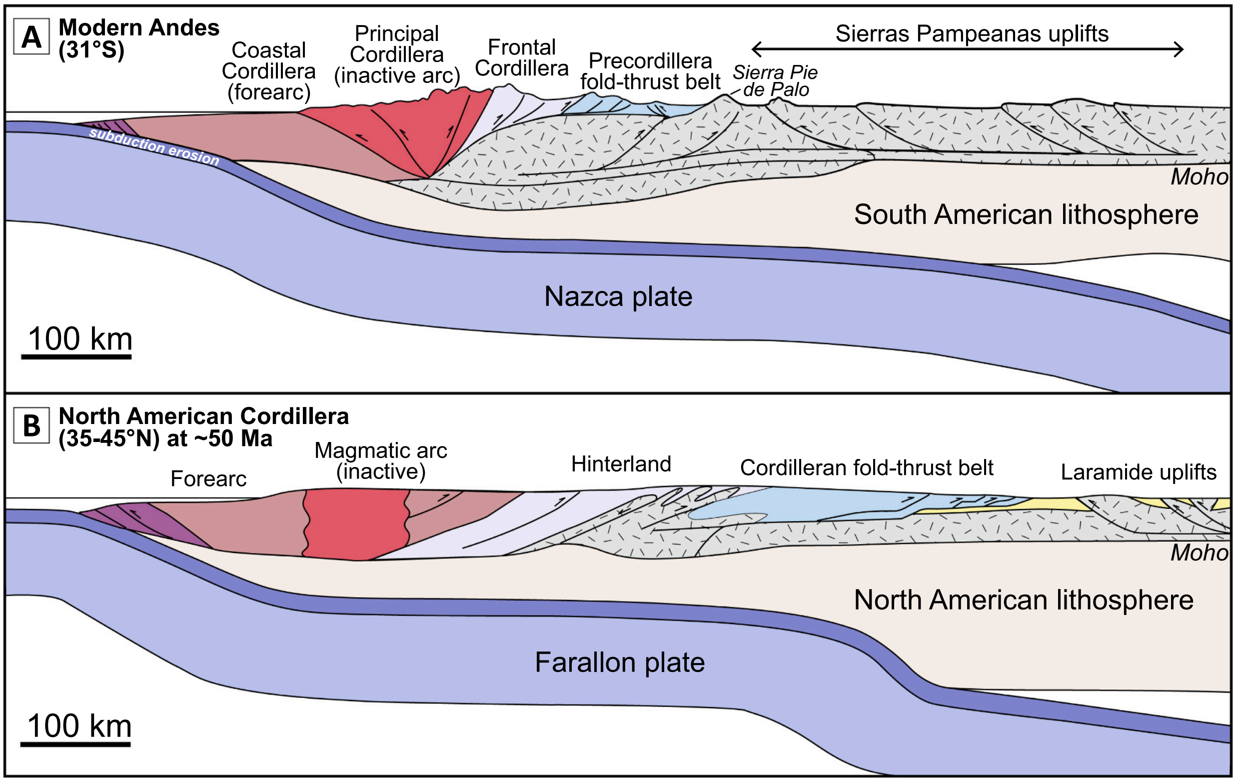

Fig. 3. (A) Present-day cross section of the Andean orogenic belt and Pampean broken foreland, southern central Andes, South America (after Cristallini and Ramos, 2000; Bellahsen et al., 2016). (B) Schematic cross section of the North American Cordillera and Laramide broken foreland at ~50 Ma (after Yonkee and Weil, 2011, 2015).

bounding faults dip 35°–70° near the surface, commonly split into several splay faults in the uppermost crust (<5 km depth), and have listric geometries at depth (Fig. 3A) (González Bonorino, 1950; Jordan and Allmendinger, 1986; Ramos et al., 2002; Alvarado and Ramos, 2011). The principal faults have been seismically imaged to mid-crustal depths (>15–30 km) and some may penetrate into the lower crust (Comínguez and Ramos, 1995; Zapata, 1998; Cristallini et al., 2004; Alvarado et al., 2005; Vergés et al., 2007). Most faults are interpreted to reactivate preexisting basement-involved faults or fabrics of pre-Cenozoic age (e.g., Schmidt et al., 1995; Martino et al., 2016; Zapata et al., 2020; Ortiz et al., 2021). Reverse displacement accounts for ~2–8 km of structural relief across individual faults, with roughly 10–20 km of cumulative horizontal shortening (~2%) across the Sierras Pampeanas (Jordan and Allmendinger, 1986; Ramos et al., 2002). Although strike-slip displacement is negligible, transtensional and transpressional deformation occurred near the northern and southern tips of overlapping (possibly en echelon) contractional structures and along transverse structures oblique to the regional N-S tectonic strike (Alvarado and Beck, 2006; Meigs et al., 2006; Seggiaro et al., 2014; Quiroga et al., 2021).

3.1.2. *Laramide broken foreland, North America*

The Laramide province of western North America represents an ancient broken foreland province that formed far inboard of the north-trending Cordilleran retroarc orogenic belt during Late Cretaceous–Paleogene subduction of the oceanic Farallon plate (Fig. 2B). Intraplate deformation affecting Precambrian crystalline basement reached cratonic regions up to 1000–1500 km east of the former subduction trench. The Laramide province corresponds to the modern Rocky Mountains in the USA, spanning ~1500 km along strike (N-S) and ~ 600 km across strike (E-W) at 32°–46°N (Yonkee and Weil, 2015). The Laramide foreland was partitioned by ~20 basement-involved faults and related folds into a series of broken foreland basins (Dickinson et al., 1988; Lawton, 2019). An anastomosing network of contractional structures exhibits a wide range of orientations, with predominantly N- to NW-trending ranges developed above E/NE- or W/SW-dipping structures (but with important exceptions such as the E-trending Uinta Range above N- and S-dipping structures) that are disconnected from the thin-skinned thrust-belt structures that mainly involve sedimentary rocks of the Cordilleran orogenic wedge to the west (Figs. 2B and 3B).

Most Laramide uplifts are linked to a single major reverse fault that penetrates Precambrian basement and displays strike lengths of several tens of kilometers, commonly up to 150–300 km (Kelley, 1955; Berg, 1962; Love, 1970; Tweto, 1979; Love and Christiansen, 1985; Blackstone, 1993a; Erslev, 1993). Some fault tips remain blind (non-emergent), with only large doubly plunging folds present at the surface. Seismic data show that most range-bounding reverse faults exhibit moderate dip values (30°–40°) and, where resolved, penetrate down to middle or lower crustal levels (~25–35 km) (Smithson et al., 1979; Gries, 1983; Allmendinger, 1992). Individual faults record maximum displacements of 5–15 km, resulting in a cumulative horizontal shortening of 40–50 km (~10–15%) across the province (Brown, 1988; Blackstone, 1993b; Stone, 1993; Hoy and Ridgway, 1997; Yonkee and Weil, 2015). Although the Laramide broken foreland contains many obliquely oriented structures, kinematic fault-slip and layer-parallel shortening analyses suggest a relatively uniform WSW-ENE compression direction (Erslev, 1993; Bird, 1998; Erslev and Koenig, 2009; Neely and Erslev, 2009; Yonkee and Weil, 2015) with local strike-slip deformation focused on transverse structures. The wide range of intraforeland orientations for Laramide basement arches may reflect contractional reactivation of heterogeneous inherited sutures, faults, and fabrics of chiefly Precambrian age (e.g., Brown, 1988; Stone, 2002; Worthington et al., 2016; Bader, 2018).

3.2. Plate tectonic configuration

3.2.1. Pampean broken foreland, South America

The late Cenozoic evolution of the Pampean broken foreland is strongly correlated with the geometry of the subducting oceanic slab beneath the South American plate. Along the western continental margin, the Nazca slab dips relatively uniformly ~30° eastward and penetrates to lower mantle depths of 1000–1100 km (Cahill and Isacks, 1992; Portner et al., 2020; Rodríguez et al., 2021). This pattern, however, is disrupted in several regions of subhorizontal (flat) slab subduction and corresponding spatial gaps in the Andean magmatic arc. At 27°–33°S, the flat Pampean segment of the Nazca slab is situated at ~100–120 km depth with an E-W width of up to ~300–400 km (Fig. 3A); this flat slab is situated medially between steeper, generally ~30° east-dipping segments of the contiguous Nazca slab near the trench and beneath the distal eastern foreland (Anderson et al., 2007; Gans et al., 2011). To the north and south, the Pampean flat slab is flanked by a uniformly east-dipping Nazca slab and active magmatic arc (Barazangi and Isacks, 1976; Jordan et al., 1983; Cahill and Isacks, 1992; Ramos, 1999b).

The spatial and temporal correspondence between the Sierras Pampeanas and the flat slab segment suggests that the basement-cored uplifts are related to the geometry of the subducting Nazca slab. However, the lack of a thick package of sedimentary cover rocks in the foreland region east of the thin-skinned Precordillera fold-thrust belt may have further promoted basement-involved deformation within the foreland (Allmendinger et al., 1983). The Pampean flat slab has been credited to subduction of the thick buoyant oceanic crust composing the aseismic Juan Fernández Ridge (Pilger, 1981; Gutscher et al., 2000; Ramos, 2009; Ramos and Folguera, 2009). A late Miocene onset of flat-slab conditions has been estimated at 12–10 Ma on the basis of plate reconstructions and the progressive inboard advance and ultimate cessation of arc magmatism (Kay et al., 1988; Yáñez et al., 2001; Kay and Mpodozis, 2002; Ramos et al., 2002). Thermochronological data indicate accelerated exhumation at this time within the orogenic wedge, with more broadly dispersed cooling ages across the Sierras Pampeanas likely due to complex pre-Andean thermal histories and the low magnitude (mostly <2 km) of late Cenozoic exhumation (Levina et al., 2014; Fosdick et al., 2015; Ortiz et al., 2021). Several uplifts within the Pampean foreland show modest bedrock cooling prior to slab flattening (Coughlin et al., 1998; Bense et al., 2013; Löbens et al., 2013; Zapata et al., 2020), although the regional stratigraphic continuity across multiple basins was not disrupted until late Miocene time (Capaldi et al., 2020; Mackaman-Lofland et al., 2022).

3.2.2. Laramide broken foreland, North America

Structural partitioning of the Cordilleran foreland basin during the Laramide orogeny has been ascribed to the mechanical effects of flat slab subduction. The shift from steep to shallow subduction is preserved in the inboard sweep of arc magmatism, which has tracked the progressive advance of the leading edge of the growing zone of flat-slab subduction (Coney and Reynolds, 1977; Dickinson and Snyder, 1978; Constenius, 1996; Bird, 1998; Constenius et al., 2003; Saleeby, 2003; Erslev, 2005; Fan and Carrapa, 2014; Yonkee and Weil, 2015; Copeland et al., 2017; Chapman et al., 2018; Lawton, 2019). The roughly 80–40 Ma phase of flat slab subduction matches the late Campanian–Eocene timing of intraplate shortening and exhumation in Wyoming and Colorado, the principal segments of the Laramide broken foreland (Fig. 2B).

Several studies have suggested a pre-flat slab (prior to ~80 Ma) onset of basement involvement in the northern Laramide province, in southwestern Montana, where most basement structures spatially overlap or are in proximity (<50–150 km) to the frontal thin-skinned structures of the Cordilleran fold-thrust belt (Suttner et al., 1981; Schwartz, 1982; DeCelles, 1986; Lageson and Schmitt, 1994; Carrapa et al., 2019; Garber et al., 2020; Orme, 2020; Vuke, 2020). Others have similarly proposed early phases of Laramide basement deformation up to 300 km inboard of the fold-thrust belt, principally on the basis of unconformities or local condensed sections within the Upper Cretaceous interval of the Cordilleran foreland basin (including the Moxa Arch, San Rafael Swell, Rock Springs Uplift, Douglas Creek Arch, Uncompahgre Uplift, Sierra Madre Uplift, and Rawlins Uplift of Wyoming, Utah, and Colorado; Lawton, 1986; Miall and Arush, 2001; Leva López and Steel, 2015; Rudolph et al., 2015; Minor et al., 2022). However, the regional Upper Cretaceous stratigraphic continuity across the Western Interior Seaway and the lack of fault-proximal facies adjacent to these basement-cored features suggests that any surface expression of these blocks prior to the late Campanian was restricted to highly localized areas and generated limited structural relief. In sharp contrast, late Campanian–Eocene shortening during flat-slab subduction (~80–40 Ma), with a possible peak during Paleocene–early Eocene time (~66–49 Ma), generated large contractional structures (many with >5–10 km structural relief and > 50 km strike lengths) across the Laramide broken foreland that led to exhumation of Phanerozoic sedimentary rocks and underlying Precambrian basement.

The temporal framework for Laramide deformation derives largely from stratigraphic, sedimentologic, and vertebrate and invertebrate biochronologic data that indicate abrupt shifts in stratigraphic thicknesses and sedimentary facies due to basement-involved deformation (e.g., Dorr et al., 1977; Dickinson et al., 1988; Lillegraven, 1993; Gunnell et al., 2009; Lynds and Slattery, 2017; Minor et al., 2022). An absolute geochronological context is provided by isotopic ages that constrain regional magmatism and the depositional ages of synorogenic Laramide basin fill (e.g., Tweto, 1975; Snyder et al., 1976; Coney and Reynolds, 1977; Dickinson and Snyder, 1978; Bryant et al., 1989; Armstrong and Ward, 1993; Constenius, 1996; Constenius et al., 2003; Chapin et al., 2004; Smith et al., 2003; Chapman et al., 2018). Erosional unroofing of Paleozoic-Mesozoic cover strata and exposure of Precambrian crystalline basement, as recorded by sandstone and conglomerate clast compositions, paleocurrents, detrital geochronological data, and bedrock thermochronological data (Cerveny and Steidtmann, 1993; Omar et al., 1994; DeCelles et al., 1991a, 1991b; Cather, 2004; Kelley and Chapin, 2004; Carroll et al., 2006; Cather et al., 2012, 2019; May et al., 2013; Peyton and Carrapa, 2013; Fan and Carrapa, 2014; Bush et al., 2016; Stevens et al., 2016), provide direct evidence for the ~80–40 Ma main phase of Laramide orogenesis and associated growth of positive topographic barriers within the broken foreland province (Figs. 2B and 3B).

4. Designation of the Andean retroarc foreland

4.1. Andean topographic front vs. foreland deformation front

The Andean orogenic belt provides an opportunity to evaluate the modern configuration of a retroarc foreland region and the scope of structural and sedimentary processes within late Cenozoic broken foreland basins (Fig. 4). In present-day South America, three separate broken foreland provinces are readily defined by the structural disruption and topographic compartmentalization of an otherwise uninterrupted foreland basin. The Peruvian (5°–14°S), Pampean (27°–33°S), and northern Patagonian (45°–48°S) broken foreland regions are recognized through the delineation of two key tectonomorphic elements—the *Andean topographic front* and the *foreland deformation front*—both in map view (Fig. 4) and in trench-normal cross sections (Fig. 5).

First, the *Andean topographic front* is defined by the sharp break between the Andean fold-thrust belt and the foreland plains (Figs. 4 and 5). Along the ~8000 km length of the Andes, this modern topographic break corresponds to the frontal (easternmost) surface-breaking fault of the thin-skinned fold-thrust belt, generally an east-directed thrust, although antithetic west-directed backthrusts and triangle zones are also present. With few exceptions, this boundary is mutually defined on the basis of topographic relief and mapped late Cenozoic faults, including several active faults (Proyecto Multinacional Andino, 2009; Veloza

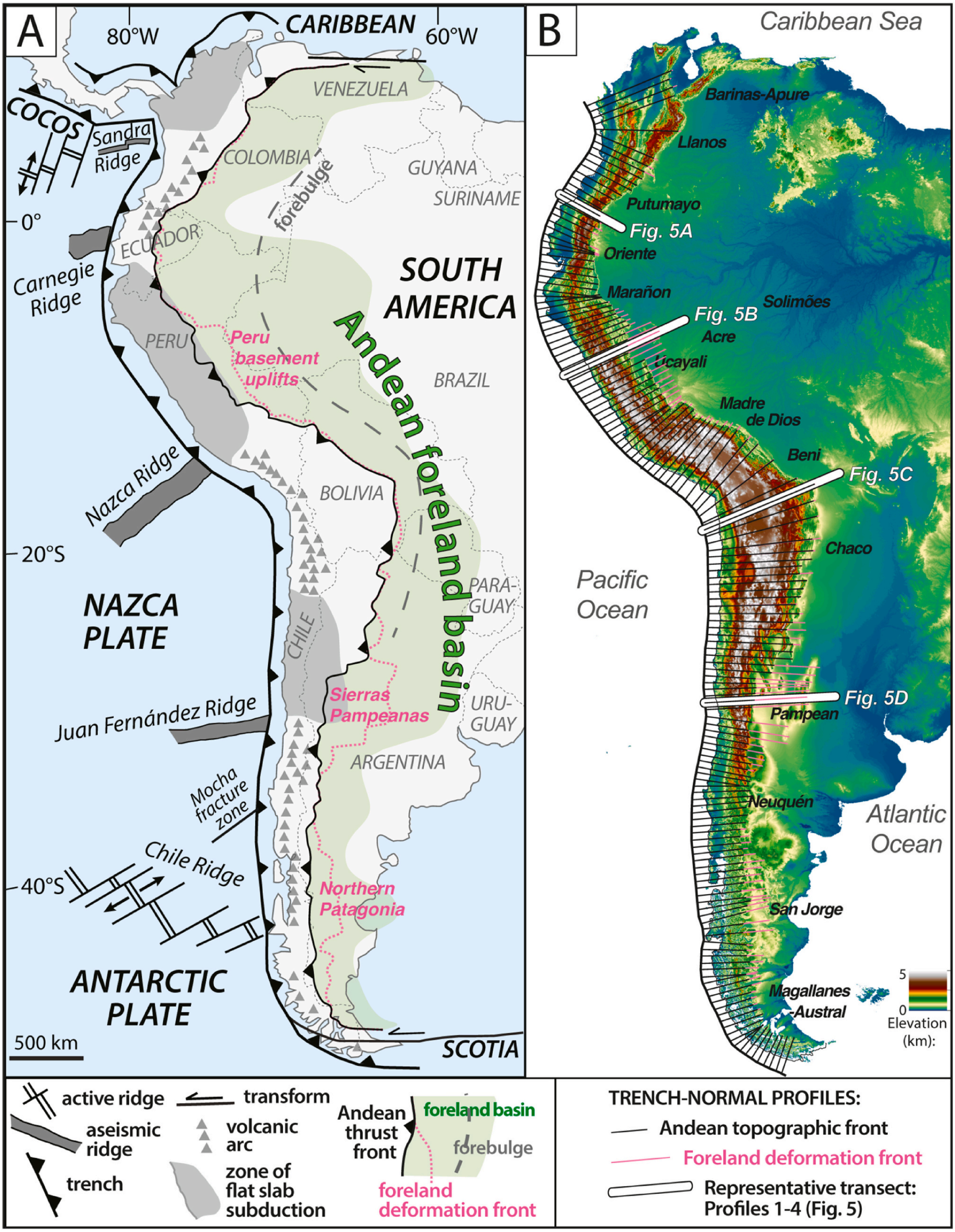

Fig. 4. (A) Tectonic map and (B) shaded topography of western South America showing plate boundaries, zones of flat slab subduction, the Andean magmatic arc, and the retroarc foreland basin system (after Horton et al., 2022). Broken foreland provinces are defined by zones where the foreland deformation front (pink dashed line) is situated far inboard of the topographic front of the Andean fold-thrust belt (black barbed line). Locations of topographic profiles A, B, C, and D (Fig. 5) are indicated.

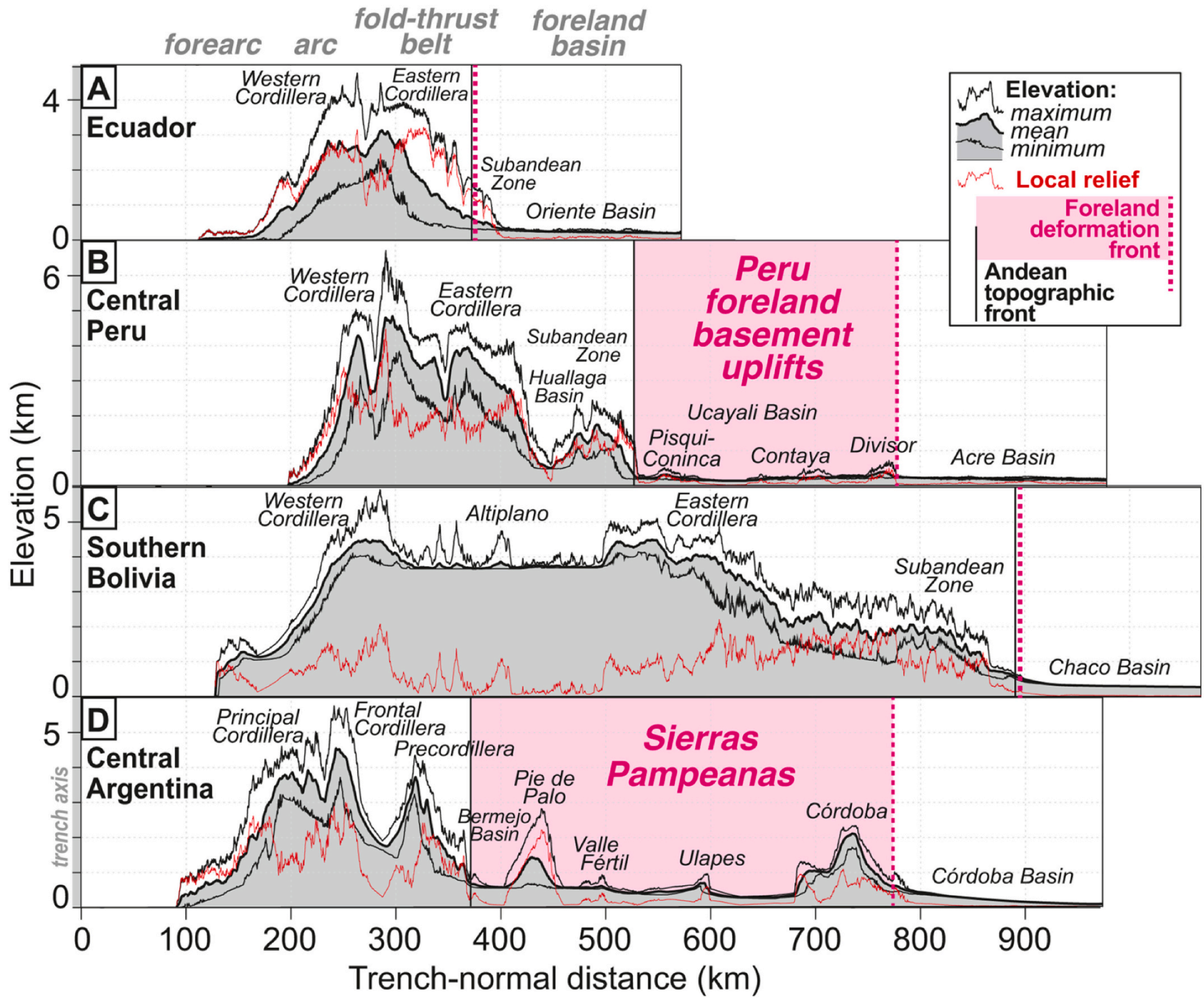

Fig. 5. Representative trench-normal profiles showing swath-averaged topography (minimum, maximum, and mean elevation; black lines), relief (red line), and the traces of the Andean topographic front (black vertical line) and foreland deformation front (pink vertical dashed line) (after Horton et al., 2022). Pink shading shows broken foreland zones where the foreland deformation front is situated far inboard of the Andean mountain front.

et al., 2012; McClay et al., 2018; Costa et al., 2020; Styron and Pagani, 2020; Horton et al., 2022).

Second, the *foreland deformation front* is defined by the maximum inboard extent of late Cenozoic structures (Figs. 4 and 5). Although locally discontinuous, this feature is marked by contractional faults or folds that generate positive surface topography at the greatest distances from the subduction trench. The late Cenozoic age of these structures is confirmed by seismic activity and/or the involvement of Neogene rock units (Proyecto Multinacional Andino, 2009; Veloza et al., 2012; Anselmi et al., 2015; Folguera et al., 2015; Costa et al., 2020; Styron and Pagani, 2020; Horton et al., 2022). Along the length of the orogenic system, the foreland deformation front either coincides with the Andean topographic front or is positioned farther inboard within the surrounding low-relief foreland plains (Fig. 4).

Systematic identification of these two late Cenozoic tectonomorphic features enables a clear discrimination of broken versus unbroken segments of the Andean foreland basin. Specifically, a contiguous or unbroken foreland is defined where the foreland deformation front coincides with the Andean topographic front, with no major intraforeland structures. Examples include (i) the narrow retroarc fold-thrust belt in the northern Andes of southern Colombia and Ecuador (2°N–5°S) and (ii) the wide fold-thrust belt in the central Andes of southern Peru, Bolivia and northernmost Argentina (15°–25°S) (Fig. 4), where broad low-relief foreland plains are represented by (i) the Putumayo and Oriente basins (Fig. 5A) and (ii) the Madre de Dios, Beni, and Chaco basins (Fig. 5C), respectively. Conversely, a broken foreland is defined where the foreland deformation front is positioned significantly inboard of the Andean topographic front, including the intraforeland positive topography generated by separate basement-involved structures of Peru (5°–14°S; Fig. 5B), west-central Argentina (27°–33°S; Fig. 5D), and southern Argentina (45°–48°S).

The positions of the Andean topographic front and foreland deformation front (Figs. 4 and 5) have varied over the Late Cretaceous–Cenozoic history of crustal shortening. Accurate delineation of these two key elements in time and space will enable tracking of the cratonward advance of the fold-thrust belt and identification of possible earlier phases of broken foreland conditions within the Andean orogenic system.

4.2. Andean broken foreland provinces

In South America, three major broken foreland provinces are defined by substantial gaps between the positions of the Andean topographic front and foreland deformation front. In the Peruvian (5°–14°S), Pampean (27°–33°S), and northern Patagonian (45°–48°S) broken foreland regions (Fig. 4), the foreland deformation front reaches orthogonal distances up to 800 km from the trench, and up to 400 km inboard of the Andean topographic front (Fig. 5). The roughly 200–400 km cross-strike widths for the broken foreland provinces are compatible with typical wavelengths for Andean flexural depocenters (e.g., Horton and DeCelles, 1997; Chase et al., 2009). These broken foreland regions, which constitute about one-third of the modern foreland system of South America (Fig. 4), contain isolated topographic features linked to basement-involved contractional structures.

These broken foreland regions are structurally partitioned by a series of basement structures that generate positive topographic features that protrude above the regional foreland plains to varying degrees. In the broken foreland of Peru (including the Sierra del Divisor along the Peru-Brazil border), the surface expressions of the basement highs reach up to 400 m above a continuous foreland plain (delimited by the Ucayali and Juruá river systems) at 200–300 m elevation (Fig. 5B). In contrast, Pampean basement highs rise up to 1500–2500 m above a series of segregated basins with basin floors variably situated between 100 and 1200 m elevation (Fig. 5D). The more-accentuated topographic relief and basin compartmentalization in the Pampean segment could reflect greater vertical displacement (throw) on intraforeland structures and/or reduced sediment accumulation relative to the Peruvian segment. The basement-involved structures in Peru are comparable in magnitude to Pampean structures, with maximum throws of 2–5 km along individual faults (Oliveira et al., 1997; Hermoza et al., 2006; Wanderley-Filho et al., 2010; Baby et al., 2018; McClay et al., 2018). However, amplified foreland accumulation in Peru (up to 3–6 km) could be the product of enhanced erosion and more-efficient sediment transport from the Andean orogenic wedge to the foreland, thus reducing topographic relief between adjacent basins and ranges, as well as the relief among successive basin floors.

In comparison to the Peruvian and Pampean segments, the northern Patagonian broken foreland lacks large zones of active sediment accumulation (e.g., Bilmes et al., 2013; Echaurren et al., 2016). Although broken by intraforeland basement structures that involve Neogene sedimentary and igneous rocks (Proyecto Multinacional Andino, 2009; Costa et al., 2020; Horton et al., 2022 and references therein), most shortening and foreland sedimentation within northern Patagonia occurred during Miocene orogenesis (Orts et al., 2012; Ramos et al., 2015; Folguera et al., 2018). The Patagonian retroarc region is situated 500–1000 m above sea level and is subjected to minor erosion, with modern Andean sediment bypassing the foreland and reaching offshore Atlantic basins (Ramos, 2005; Orts et al., 2015; Ghiglione et al., 2016; Horton, 2022). The variable accommodation situations in the three broken foreland provinces underscore the complex interactions among sediment accumulation, erosion, and bypass. These contrasts may be attributable to different geodynamic, structural, or climatic settings, which show large variations along the western margin of South America (Mpodozis and Ramos, 1990; Ramos, 1999b, 2009; Horton, 1999, 2018a, 2018b, 2022; Montgomery et al., 2001).

4.3. Modern depositional systems

Evaluation of modern erosional and depositional systems in an active broken foreland in South America (Fig. 6) illustrates the range of sedimentary processes and environments within broken foreland basins. A suite of ~10 topographically distinct basins occupy the lowland areas (mostly 200–600 m above sea level) adjacent to the ranges that form the Sierras Pampeanas (with most crestlines up to 1–4 km high). These broken foreland basins contain Cenozoic basin fill up to 3000 m in thickness. Map-view interpretations based on satellite images and digital elevation data enable the identification of modern erosional regions, as defined by incised bedrock fluvial systems, within the Precordillera fold-thrust belt and the basement-cored uplifts of the western Pampean foreland in Argentina (Fig. S1). Within the ~30,000 km^2 map area (Fig. 6A), active depositional systems include alluvial fan, braided fluvial channel, fluvial megafan, fluvial overbank/floodplain, playa lake, and eolian dune field environments.

The erosional drainage networks and corresponding depositional systems within the independent basement ranges of the foreland are sharply different from their counterparts in the thin-skinned Precordillera fold-thrust belt. The Sierra Pie de Palo and Sierra Valle Fértil basement ranges are dominated by a series of small drainages (<500 km^2) that feed local alluvial fans (<50 km^2) that coalesce into a mountain-front bajada. Conversely, within the thrust belt, sediment loads derived from large drainage catchments (>5000 km^2) debouch onto the westernmost foreland as separate fluvial megafans with depositional areas >500 km^2, far in excess of local alluvial fans (Damanti, 1993; Milana, 2000; Horton and DeCelles, 2001).

In addition to sourcing local alluvial fans, the basement uplifts of the Pampean broken foreland constitute topographic barriers that affect fluvial and local lacustrine systems. These elongate topographic highs guide the courses of river systems that navigate through the Pampean foreland, forming axial (longitudinal rivers) parallel to NNW-trending ranges such as the Sierra Valle Fértil. Intersections among topographic highs are commonly restricted to narrow gaps between adjacent topographic highs, such as the ~10 km wide zone between alluvial fans from the Pie de Palo and Sierra Valle Fértil (Fig. 6A). In some cases, these gaps are closed by constructional alluvial fans or uplifted bedrock, forming topographic sills that impound drainage systems and form lakes.

Both emergent (surface-breaking) and non-emergent (blind or subsurface) contractional faults exert considerable influence on foreland depositional systems. The Pie de Palo represents a N-trending, doubly plunging anticline formed above blind crustal-scale reverse faults with upper-crustal splays that only locally breach the surface along the ~80 km length of the fold (Jordan and Allmendinger, 1986; Fielding and Jordan, 1988; Smalley et al., 1993; Zapata, 1998; Vergés et al., 2007). In a departure from earlier studies, Bellahsen et al. (2016) used structural, seismic, and geomorphic data to demonstrate that shallow east-dipping faults along the western margin of the Pie de Palo are antithetic to a deeply rooted, west-dipping master fault that principally controlled the growth of the range (Fig. 6B). Toward the foreland, the NNW-trending Sierra Valle Fértil formed above an emergent east-dipping reverse fault that persists along strike over a ~ 350 km distance (Ramos et al., 2002; Ortiz et al., 2021). Although the Pie de Palo and Sierra Valle Fértil are among the smallest and largest structures within the Pampean foreland, respectively, both systems successfully form 2500–3000 m high topographic barriers (Fig. 6) that similarly deflect fluvial and eolian systems (Capaldi et al., 2019; Garzanti et al., 2022).

Most of the modern lakes and eolian systems in the proximal Pampean foreland have developed in broad floodplain regions adjacent to braided river systems that ultimately drain to the Atlantic Ocean (Garzanti et al., 2021). These settings include local overbank areas adjacent to small streams and much larger inter-megafan areas situated between the major outlet rivers that feed fluvial megafans in the most proximal foreland. Most of the lakes represent ephemeral playa systems related to seasonal overbank flooding. Large eolian dune fields originate from windblown materials derived from fluvial channels and deflated floodplain areas. A prominent example is the 2000 km^2 Medanos Grande dune field (Fig. 6), in which sediments derived from the active Río San Juan and Río Tunuyán fluvial channels and adjacent floodplains are transported northward and confined by topographic barriers formed by the Pie de Palo and Sierra Valle Fértil basement ranges (Capaldi et al., 2019). This dune field represents an isolated western satellite of the broad Pampean Sand Sea of central Argentina (Iriondo, 1999; Tripaldi and Forman, 2016; Garzanti et al., 2022).

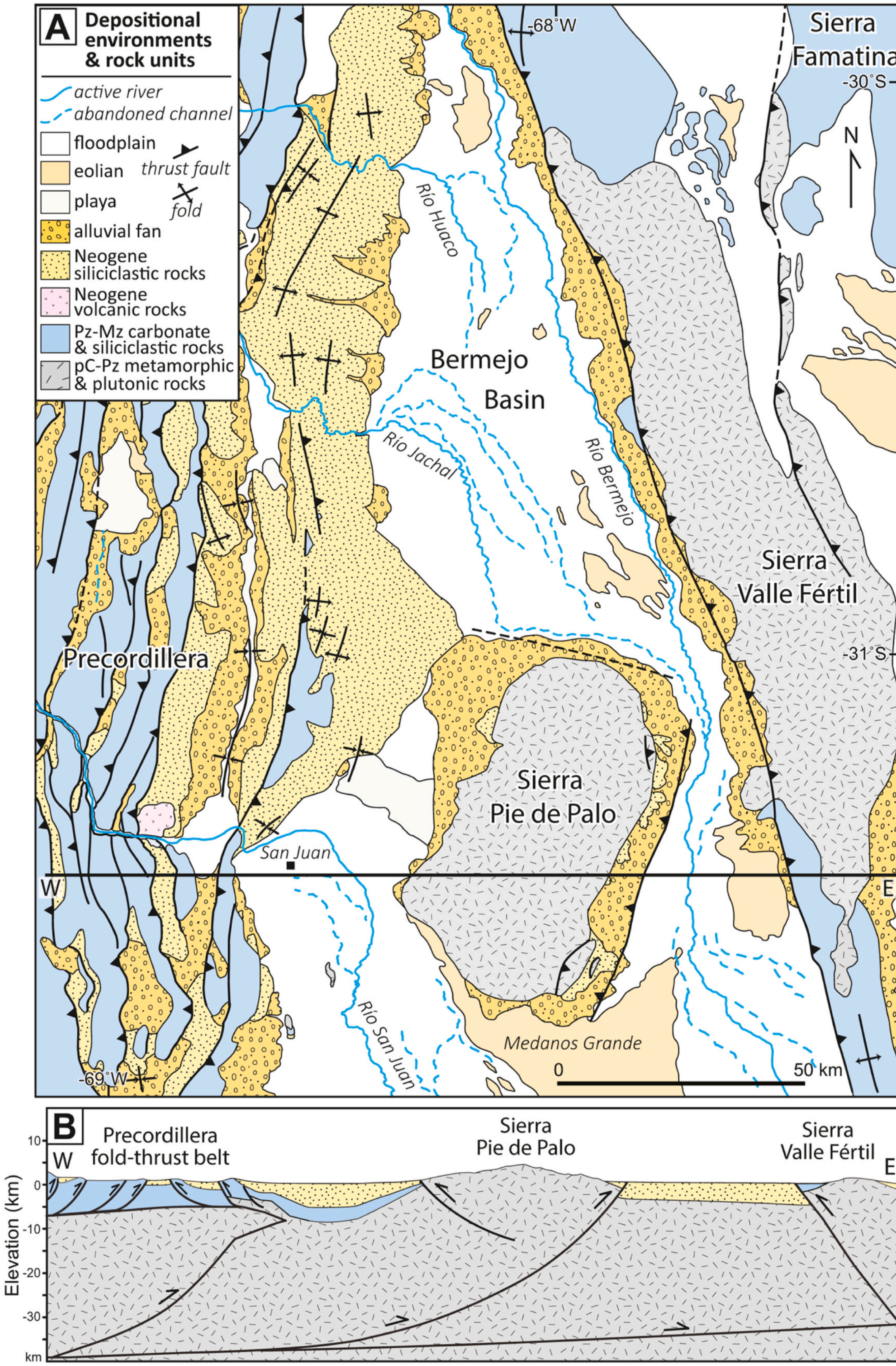

Fig. 6. (A) Map of modern depositional environments and major geologic units (corresponding to satellite image in Fig. S1; modified from Fielding and Jordan, 1988) and (B) W-E cross section of the southern central Andes and proximal western segment of the Pampean broken foreland, west-central Argentina (modified from Vergés et al., 2007; Bellahsen et al., 2016).

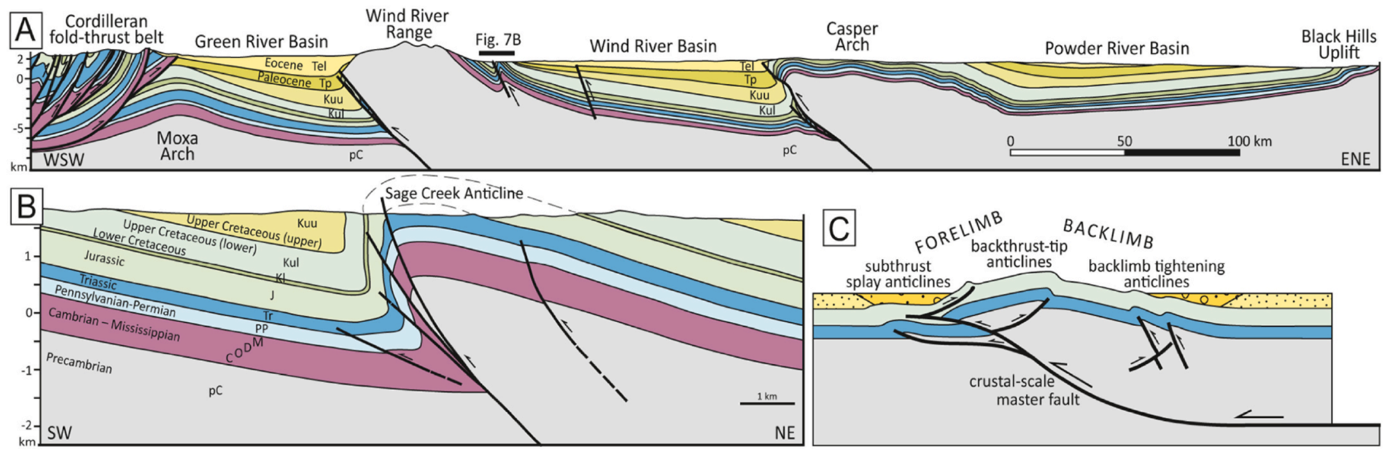

Fig. 7. (A) Regional cross section of representative broken foreland basins (Green River, Wind River, and Powder River basins) and flanking basement-cored uplifts (Wind River Range, Casper Arch, and Black Hills Uplift) within the Wyoming segment of the Laramide broken foreland province (redrawn from Love and Christiansen, 1985). (B) Detailed cross section showing subsidiary structures within the Sage Creek anticline of the western Wind River Basin (redrawn from Stone, 1993). (C) Generalized cross section depicting basement structural geometries and contrasting forelimb and backlimb settings for broken foreland basins (after Erslev et al., 2001; Erslev, 2005).

5. Intraforeland structure and basin architecture

5.1. Structural configuration

Regional cross sections across an ancient broken foreland in North America highlight some of the structural geometries associated with basement-involved intraplate deformation and the evolution of intervening basins (Fig. 7). A ~ 600 km regional cross section through Wyoming (Fig. 7A) shows the spatial transition from the Cordilleran fold-thrust belt to the Laramide broken foreland and a series of basement block uplifts (the Wind River Range, Casper Arch, and Black Hills Uplift) and successive basins (the Green River, Wind River, and Powder River basins) (Love and Christiansen, 1985; Stone, 1993; Yonkee and Weil, 2015). The frontal thrust belt is defined by thin-skinned structures arranged into a foreland-directed imbricate fan that deformed thick (>5–10 km) Phanerozoic cover strata above a single shared décollement near the basement-cover interface. In contrast, the broken foreland is typified by basement-involved intraforeland structures that are each controlled by a single principal fault with common splay faults at shallow levels within a relatively thin (<2 km) sedimentary cover (Fig. 7B; Berg, 1962; Smithson et al., 1979; Gries, 1983; Brown, 1988; Blackstone, 1990, 1993b; Allmendinger, 1992; Stone, 1993; Hennings and Hager, 1996: Lillegraven, 2015). Laramide basement structures show variable foreland- and hinterland-dipping geometries, as clearly expressed in regional maps (Fig. 2B), but individually they share several common characteristics, as summarized in a schematic crustal cross section (Fig. 7C; Erslev et al., 2001; Erslev, 2005).

Each basement-cored uplift exhibits a topographic and structural asymmetry expressed as a steep forelimb and gentle backlimb (Fig. 7C). This anatomy is assigned to a single controlling fault with a broadly listric geometry in which the fault penetrates crystalline basement at a moderate dip and soles into a subhorizontal décollement within the middle to lower crust. At shallow levels (and commonly observed at the surface), most master faults and subsidiary splay faults are expressed as steeply dipping features that yield complex geometries with sheared limbs and steep to overturned footwall units. On the forelimb, near-surface geometries entail: (i) low-angle footwall splays (e.g., short-cut faults, out-of-basin thrusts, and out-of-syncline thrusts) that follow anisotropies within the sedimentary cover or shallow basement; (ii) basement-involved backthrusts (including wedge faults and the generation of triangle zones); and (iii) shallow backthrusts confined to the sedimentary cover (including rabbit-ear anticlines) (Fig. 7C). On the backlimb, secondary structures either synthetic or antithetic to the main fault form in the sedimentary cover and shallow basement in response to tightening above the deeper ramp.

The comparable geometries of many Laramide basement arches suggest that their controlling faults may share a deep crustal shear zone (or regional décollement) that approximates the brittle-ductile transition for continental basement rocks of granitic composition (Oldow et al., 1989; Erslev, 1993; McQuarrie and Chase, 2000). These widely spaced structures, however, lack a single preferred direction of tectonic transport (or vergence), and contain many secondary structures antithetic to the master faults responsible for individual basement uplifts. This pattern of diffuse intraplate shortening with no preferred vergence may reflect the uniformly thin pre-orogenic sedimentary cover across the region (i.e., no inherited supracrustal stratigraphic wedge; Boyer, 1995) and the diversity of preexisting basement discontinuities (igneous and metamorphic fabrics; faults, and sutures; Yonkee and Weil, 2015).

5.2. Basin configuration

The architecture of compartmentalized basins within a broken foreland is closely linked to the geometry of the bounding structures (Fig. 7). Most importantly, basin development is largely dictated by position on the steep forelimb or the gentle backlimb of a single crustal-scale basement-cored uplift (Fig. 7C). Most basin depocenters are situated in footwall positions near the forelimbs of major reverse faults, consistent with greater flexural loading in proximity to topographic loads. These forelimb basin margins also have the highest degree of structural disruption, with commonly steep to overturned units and growth strata produced by progressive tilting of proximal basin fill adjacent to the primary bounding structure (Bryant et al., 1989; DeCelles et al., 1991b; Lageson and Schmitt, 1994; Zapata and Allmendinger, 1996a; Hoy and Ridgway, 1997). In contrast, basin development along the gently dipping backlimb generally marks the distal basin margin, with stratigraphic onlap or pinchout onto the corresponding gentle topographic slope.

These contrasts in forelimb versus backlimb setting impart several distinct configurations for potential broken foreland basins. First, asymmetric basins may form between opposing basin-margin structures defined by the forelimb of one structure and the backlimb of a separate structure (e.g., Wind River Basin, Fig. 7A); such basins exhibit asymmetric, wedge-shaped cross-sectional profiles reminiscent of foredeeps, but at a more localized scale (e.g., Hagen et al., 1985; Yang and Dorobek, 1995). A second option represents a basin situated between two facing forelimbs of separate basin-directed structures (e.g., Green River Basin,

Fig. 7A), yielding a relatively symmetric basin with similar depocenters along opposite margins (e.g., Cobbold et al., 1993; Cunningham, 2005). A third possibility constitutes a broad, low-relief “sag” or saucer-shaped basin positioned on the backlimbs of two separate structures that dip toward the central basin (e.g., Powder River Basin, Fig. 7A), generating a modest topographic low containing basin fill of limited thickness (Yin and Ingersoll, 1997).

The structural controls on basin geometry (Fig. 7C) also influence surface topographic gradients, and thus depositional systems within individual basins and among separate basins. Proximal and distal facies will be preferentially focused along forelimb and backlimb basin margins, respectively. The maximum topographic lows, which are prone to axial fluvial or lacustrine deposition, tend to form near basin centers or forelimbs, away from gently inclined backlimbs. In addition, the contrasting structural arrangements may play a pivotal role in the mode and magnitude of accommodation within different sectors of a broken foreland.

5.3. Accommodation mechanisms

Broken foreland basins are affected by a variety of accommodation mechanisms ranging from local to continental-scale processes. We emphasize five modes of accommodation generation (Table 1), recognizing the likelihood of variations among these factors as a function of plate tectonic setting, geodynamic parameters, structural architecture, and various influences on the supply and transport of sediment.

(1) Flexural subsidence is driven by intraplate crustal thickening and proximal loading by basement blocks bounding broken foreland basins (Hagen et al., 1985; Dickinson et al., 1988; Hall and Chase, 1989; Heller and Liu, 2016; Hindle and Kley, 2021). The amount of accommodation generation scales with the magnitude of topographic loading. Although horizontal shortening may be secondary to vertical motions in broken foreland provinces, the large vertical displacements on individual faults generate considerable structural relief and hence sufficient topographic loads to generate crustal flexure.

(2) Additional flexural subsidence may be the product of loading by a thin-skinned fold-thrust belt bordering the broken foreland province (Kauffman and Caldwell, 1993; DeCelles, 2004; Yonkee and Weil, 2015; Gentry et al., 2018). Such accommodation corresponds with the proximity and size of the thrust-belt load. Foreland structural partitioning may ultimately be accompanied by a reduction in thrust-belt shortening and/or weakening of foreland lithosphere, possibly suggesting a diminished role of thrust-belt induced flexure over time (Gao et al., 2016; Saylor et al., 2020).

(3) Long-wavelength dynamic subsidence across a broken foreland is generally affiliated with mantle flow or coupling between the overriding continental plate and a subducting/underthrusting plate. The mechanical interactions involved in dynamic subsidence are sensitive to the age, composition, density, thickness, and overall geometry (particularly the dip) of the subducting slab (Cross, 1986; Mitrovica et al., 1989; Liu et al., 2014; Li and Aschoff, 2022).

(4) Motion along crustal-scale reverse faults generates structural tilting of compartmentalized, fault-bounded blocks (beams) within a broken foreland, independent of flexural or dynamic processes. Accommodation in proximal forelimb basin settings is amplified by footwall block tilting toward the bounding structure (McQueen and Beaumont, 1989; Jordan, 1995; Fernández-Lozano et al., 2011; Simpson, 2014). In contrast, backlimb settings are likely to experience low-magnitude uplift as the hangingwall block is tilted during translation along a crustal-scale ramp.

(5) Broken foreland basins are well suited to accommodation generation through endorheic (internal drainage) conditions imparted by topographic barriers. Sediment accumulation or “ponding” in such closed basins requires long-term preservation of basin-margin topography, as common in structurally partitioned plateau regions where uplift exceeds erosive stream power (Métivier et al., 1998; Sobel et al., 2003; Horton, 2012; Li et al., 2020).

6. Broken foreland sedimentation

6.1. Sediment accumulation and chronostratigraphic patterns

Sediment accumulation rates within a broken foreland reflect temporal variations in short- and long-wavelength accommodation along with local subsidence or uplift directly related to structural geometry. Variable sediment accumulation histories are recorded in broken foreland systems (Dickinson et al., 1988; DeCelles et al., 1991a, 1991b; Steidtmann and Middleton, 1991; Lillegraven, 2015; Vuke, 2020), as exemplified by successive basins across the Wyoming segment of the Laramide province (Fig. 7A). Fan and Carrapa (2014) report accumulation histories for the Green River, Wind River, and Powder River basins (Fig. 8A) indicative of sustained continuous accumulation during two stages of Laramide deformation in this region at ∼71–58 Ma and ∼ 58–50 Ma (stage 1 and stage 2, respectively). Whereas the Green River and Wind River basins show a pronounced acceleration in sediment accumulation (a roughly 50–100% increase) from stage 1 to stage 2, no significant change is recorded in the relatively thinner Maastrichtian–Eocene succession of the Powder River Basin. This discrepancy for the Powder River Basin may represent (i) limited flexure owing to its more inboard position, farther from the Cordilleran thrust-belt load, and/or (ii) diminished subsidence due to its backlimb structural position, in contrast to rapid flexure and footwall tilting in the forelimb settings of the Green River and Wind River basins (Figs. 7A and 8A). These differences underscore the importance of distinct structural configurations, including the proximity to crustal loads, in determining variations in sediment accumulation.

Many broken foreland basins, including the Laramide and Pampean broken forelands (Fig. 2), are successors to precursor contiguous (unbroken) foreland basins. The inception of a broken foreland is commonly expressed as an increase in local accommodation within more inboard positions (e.g., Reynolds et al., 1990; Ramos and Folguera, 2009). This shift, however, depends on the cumulative effect from multiple accommodation mechanisms (section 5.3). For some localities, a switch from an unbroken to broken foreland may have a limited effect on the pace of sedimentation (e.g., Fan and Carrapa, 2014; Capaldi et al., 2020). A potentially more direct measure of broken foreland conditions may involve spatial changes in sedimentation caused by new accommodation generation in distal foreland locations toward the plate interior.

The Pampean broken foreland recorded late Cenozoic compartmentalization of the predecessor foreland basin and a large inboard advance of accommodation. Several time-space patterns are revealed by available accumulation histories derived from thick Neogene stratigraphic records of the proximal to distal foreland (including the Manantiales, Talacasto, Albarracín, proximal Bermejo (Mogna), and distal Bermejo (Pie de Palo) basin localities; Vergés et al., 2001; Milana et al., 2003; Ciccioli et al., 2014; Levina et al., 2014; Amidon et al., 2016; Collo et al., 2017; Pinto et al., 2018; Capaldi et al., 2020; Mackaman-Lofland et al., 2020). First, the generally Oligocene to early Miocene onset of rapid foreland sedimentation is 5–10 Myr earlier in the most proximal (westernmost) sector (Fig. 8B; curves A and B), consistent with an inboard (eastward) advance of accommodation (Fig. 8B; curves C–F) in an originally unified foreland basin controlled by progressive flexural loading in the Principal Cordillera and Frontal Cordillera of the Andean orogen (Jordan et al., 1996, 2001; Irigoyen et al., 2000; Giambiagi et al., 2001; Levina et al., 2014; Horton and Fuentes, 2016; Buelow et al., 2018; Stevens Goddard and Carrapa, 2018; Capaldi et al., 2020;

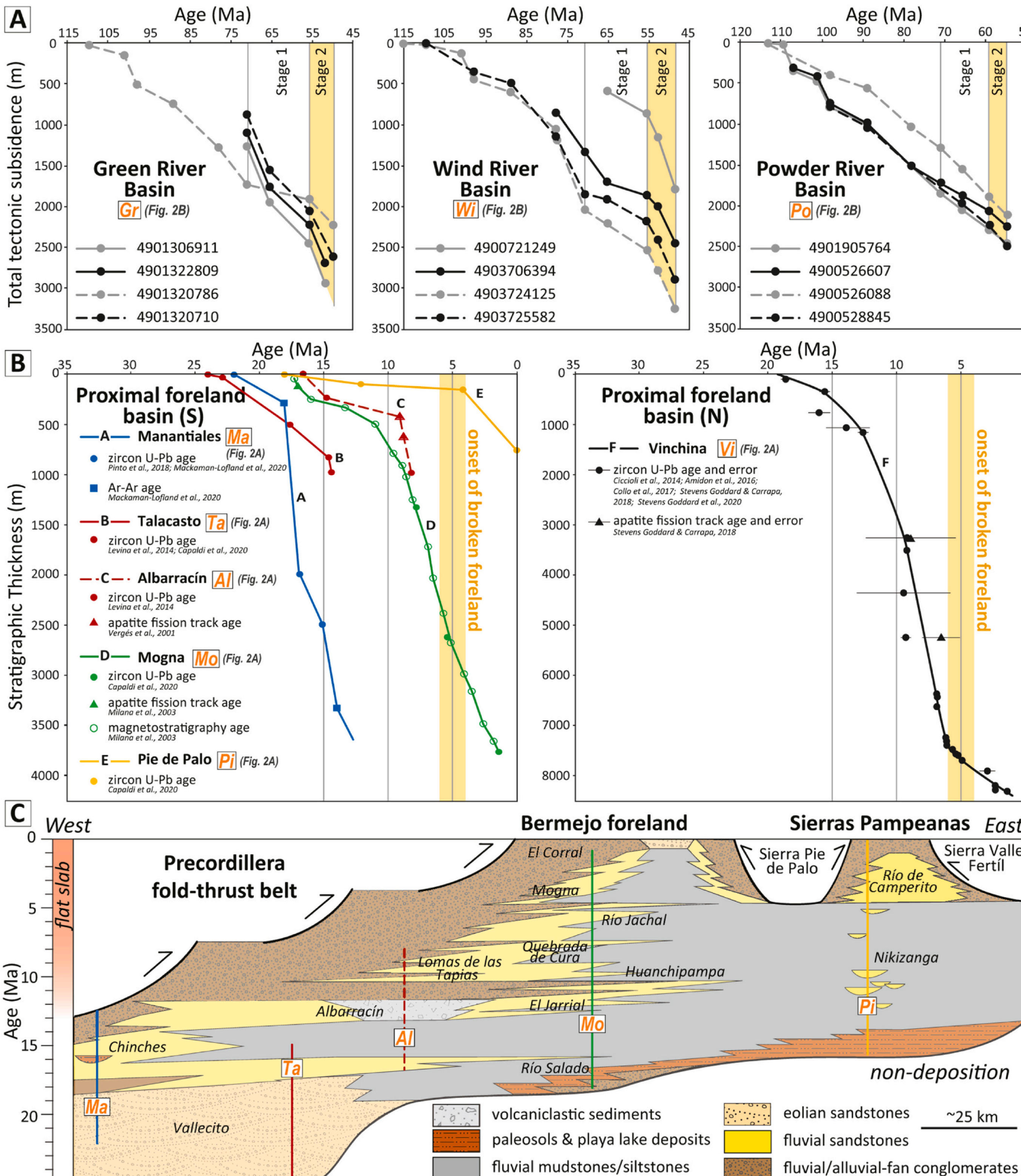

Fig. 8. Sediment accumulation histories for (A) Laramide broken foreland basins in Wyoming (Figs. 2B and 7A; Fan and Carrapa, 2014) and (B) the proximal segments of the Pampean broken foreland, west-central Argentina (Figs. 2A and 6; Capaldi et al., 2020; Mackaman-Lofland et al., 2022). (C) Time-stratigraphic (Wheeler) diagram for the Precordillera fold-thrust belt and Pampean broken foreland (corresponding to Fig. 6B) showing the generalized depositional framework for the Neogene transition from a contiguous to broken foreland basin system (Capaldi et al., 2020).

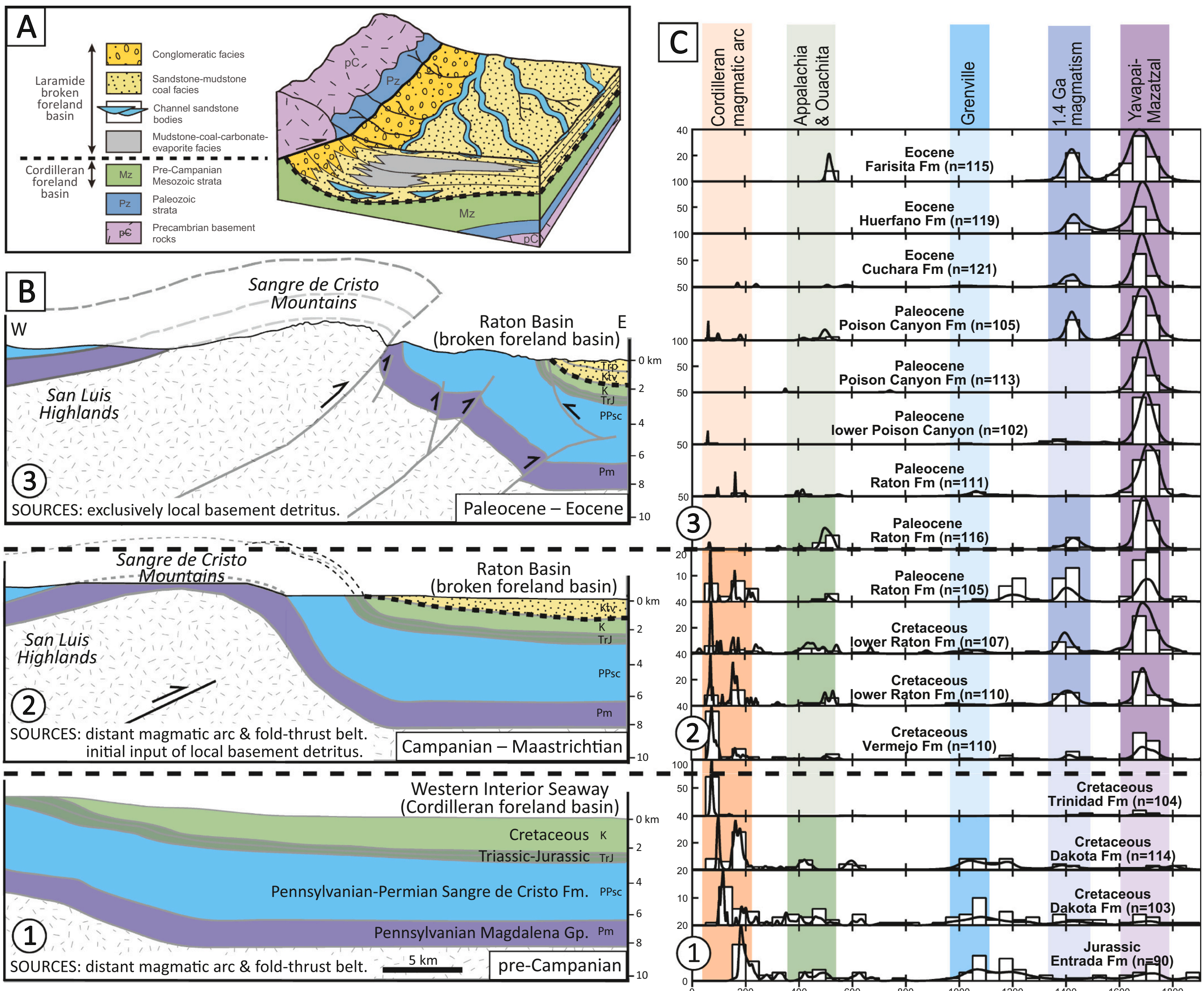

Fig. 9. (A) 3D block diagram showing depositional environments and associated facies for broken foreland basins (after Lawton, 2019). (B) Schematic cross sections showing multiphase evolution (steps 1–3) of a basement-involved intraforeland uplift in the southern Colorado segment of the Laramide broken foreland (northern Sangre de Cristo Range; Bush et al., 2016) and (C) detrital zircon U-Pb age distributions showing corresponding shifts (steps 1–3) from the regional provenance of a contiguous (unbroken) foreland basin to the local provenance of a broken foreland basin (Bush et al., 2016).

Mackaman-Lofland et al., 2020, 2022). The absence of a thick antecedent clastic succession of Eocene age contradicts interpretations of important shortening and flexural subsidence by ~40–35 Ma (e.g., Coughlin et al., 1998; Fosdick et al., 2017; Lossada et al., 2017). Second, the phase of maximum accumulation within each succession occurred progressively later in distal (eastern) localities (Fig. 8B; curves C–E); this time-transgressive pattern is the combined product of advancing deformation within the Precordillera fold-thrust belt and initial intraforeland shortening (Reynolds et al., 1990; Jordan et al., 1993; Fosdick et al., 2015; Ortiz et al., 2021). Third, the onset of rapid accumulation within distal segments of the broken foreland basin appears to broadly coincide (at ~6–4 Ma) with a decrease in accommodation generation in proximal regions (Fig. 8B; curves D and F), possibly attesting to the increased role of intraforeland crustal loading relative to topographic loading within the flanking Precordillera fold-thrust belt (Capaldi et al., 2020; Mackaman-Lofland et al., 2022).

A chronostratigraphic (Wheeler) diagram across the Andean foreland of west-central Argentina (Fig. 8C) shows the time-stratigraphic and sedimentary facies record of a switch from an integrated (unbroken) foreland basin to a structurally partitioned series of subbasins. The W-E profile (Fig. 8C) highlights past transitions between net accumulation and nondeposition or erosion (including the local onset and local termination of sedimentation), with four components identified. (1) Initial flexural foredeep conditions were first recorded in western localities by a chiefly Oligocene–early Miocene inception of sediment accumulation. (2) The eastward advance of flexural foredeep accommodation and corresponding shift from moderate to rapid accumulation (Fig. 8B) coincided with the eastward advance of Miocene deformation into the Precordillera thin-skinned fold-thrust belt. (3) A late Miocene shift from accumulation to erosion in western sectors represents incorporation of the proximal foredeep into the advancing fold-thrust belt. (4) An abrupt stepwise disruption of the once-contiguous foredeep marked the latest Miocene–Pliocene initiation of intraforeland shortening, which compartmentalized zones of deposition from discrete zones of erosion above actively growing basement uplifts. Although this multiphase history has been previously demonstrated from various structural and stratigraphic datasets (Fielding and Jordan, 1988; Jordan, 1995; Ramos et al., 2002; Levina et al., 2014; Capaldi et al., 2020; Mackaman-Lofland et al., 2020), the construction of a chronostratigraphic (Wheeler) diagram (Fig. 8C) helps elucidate the accommodation shifts and missing parts of the stratigraphic record that pinpoint the shift to a broken foreland situation.

6.2. Sediment routing, provenance, and drainage reorganization

Broken foreland basins record major changes in sediment provenance, sediment dispersal, and drainage configurations. Whereas contiguous foreland basins may have subsurface structural highs that affect spatial patterns in accommodation, these non-emergent (blind) features do not alter sediment routing patterns. In contrast, broken foreland systems are the product of structural partitioning by emergent basement structures that induce not only shifts in accommodation patterns, but also form barriers to sediment dispersal (Fig. 6A).

Depositional systems and facies distributions in nonmarine broken foreland settings (Fig. 9A) are principally guided by major structures that dictate topographic slopes, zones of erosion, and zones of sediment accumulation (e.g., Flores and Ethridge, 1985; Beck et al., 1988; DeCelles et al., 1991a; Flemings and Nelson, 1991; Steidtmann and Middleton, 1991; Lawton, 2019). This structural influence generally leads to lacustrine or axial fluvial systems parallel to bounding faults and folds, with alluvial fan and fan-delta systems restricted to basin margins along the flanks of topographic highs.

The emergence of structural highs further modifies landscape evolution during progressive exhumation of weak sedimentary cover rocks into stronger (less erodible) crystalline basement lithologies, which can lead to decelerated erosion, diminished sediment flux, and enhanced relief (Flowers and Ehlers, 2018; Bernard et al., 2019). An associated shift in sediment delivery to the flanking basin can be manifest as changes in grain size and depositional facies (DeCelles et al., 1991b; Carroll et al., 2006).

The growth of structurally controlled topographic barriers revises surface slopes, basin hydrography, and may lead to complete drainage isolation as internally drained (closed) basins. Even without complete drainage isolation, cases of drainage reorganization will affect the hydrologic linkages between adjacent basins, with alternating cutoff and reestablishment of drainage connectivity (e.g., Dickinson et al., 1988; Métivier et al., 1998; Davis et al., 2008; Smith et al., 2014; Saylor et al., 2017; Lawton, 2019).

In addition to sediment routing, a fundamental shift accompanies the creation of small drainage networks on newly developed topographic features above basement-cored uplifts. This trend is well defined by geomorphic and provenance studies of active broken forelands (Damanti, 1993; Capaldi et al., 2017; Garzanti et al., 2021, 2022). Expected provenance signatures of foreland compartmentalization would entail a temporal shift from regional-scale drainage networks spanning large segments of the fold-thrust belt to localized drainages limited to restricted ranges within the broken foreland. Such an example is reported for the stepwise growth of a basement uplift along the deformation front of the Laramide province, where the Sangre de Cristo Range was uplifted during motion on a range-bounding contractional fault system (Fig. 9B; Lindsey, 1998; Bush et al., 2016).

Detrital zircon U-Pb age distributions for Upper Cretaceous–Eocene basin fill in the Raton basin of southern Colorado and northern New Mexico (Fig. 9C) show the erosional exhumation of the Sangre de Cristo Range (Bush et al., 2016). Pre-deformational age distributions show exclusive derivation from the Cordilleran fold-thrust belt (as denoted by 200–1300 Ma ages) and magmatic arc (<200 Ma ages). During early Laramide deformation, the detrital signatures show initial unroofing of Precambrian basement rocks of the Rocky Mountain province with a combination of far-traveled thrust-belt (<1300 Ma) and locally sourced basement (>1300 Ma) detritus. During advanced Laramide deformation, the detrital signatures show elimination of Cordilleran magmatic arc detritus (<200 Ma) and exclusive derivation from local basement (>1300 Ma). These upsection provenance trends (Fig. 9C) constrain the sequential structural evolution (Fig. 9B) by showing the unambiguous evolution from (i) regional drainage systems that encompassed the Cordilleran orogenic system to (ii) small local drainages with short transport distances from a single basement uplift (Sangre de Cristo Range) within the Laramide broken foreland province (Cather, 2004; Bush et al., 2016). Other parts of the Laramide province show a comparable shift from regional to local sourcing, with recognition of the potential complications involved in recycling of older foreland basin fill (e.g., Fan et al., 2011; May et al., 2013; Pecha et al., 2018; Lawton, 2019).

7. Driving mechanisms of foreland partitioning

We propose two sets of requirements for the development of broken foreland basins: first, favorable *conditions* inherited from the preceding geologic history and, second, specific *catalysts* during orogenesis that trigger heterogeneous intraforeland shortening. We propose that basin genesis can be linked to: (i) tectonic inheritance in the form of preexisting structural, stratigraphic, rheological, and thermal configurations; and (ii) mechanical triggers that may include elevated stress, enhanced stress transmission, fluid influx, or irregular strengthening and weakening within the intraplate regions that host broken foreland basins.

7.1. Conditions

In considering the necessary components for the generation of broken foreland basins, we offer perspectives on some underlying *conditions* that may promote intraforeland partitioning. Recognizing that most broken foreland regions have a rich geologic heritage, we utilize the concept of tectonic inheritance to explore the role of precursor structural, stratigraphic, rheological, and thermal parameters in guiding basement-involved deformation (Fig. 10). We regard these four elements within a broad framework of potentially overlapping variables that may influence deformation, individually or collectively, but are not uniquely sufficient to induce a broken foreland configuration.

7.1.1. Structural inheritance

Structural reactivation of preexisting faults, fabrics, and sutures (Fig. 10A) is a common theme in intraplate settings. The Pampean foreland recorded reactivation of pre-Andean structures consisting of Cretaceous normal faults, Paleozoic faults, and Precambrian faults, sutures, and metamorphic fabrics (e.g., Schmidt et al., 1995; Martino et al., 2016; Zapata et al., 2020; Ortiz et al., 2021; Wimpenny, 2022). Reactivated structures in the Laramide province include Precambrian sutures, faults, and igneous and metamorphic fabrics, as well as late Paleozoic basement-involved faults related to development of the Ancestral Rocky Mountains (e.g., Brown, 1988; Bryant and Nichols, 1988; Nelson, 1993; Marshak et al., 2000; Stone, 2002; Neely and Erslev, 2009; Chapin et al., 2014; Worthington et al., 2016; Bader, 2018). Although selective fault reactivation and basin inversion are also common in thin-skinned fold-thrust belts that mainly affect cover strata (e.g., Cristallini and Ramos, 2000; Giambiagi et al., 2008; Macellari and Hermoza, 2009; Parra et al., 2012; McGroder et al., 2015; Fuentes et al., 2016; Perez et al., 2016; Hafiz et al., 2019; Mackaman-Lofland et al., 2019; Horton et al., 2020; Mora et al., 2020), the emphasis here is on antecedent structures that affected deeper levels of crystalline basement within the plate interior.

7.1.2. Stratigraphic inheritance

Basement deformation may be fostered in intraplate regions by the absence of the thick stratigraphic prisms that host thin-skinned ramp-flat structural systems (Fig. 10B). The pre-orogenic stratigraphic cover within continental plate interiors tends to be markedly thinner and more laterally uniform than correlative plate-margin successions in thin-skinned fold-thrust belts. In Argentina, basement structures are preferentially developed in eastern foreland regions that lack the thick

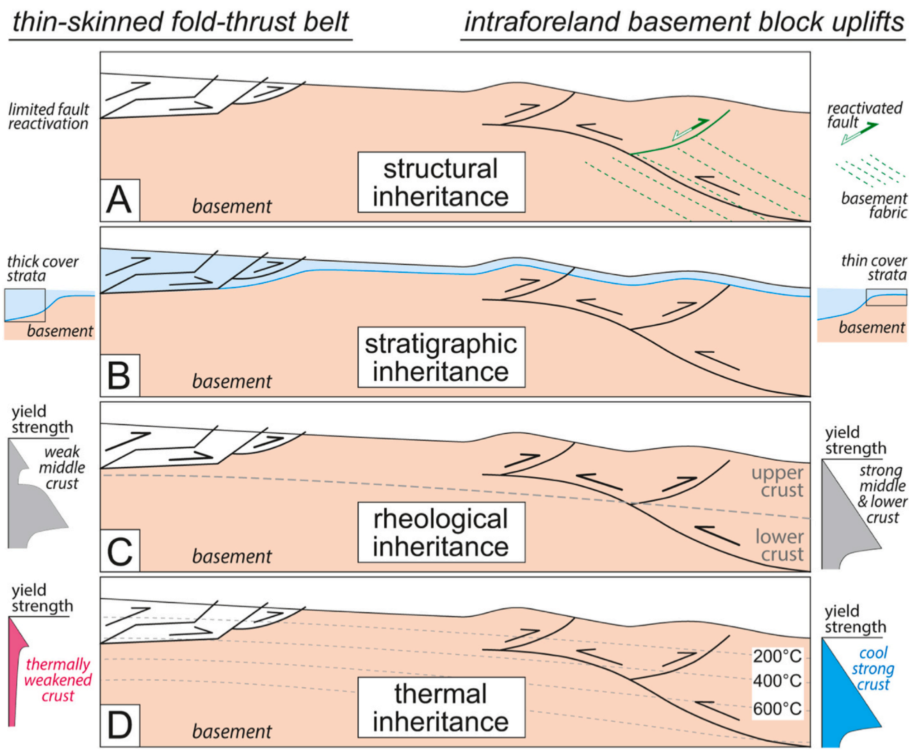

Fig. 10. Concept of tectonic inheritance in promoting intraplate deformation and development of broken foreland basins. (A) Structural inheritance, with reactivation of preexisting faults or fabrics (right). (B) Stratigraphic inheritance, with the geometry and thickness of precursor stratigraphic package guiding thin-skinned shortening (left) versus intraforeland basement deformation (right). (C) Rheological inheritance, with a strong crustal/lithospheric profile (right) facilitating deeply rooted deformation. (D) Thermal inheritance, with schematic strength profiles for continental crust showing a thermally weakened profile (left) relative to a strong profile favoring intraforeland basement deformation (right). After Lacombe and Bellahsen, 2016; Horton and Folguera, 2022.

Paleozoic stratigraphic package of the flanking thin-skinned fold-thrust belt within the Andes (Allmendinger et al., 1983; Kley et al., 1999; McQuarrie, 2002; Jacques, 2003; Pearson et al., 2013). In the Laramide foreland, the uniformly thin (<1–2 km) pre-deformational (pre-Campanian) stratigraphic cover likely helps explain the lack of a preferred vergence direction within basement structures (Erslev, 1993; Yonkee and Weil, 2015; Parker and Pearson, 2021).

7.1.3. Rheological inheritance

The rheological framework, in the form of spatially variable strength parameters, helps dictate areas of strain localization along mechanical anisotropies and heterogeneities within broken foreland regions (Fig. 10C). Strong intraplate regions that show progressively higher yield strength with depth in continental crust and mantle lithosphere are prone to decoupling at relatively deeper levels (Barrionuevo et al., 2021; Ibarra et al., 2021). This scenario contrasts with plate-margin regions characterized by mid-crustal weaknesses that facilitate decoupling between the upper and lower crust (Giambiagi et al., 2015, 2022; Lacombe and Bellahsen, 2016; Wolf et al., 2021). Foreland crust and mantle lithosphere with high integrated strength will favor solitary crustal-scale ramps rather than multiple shallow décollements in upper crust. This pattern is not unique, however, as rheology is also strongly dependent on the age, thickness, composition, temperature, and fluid conditions within the crust and lithosphere (Mouthereau et al., 2013; Pfiffner, 2017; Martinod et al., 2020). Rheological contrasts may account for an observed delay in strain localization in which the locus of shortening ultimately shifts from a principal décollement along the basement-cover interface within the fold-thrust belt to deeper basement levels in the foreland (e.g., Lacombe and Mouthereau, 2002; Madritsch et al., 2008; Lacombe and Bellahsen, 2016; Tavani et al., 2021).

7.1.4. Thermal inheritance

The initial thermal structure can affect strain patterns in convergent orogens, including not only near-trench or magmatic arc localities, but also more-distal inboard regions (Fig. 10D). The inherited thermal configuration is largely governed by earlier magmatism, sedimentary burial, and crustal/lithospheric thinning or thickening. Pre-orogenic heating of continental crust results in thermal weakening that affects the strength profile and may promote or impede basement involvement during orogenesis (Lacombe and Bellahsen, 2016). A thermally weakened retroarc region may experience enhanced dislocation creep in the lower crust and an increased potential to decouple lower from upper crustal deformation, possibly limiting inboard stress transmission to the distal foreland. In contrast, a cool foreland lithosphere with a lower geothermal gradient, possibly aided by the presence of a strong lithospheric mantle keel, may lead to distributed shortening, with potential localization along preexisting faults and basement weaknesses. These conditions may result in relatively distributed shortening with deeply rooted structures equally involving upper and lower crustal levels (e.g., Yonkee and Weil, 2015; Giambiagi et al., 2022). Along-strike and across-strike variations in both pre- and synorogenic thermal processes help shape orogenic topography and may lead to temporal changes in structural style (e.g., Isacks, 1988; Whitman et al., 1996; Beaumont et al., 2006; Wolf et al., 2021).

7.2. Catalysts

The aforementioned *conditions*—including inherited structural, stratigraphic, rheological, and thermal parameters (section 7.1)—are conducive but likely insufficient to exclusively prompt broken foreland development. In addition to tectonic inheritance, we suggest that a separate *catalyst* or trigger may be required to structurally and topographically partition a foreland region into a series of broken foreland basins. Below we outline four potential *catalysts* that are categorized according to stress, thermal, fluid, and strength-related processes (Fig. 11). Given the interdependence of these variables in subduction zone settings (e.g., Hyndman et al., 2005; Currie and Hyndman, 2006; Van Keken et al., 2011), we recognize that these triggers may operate independently or collectively.

7.2.1. Stress trigger

The initiation of a broken foreland may be triggered by a shift to elevated stress conditions within intraplate regions (Fig. 11A), a hypothesis supported by modern and ancient estimates of differential

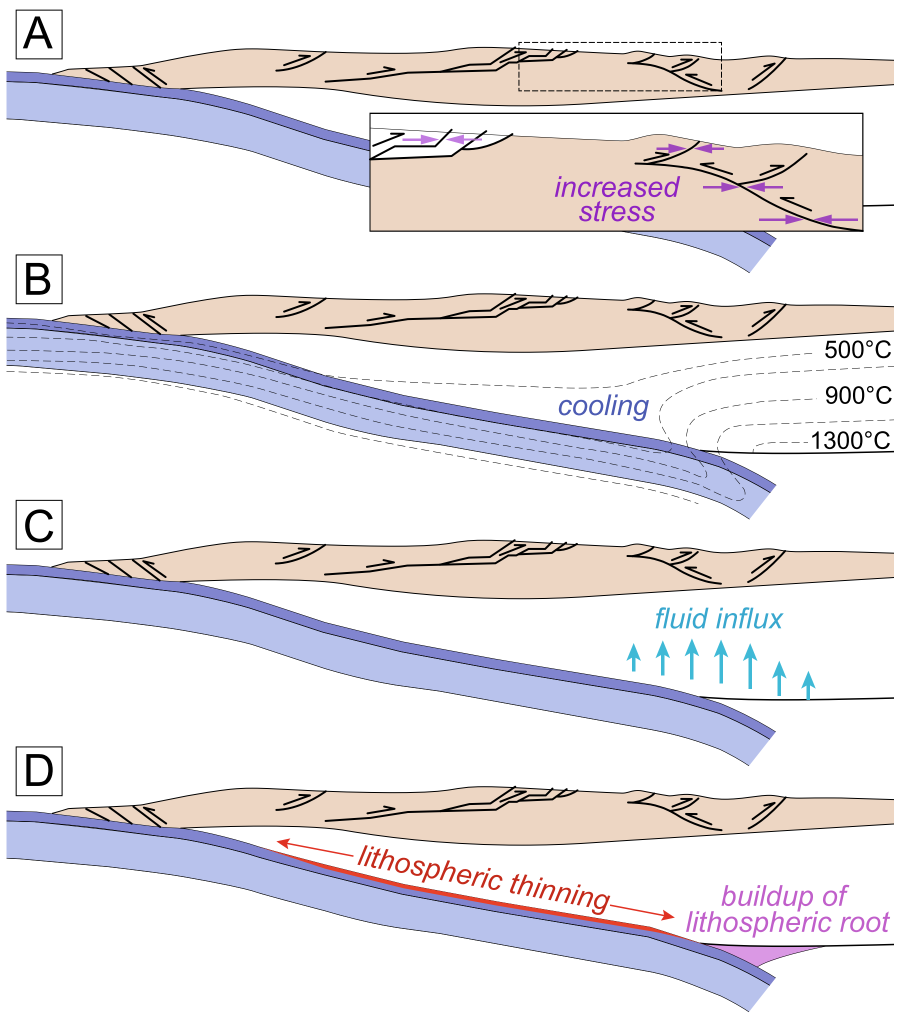

Fig. 11. Concept of mechanical triggers in which shifts in key parameters help catalyze intraplate basement deformation and attendant development of broken foreland basins. (A) Increased stress, which enhances long-distance stress transmission. (B) Decreased temperature (and resulting increase in strength), which fosters inboard stress transmission. (C) Enhanced fluid flux (and resulting decrease in strength), which localizes strain (failure) in intraplate regions. (D) Decrease or increase in strength, potentially involving spatially variable thinning (weakening) and thickening (strengthening) of continental lithosphere. After James and Sacks, 1999; Humphreys, 2009; Behr and Smith, 2016; Axen et al., 2018; Beaudoin et al., 2020; Lacombe et al., 2021.

stresses within continental plate interiors (e.g., Raimondo et al., 2014; Beaudoin et al., 2020; Stephenson et al., 2020; Lacombe et al., 2021). The precise mechanisms may be attributable to in-plane stresses during increased end loading along distant plate boundaries (e.g., Ziegler et al., 1995, 2002; Cunningham, 2005; Kley and Voigt, 2008; Silva et al., 2018). Alternatively, heightened intraplate shear stresses may be the product of enhanced coupling due to a diminished thickness of trench-fill sediments (Lamb and Davis, 2003; Hu et al., 2021) or greater basal traction due to regional coupling with a shallowly subducting/underthrusting plate with resulting local mantle flow (Bird, 1984, 1998; Jones et al., 2011). Further, temporal changes in fluid pressure (Amrouch et al., 2010; Beaudoin et al., 2014; Lacombe et al., 2021) and the thickness of sedimentary cover strata (Jones et al., 2011; Ballato et al., 2019) may lead to variable stress conditions that promote or suppress brittle failure during progressive shortening.

7.2.2. Thermal trigger

The activation of basement-involved deformation may be related to long-distance transmission of plate-margin stresses toward the plate interior, as triggered by regional crustal/lithospheric cooling and the attendant increase in continental strength (Fig. 11B). Flat slab subduction generates major thermal effects that are not limited to abrupt refrigeration of the forearc, but also lead to cooling and hence lithospheric strengthening above the flat slab (Henry and Pollack, 1988; Gutscher et al., 2000; Manea and Manea, 2011; Behr and Smith, 2016). The time scales involved with the thermal perturbations induced by flat slab subduction are dependent on various factors, including the thickness, composition, thermal conductivity, and conductive versus convective modes of heat transfer within the asthenospheric wedge and overriding plate (e.g., Liu and Currie, 2016; Axen et al., 2018; Liu et al., 2021). Modifications to the thermal profile of the foreland crust and lithosphere may have prompted inboard stress transmission for several hundreds of kilometers in both the Laramide and Pampean broken foreland provinces (Dumitru et al., 1991; Gutscher, 2002; Collo et al., 2017; Christiansen et al., 2022; Rodriguez Piceda et al., 2022).

7.2.3. Fluid trigger

Intraforeland basement deformation may be triggered by enhanced fluid flux and associated strain localization (Fig. 11C). In the case of flat slab subduction, an influx of slab-derived hydrous fluids (slab dewatering) has been interpreted to induce hydration of the overriding lithosphere (Wagner et al., 2005; Behr and Smith, 2016) and selectively weaken segments of the Laramide broken foreland (Saylor et al., 2020). Such fluid-induced weakening may be maximized above the leading hinge of the subducted slab, at the inboard transition from the flat slab segment to the steep deeper segment (James and Sacks, 1999; Humphreys et al., 2003; Humphreys, 2009; Currie and Beaumont, 2011; Thacker et al., 2022). This spatial focusing may lead to an advancing front of fluid-induced weakening that would facilitate progressive strain localization through the diachronous activation or reactivation of structures toward the plate interior.

7.2.4. Strength-related trigger

Several processes capable of catalyzing an increase or decrease in plate strength may trigger the onset of broken foreland conditions (Fig. 11D). Of many possibilities, four options are listed here. First, zones of lithospheric thinning within the foreland may be weakened sufficiently to promote basement deformation (e.g., Ziegler et al., 1995). Second, shifts between felsic and mafic compositions, possibly related to the buildup and removal of dense lithospheric roots, may variably cause weakening or strengthening that would influence intraplate shortening; such processes are more likely to affect magmatic arc and hinterland regions (Babeyko et al., 2006; Wang and Currie, 2017; Comeau et al., 2021). Third, the breakoff of a subducting/underthrusting slab or development of a slab window during oceanic ridge subduction may foster weakening capable of focusing intraplate deformation (Buiter et al., 2002; Bradley et al., 2003). Fourth, mechanical or strain weakening from alteration and grain size reduction during fault slip, reactivation of basement weaknesses, and/or progressive linkage of fault segments may further reduce overall strength and help trigger foreland deformation (Beaumont et al., 2006; Liu et al., 2021).

8. Discussion: Drivers, caveats, and opportunities

8.1. Role of flat slab subduction

The process of flat slab subduction satisfies many of the proposed *conditions* and *catalysts* (sections 7.1 and 7.2; Figs. 10 and 11) that bring about the development of broken foreland basins. This profound connection reinforces decades of investigations on the structure, stratigraphic framework, and geodynamic setting of modern and ancient systems (e.g., Dickinson and Snyder, 1978; Coney and Reynolds, 1977; Dickinson et al., 1988; Jordan, 1995; Constenius, 1996; Bird, 1998; Ramos et al., 2002; Ramos, 2009; Finzel et al., 2011; Yonkee and Weil, 2015; Bishop et al., 2017; Horton et al., 2022). Flat slab subduction is a fundamental tectonic process with implications for sedimentary basin evolution, continental deformation, arc magmatism, crustal evolution, and craton growth and destruction (e.g., Smithies et al., 2003; Li and Li, 2007; Humphreys, 2009; Kusky et al., 2014; Wu et al., 2019; Capaldi et al., 2021; Gianni and Pérez Luján, 2021). Past phases of flat slab subduction are likely common, and may be somewhat aliased in the geologic record by a restricted duration, limited strike length, surface erosion, subduction erosion, or igneous/structural overprinting (e.g., Sandeman et al., 1995; Kay et al., 2005; Kay and Coira, 2009; Ramos and Folguera, 2009; Folguera and Ramos, 2011; Wagner et al., 2017; Perez and Levine, 2020; Runyon et al., 2022).

Nevertheless, we caution against interpretations in which the genesis of broken foreland basins is entirely attributed to flat slab subduction. Specifically, we disagree with the suggestion that the occurrence of intraplate shortening necessitates a phase of flat slab subduction, without consideration of other potential processes. Such overemphasis on flat slab subduction likely stems from simplicity, in that continental deformation hundreds or thousands of kilometers from plate boundaries can be difficult to explain from a conventional view of plate tectonics with rigid plate interiors (Dewey and Bird, 1970). Importantly, a range of additional explanations for intraplate deformation have been identified, including increased compressional stresses along plate margins, more-effective horizontal transmission of such stresses, and forces originating within plate interiors (Burov and Cloetingh, 2009; Raimondo et al., 2014; Stephenson et al., 2020; Lacombe et al., 2021). Therefore, a geologic record of intraplate deformation or a broken foreland does not, *a priori*, require a contemporaneous flat slab subduction history.

With these caveats, we recommend further scrutiny when assessing the variety of processes that accompany flat slab subduction—namely the broad range of *conditions* and *catalysts* (section 7). We highlight four underlying *conditions* associated with preexisting elements—referred to as (1) structural inheritance, (2) stratigraphic inheritance, (3) rheological inheritance, and (4) thermal inheritance (Fig. 10) (Lacombe and Bellahsen, 2016; Horton and Folguera, 2022). We also discuss several *catalysts* or mechanical triggers: (1) increased stress, (2) long-distance stress transmission within a cooled plate, (3) enhanced fluid flux localizing failure within a plate interior, and (4) changes in strength related to plate thickness, composition, or mechanical (strain) weakening (Fig. 11).

8.2. Broken foreland systems in the geologic record

The modern Andean foreland provides a proof of concept for a simple classification scheme based on two key tectonomorphic elements—the *Andean topographic front* and the *foreland deformation front* (Fig. 4). Unbroken foreland regions are defined where these two tectonomorphic elements are co-located, and broken foreland provinces are defined where they diverge (Fig. 5). Thus, the boundaries of the structurally partitioned, or broken, provinces within the Andean foreland are demarcated through the delineation of the Andean topographic front and the foreland deformation front. Andean broken foreland regions are up to 400 km wide and reach up to 800 km inboard of the subduction trench (Figs. 2–5).

This rationale provides a sound foundation for defining ancient broken foreland basins in the geologic record, provided the positions of the thrust-belt topographic front and foreland deformation front can be determined through growth structures, depositional systems, and exhumational histories from thermochronological or sediment provenance studies. In practice, most cases offer a clear separation between upper-crustal thrust-belt structures and intraforeland basement structures; although both systems involve crystalline basement, the former embody an integrated family of ramp-flat structures, whereas the latter constitute widely spaced crustal-scale structures. For example, the Laramide broken foreland is well defined as the zone between the Cordilleran thrust front and the Laramide deformation front, a region up to ~600 km wide that reached up to 1000–1500 km inboard of the former subduction trench (Figs. 2B and 3B).

Although numerous criteria are employed in basin classification (Table 1), we recognize several areas of potential complexity in the discrimination of broken foreland basins from other basin types. The first issue concerns non-compressional stress regimes. The distal zones of some foreland basins may be disrupted by non-contractional structures, including extensional faults generally related to plate bending in the distal foredeep or forebulge (e.g., Gustason, 1989; Bradley and Kidd, 1991; Delgado et al., 2012; Tavani et al., 2015; Enriquez St. Pierre and Johnson, 2022). Such faults are commonly limited to the subsurface and therefore do not generate the topographic compartmentalization required for designation as a broken foreland basin. Potential exceptions include large-magnitude normal or strike-slip faults that generate positive surface topography in the distal foreland during contemporaneous foredeep sedimentation (e.g., Krzywiec, 2001; Cunningham, 2005; Gianni et al., 2015; Sun and Dong, 2020).

Two additional complexities are discussed below. First, complications in basin categorization may be introduced by a potential structural connection between the thin-skinned fold-thrust belt and intraforeland uplifts (section 8.3). Second, the burial of actively growing intraforeland arches by high-volume sedimentation may preclude the surface structural expression necessary for foreland partitioning (section 8.4).

8.3. Identification of structural style

Most broken foreland basins are affiliated with widely spaced intraforeland structures that are deeply rooted in crystalline basement (Figs. 2 and 3). In most cases, each basement uplift is tied to a single master fault defined by a deeply penetrating fault ramp, rather than an array of interconnected ramp-flat structures that form an organized fold-thrust belt and orogenic wedge (Fig. 7). However, potential ambiguity may arise in situations where basement-involved structures of the foreland are geometrically and kinematically linked to the thin-skinned fold-thrust belt. Possible ancient candidates from North America include basement arches that overlap spatially with the frontal structures of the thin-skinned thrust system: for example, (i) the Uinta, Gros Ventre, and subsurface Moxa arches near the Idaho-Wyoming thrust front (Royse et al., 1975; Dorr et al., 1977; Kraig et al., 1987; Bradley and Bruhn, 1988; Bryant and Nichols, 1988; Yonkee and Weil, 2011) and (ii) overlapping Laramide basement and Cordilleran thrust belt structures in southwestern Montana (Ruppel and Lopez, 1984; Schmidt et al., 1988). Ancient broken foreland basins in South America are best expressed in the structural record of basement uplifts in northern Patagonia, which may be connected in the subsurface to structures in the Andean fold-thrust belt (e.g., Orts et al., 2012; Gianni et al., 2015; Echaurren et al., 2016; Folguera et al., 2018; Horton, 2018a; Butler et al., 2020). Past broken foreland settings have also been proposed for selected parts of the eastern Andes on the basis of anomalous Paleogene stratigraphic and provenance trends, but with limited evidence for coeval contractional structures of large magnitude (e.g., Bayona et al., 2013, 2020; del Papa et al., 2013; Montero-López et al., 2018).

For modern examples in South America, the proximity of the thin-skinned Andean thrust front to opposing basement structures suggests either overlap of two contrasting structural styles, or complex geometric linkages within a hybrid structural style (Figs. 2, 3, and 6). Examples from flat slab provinces (Figs. 4 and 5) include interactions among the eastern front of the Precordillera fold-thrust belt and westernmost Sierras Pampeanas in Argentina (von Gosen, 1992; Smalley et al., 1993; Zapata and Allmendinger, 1996b; Zapata, 1998; Meigs et al., 2006; Vergés et al., 2007; Venerdini et al., 2020) and the Subandean thrust front and intraforeland uplifts of Peru (Macellari and Hermoza, 2009; Espurt et al., 2008; Gautheron et al., 2013; Baby et al., 2018; McClay et al., 2018). Comparable late Cenozoic occurrences are observed in continental collisional systems, including the Shillong Plateau of the Himalayan foreland (e.g., Yin et al., 2010; Coutand et al., 2016) and the Mazatagh high (Bachu Uplift) of the Tarim Basin (Wang et al., 2014; Suppe et al., 2019; Li et al., 2020; Chen et al., 2022). These cases raise the possibility of local uncertainty in broken versus unbroken foreland basin designations.

We suggest that most potential ambiguity arises from structural assessments at different scales. For example, a collection of variably oriented basement structures with opposing vergence directions in a single broken foreland may ultimately root into a single deep shear zone (or décollement) in the lower crust or uppermost mantle (Oldow et al., 1989; Erslev, 1993; Meyer et al., 1998; Tapponnier et al., 1990). Although ostensibly similar to imbricate fan and backthrust (or triangle zone) geometries within a thin-skinned thrust belt, these deeply rooted structural systems within most broken forelands are decoupled at much deeper levels (>20–30 km depths), with larger spacing between successive structures (>20–100 km), and greater diversity in structural orientation and tectonic transport. These foreland provinces are distinguished by isolated structural highs and lack the regional topographic continuity and foreland-sloping upper surface expressed in the thin-skinned fold-thrust belts of most orogenic wedges (e.g., Yonkee and Weil, 2011, 2015; Horton et al., 2022).

8.4. Influence of sediment accumulation

The contrast between broken and unbroken conditions directly relates to the topographic expression of basement-involved structures (Fig. 1). Positive foreland topography is a key component in the definition of a broken foreland basin, given that all basin regions have some degree of small-scale faulting, folding, and fracturing. The definition of a broken foreland, therefore, excludes deformed foreland regions with low-magnitude deformation incapable of generating positive topography at the Earth's surface.

However, we acknowledge the possibility of special cases in which the delivery of extremely large volumes of sediment consistently buries active intraforeland structures of considerable magnitude. These systems would display intraforeland basement highs, but they would be recorded as zones of diminished accommodation rather than net uplift. Subsurface examples from retroarc and peripheral foreland settings show that multiple intraforeland structures represent reactivated features that were intermittently active over long periods (>50 Myr), but at sufficiently low rates that they principally remained zones of net sediment accumulation rather than uplift or erosion; specific cases include the Zagros foreland basin (Sherkati and Letouzey, 2004; Lalami et al., 2020), the Sacha-Shushufindi and Capiron–Tiputini systems in the northern Andean Oriente foreland of Ecuador (Balkwill et al., 1995; Baby et al., 2013) and the Izozog Arch in the central Andean Chaco foreland of Bolivia (Uba et al., 2006; Stewart et al., 2018).

Alternatively, late syndeformational to post-deformational sedimentation may lead to burial of relict topographic highs generated by formerly active faults; examples include the establishment of late-stage connections among Laramide basins (Lillegraven and Ostresh, 1988; Montagne, 1991; Smith et al., 2014; Lawton, 2019) and the unification of the Midland and Delaware basins within the late Paleozoic Ancestral Rocky Mountain foreland (Ewing, 2019; Fairhurst et al., 2021). Moreover, entirely post-orogenic sedimentation may generate successor basins that fill in preexisting topography at a regional scale (e.g., Dickinson et al., 1988; Graham et al., 1993; Hendrix, 2000; Carroll et al., 2010), thus reducing relief and expanding the cumulative area of a basin system.

We maintain that topographic or bathymetric disruption (in nonmarine or marine systems, respectively) is an essential component of broken foreland basins, as it affects many surface processes related to the generation, transport, and deposition of sediment. In practice, once intraforeland uplifts have structurally partitioned a foreland region and generated positive topographic or bathymetric relief, it would be most logical to adopt the broken foreland terminology. Otherwise, in extreme cases, modest changes in the ratio of sediment accumulation to vertical uplift could induce abrupt temporal fluctuations in topographic expression that could be construed as rapid alternations between broken and unbroken conditions.

8.5. Paleodrainage and basin connectivity

A broken foreland network of anastomosing ranges with broad intervening basins (Figs. 2 and 6) leads to complex evolution of fluvial drainage networks (watersheds), with phases of isolation and connectivity among adjacent basins. This leads to pronounced inter-basinal complexity and variability in the reconstruction of depositional systems. These variations led Dickinson et al. (1988) to classify three modes of Laramide broken foreland basins, consisting of ponded basins and axial basins within the interior of the Laramide province, and perimeter basins formed around its periphery. The dynamic interactions among these basins, including multiple phases of isolation and intermittent linkage with adjacent basins, are not only the product of variations in surface uplift and the establishment of topographic barriers, but also the processes of erosion and sediment accumulation, which could overtop topographic sills between adjacent basins. In addition, climate variations reflected in changes in temperature, rainfall, and sediment transport efficiency further influence basin deposystems and interbasin connectivity.

Given the elaborate drainage configurations and sediment routing possibilities, broken foreland basins are well suited for reconstruction of past sediment transport pathways. Recent studies demonstrate the power of provenance techniques such as detrital zircon U-Pb geochronology to define major shifts in paleodrainage (e.g., Fan et al., 2011; May et al., 2013; Perez and Horton, 2014; Bush et al., 2016; Gao et al., 2020; Stevens Goddard et al., 2020; Smith et al., 2020; Capaldi et al., 2020; Mackaman-

Lofland et al., 2022). Several trends emerge from such studies. First, broken foreland basins may be fed by large integrated erosional drainage systems spanning diverse sediment source regions within orogenic wedges, which include chiefly sedimentary rocks within thin-skinned fold-thrust belts and igneous and metamorphic rocks from elevated hinterland provinces, accreted terranes, and continental-margin magmatic arcs (e.g., Fuentes et al., 2011; Saylor et al., 2011; Laskowski et al., 2013; Garber et al., 2020; Rosenblume et al., 2021). Second, broken foreland provinces may be dominated by far-traveled sediment from transcontinental drainages with headwaters in cratonic or orogenic systems far removed from the geologic elements responsible for basin formation (e.g., late Paleozoic supply of Appalachian-Ouachita detritus to the Ancestral Rocky Mountains: Thomas et al., 2017; Gao et al., 2020; Leary et al., 2020; Lawton et al., 2021). Third, sediment delivery to broken foreland basins may be limited to isolated foreland block uplifts with local drainage systems confined to crystalline basement rock units (e.g., local derivation of basement detritus within Pampean and Laramide basins (Fig. 9); Bush et al., 2016; Capaldi et al., 2017; Stevens Goddard et al., 2020; Smith et al., 2020; Garzanti et al., 2022).

The sedimentary records of broken foreland basins offer valuable insights into the dynamic evolution of drainages and drainage divides, including drainage reversal and drainage reorganization at regional and continental scale. Modern and ancient broken foreland basins offer opportunities to employ field data to test a range of geomorphic models related to competition among drainage networks (Bonnet, 2009; Willett et al., 2014; Whipple et al., 2017; Viaplana-Muzas et al., 2018; Struble et al., 2021). Such intraplate basins are also instrumental in evaluating suggestions of large-scale drainage reversal in the genesis of the Amazon River (Shephard et al., 2010; Sacek, 2014), Laramide transcontinental sediment routing to the Gulf of Mexico basin (Mackey et al., 2012; Snedden and Galloway, 2019), and the use of river drainage analysis to detect continental-scale tectonic uplift histories (e.g., Rodríguez Tribaldos et al., 2017; Fernandes et al., 2019).

8.6. Climate and erosion

Broken foreland basins (Fig. 1) are particularly sensitive to variations in climate and erosion, with implications for sediment routing and erosional and depositional mass budgets. Individual basement-cored ranges are not only capable of forming barriers to surface transport of water and sediment, but also may substantially alter regional orographic effects and thus impact climate. The orographic barriers may lead to aridification, drainage closure, and diminished stream power, such that continued rock uplift further perpetuates long-lived topographic barriers (e.g., Métivier et al., 1998; Sobel et al., 2003; Coutand et al., 2006; Carroll et al., 2010). However, climate has become widely appreciated as a major control on topography, relief generation, and tectonic uplift in many orogenic systems, including broken foreland basins (e.g., McMillan et al., 2006; Heller et al., 2011; Hilley and Coutand, 2010; Strecker et al., 2012; Ghiglione et al., 2019). Despite many modern and ancient examples, discrimination of the interactions and potential cause-effect relationships among climate, erosion, and tectonics have remained elusive.

Mass redistribution is considerably reduced in broken foreland systems characterized by closed drainages, arid climate, and fluvial systems with limited erosive power. Such systems will be governed by intrabasinal sedimentation with limited sediment transport to peripheral regions beyond the foreland deformation front. This large-scale mass retention may promote shifts in the deformation front position, structural vergence, and overall orogenic architecture (e.g., Métivier et al., 1998; Horton, 1999; Sobel et al., 2003; Norton and Schlunegger, 2011; Armijo et al., 2015). More generally, if entire orogenic wedges and flanking broken-foreland basement provinces may collectively operate as self-organized, critically tapered systems (Oldow et al., 1989; Erslev, 1993; DeCelles, 2004; DeCelles and Graham, 2015), confinement of mass to the broken foreland may help regulate the pace and magnitude of deformation advance. This raises the possibility that climate and erosion may be instrumental as potential drivers capable of guiding both the structural and sedimentary development of broken foreland systems.

9. Conclusions

(1) Broken foreland basins are fundamental components of many contractional orogenic systems (Figs. 1–3). Multiple criteria distinguish broken foreland basins from their unbroken counterparts, including basin dimensions, bounding structural geometries, deformation style, shortening magnitude, stratigraphic arrangement, accommodation mechanisms, depositional environments, sediment source regions, drainage networks, sediment routing patterns, provenance evolutionary schemes, and basin lifespans (Table 1).
(2) The late Cenozoic basin architecture and structural anatomy of the Andes and its adjacent foreland demonstrate the utility of accurate determination of two key contemporaneous elements—the topographic front of the fold-thrust belt and the foreland deformation front (Figs. 4 and 5). Recognition of these features in modern systems and temporally constrained ancient systems will enable identification of broken foreland basins in both retroarc and collisional orogens.
(3) Plate tectonic and geodynamic configurations demonstrate the importance of flat slab subduction in the ancient Laramide broken foreland of North America and the modern Pampean broken foreland of South America (Figs. 2 and 3). However, flat slab subduction is not uniquely required to induce intraplate deformation and broken foreland conditions.
(4) Delineation of broken foreland basins in the geologic record is important for reconstructions of plate convergence, mechanical interactions along plate boundaries, continental deformation, arc magmatism, crustal evolution, craton growth and destruction, and the long-term preservation or elimination of synorogenic strata in foreland settings. Similarly, within the stratigraphic record, broken foreland basins provide insights into the interactions among sediment supply, accommodation, climate, paleodrainage, and synorogenic mass redistribution, as reflected in patterns of erosion, transport, and accumulation.
(5) We propose two sets of circumstances conducive to the development of broken foreland basins: first, favorable *conditions* inherited from the preceding geologic history; and second, specific *catalysts* during orogenesis that trigger distributed intraforeland shortening. We postulate that basin genesis can be ascribed to: (i) tectonic inheritance in the form of preexisting structural, stratigraphic, rheological, and thermal conditions (Fig. 10); and (ii) a mechanical trigger that may include elevated stress, long-distance stress transmission, or variable crustal strengthening or weakening within the intraplate regions that host broken foreland basins (Fig. 11). This framework builds upon previous studies that variably emphasize the role of cool, thick, strong lithosphere, preexisting crustal weaknesses, and competing effects of thermal processes (cooling) and fluid processes (lithospheric hydration) during flat slab subduction.
(6) Future efforts are required to better understand the precusor *conditions* and discrete *catalysts* in time and space. In considering inherited *conditions*, there are debates over the controls on selective reactivation of particular structural or stratigraphic anisotropies and heterogeneities (over other candidate features), the strength of fault zones over time, and the rates and processes

governing rheological and thermal changes. In terms of *catalysts*, uncertainties persist over the magnitude, time scales, and crustal/lithospheric positions of the shifts in intraplate stresses, fluid flow, strengthening, and weakening that trigger intraforeland basement deformation and the genesis of broken foreland basins.

Supplementary data to this article can be found online at https://doi.org/10.1016/j.earscirev.2022.104193.

Declaration of Competing Interest

The authors declare the following financial interests/personal relationships which may be considered as potential competing interests: Brian K. Horton reports financial support was provided by National Science Foundation.

Data availability

Data used in this synthesis are derived from published works that are referenced in the article. The satellite image used for delineation of depositional environments (Fig. 6) is provided in Fig. S1.

Acknowledgments

Our work has been influenced by discussions with Peter Hennings, Mark Helper, Whitney Behr, Andres Folguera, Piotr Krzywiec, Nadine McQuarrie, Cornel Olariu, Joel Saylor, Ron Steel, Jana Alabdullatif, Kristina Butler, Sarah Davis, Sarah George, Gabriel Giacomone, E. Gabriela Gutierrez, Lily Jackson, Keith Minor, Matt Nix, and Ben Rendall. We appreciate the detailed and constructive comments provided by two anonymous reviewers. Financial support was provided by U.S. National Science Foundation grants EAR-1918541, EAR-1925898, EAR-1946700, and EAR-1812681.

References

Allen, P.A., Eriksson, P.G., Alkmim, F.F., Betts, P.G., Catuneanu, O., Mazumder, R., Meng, Q., Young, G.M., 2015. Classification of basins, with special reference to Proterozoic examples. In: Mazumder, R., Eriksson, P.G. (Eds.), Precambrian Basins of India: Stratigraphic and Tectonic Context: Geol. Soc. London Memoir, 43, pp. 5–28. https://doi.org/10.1144/M43.2, 28.

Allmendinger, R.W., 1992. Fold and thrust tectonics of the western United States exclusive of the accreted terranes. In: Burchfiel, B.C., Lipman, P.W., Zoback, M.L. (Eds.), The Cordilleran Orogen: Conterminous U.S.: Geol. Soc. Am., The Geology of North America, G-3, pp. 583–607.

Allmendinger, R.W., Ramos, V.A., Jordan, T.E., Palma, M., Isacks, B., 1983. Paleogeography and Andean structural geometry, northwest Argentina. Tectonics 2, 1–16.

Alvarado, P., Beck, S., 2006. Source characterization of the San Juan (Argentina) crustal earthquakes of 15 January 1944 (M_w 7.0) and 11 June 1952 (M_w 6.8). Earth Planet. Sci. Lett. 243, 615–631. https://doi.org/10.1016/j.epsl.2006.01.015.

Alvarado, P., Beck, S., Zandt, G., Araujo, M., Triep, E., 2005. Crustal deformation in the south-central Andes backarc terranes as viewed from regional broad-band seismic waveform modelling. Geophys. J. Int. 163, 580–598. https://doi.org/10.1111/j.1365-246X.2005.02759.x.

Alvarado, P., Ramos, V.A., 2011. Earthquake deformation in the northwestern Sierras Pampeanas of Argentina based on seismic waveform modelling. J. Geodyn. 51, 205–218. https://doi.org/10.1016/j.jog.2010.08.002.

Amidon, W.H., Ciccioli, P.L., Marenssi, S.A., Limarino, C.O., Fisher, G.B., Burbank, D.W., Kylander-Clark, A., 2016. U-Pb ages of detrital and volcanic zircons of the Toro Negro Formation, northwestern Argentina: Age, provenance and sedimentation rates. J. S. Am. Earth Sci. 70, 237–250. https://doi.org/10.1016/j.jsames.2016.05.013.

Amrouch, K., Lacombe, O., Bellahsen, N., Daniel, J.M., Callot, J.P., 2010. Stress and strain patterns, kinematics and deformation mechanisms in a basement-cored anticline: Sheep Mountain anticline, Wyoming. Tectonics 29. https://doi.org/10.1029/2009TC002525.

Anderson, M., Alvarado, P., Zandt, G., Beck, S., 2007. Geometry and brittle deformation of the subducting Nazca Plate, Central Chile and Argentina. Geophys. J. Int. 171, 419–434. https://doi.org/10.1111/j.1365-246X.2007.03483.x.

Anselmi, G., Candeani, J.C., Chávez, S., Etcheverría, M.P., Folguera, A., Marengo, H., Negro, C., Rodríguez, M.F., Seggiaro, R., Tedesco, A., Wilson, C., Yamin, M., 2015. Mapa Geológico de la República de Argentina, scale 1:5,000,000, Servicio Geológico Minero Argentino. Instituto de Geología y Recursos Minerales, Buenos Aires, Argentina.

Armijo, R., Lacassin, R., Coudurier-Curveur, A., Carrizo, D., 2015. Coupled tectonic evolution of Andean orogeny and global climate. Earth Sci. Rev. 143, 1–35.

Armstrong, R.L., Ward, P.L., 1993. Late Triassic to earliest Eocene magmatism in the North American Cordillera: Implications for the Western Interior Basin. In: Caldwell, W.G.E., Kauffman, E.G. (Eds.), Evolution of the Western Interior Basin. Geol. Assoc. Canada Spec. Paper 39, pp. 49–72.

Axen, G.J., van Wijk, J.W., Currie, C.A., 2018. Basal continental mantle lithosphere displaced by flat-slab subduction. Nat. Geosci. 11, 961–964.

Babeyko, A.Y., Sobolev, S.V., Vietor, T., Oncken, O., Trumbull, R.B., 2006. Numerical study of weakening processes in the central Andean back-arc. In: Oncken, O., et al. (Eds.), The Andes: Active Subduction Orogeny. Springer-Verlag, Berlin, pp. 337–353. https://doi.org/10.1007/978-3-540-48684-8_24.

Baby, P., Calderón, Y., Brusset, S., Roddaz, M., Brichau, S., Eude, A., Calves, G., Quispe, A., Ramirez, L., Bandach, A., Bolaños, R., Hurtado, C., Louterbach, M., Espurt, N., 2018. The Peruvian sub-Andean foreland basin system: Structural overview, geochronologic constraints, and unexplored plays. In: Zamora, G., McClay, K.R., Ramos, V.A. (Eds.), Petroleum Basins and Hydrocarbon Potential of the Andes of Peru and Bolivia: AAPG Memoir, 117, pp. 91–119.

Baby, P., Rivadeneira, M., Barragán, R., Christophoul, F., 2013. Thick-skinned tectonics in the Oriente foreland basin of Ecuador. In: Nemčok, M., Mora, A.R., Cosgrove, J.W. (Eds.), Thick-Skin-Dominated Orogens: From Initial Inversion to Full Accretion: Geol. Soc. London Spec. Publ., 377, pp. 59–76. https://doi.org/10.1144/sp377.1.

Bader, J.W., 2018. Structural inheritance and the role of basement anisotropies in the Laramide structural and tectonic evolution of the North American Cordilleran foreland, Wyoming. Lithosphere 11, 129–148. https://doi.org/10.1130/L1022.1.

Balkwill, H.R., Rodrigue, G., Paredes, F.I., Almeida, J.P., 1995. Northern part of Oriente Basin, Ecuador: Reflection seismic expression of structures. In: Tankard, A.J., Suárez, R., Welsink, H.J. (Eds.), Petroleum Basins of South America: AAPG Memoir, 62, pp. 559–571.

Ballato, P., Brune, S., Strecker, M.R., 2019. Sedimentary loading–unloading cycles and faulting in intermontane basins: Insights from numerical modeling and field observations in the NW Argentine Andes. Earth Planet. Sci. Lett. 506, 388–396. https://doi.org/10.1016/j.epsl.2018.10.043.

Barazangi, M., Isacks, B.L., 1976. Spatial distribution of earthquakes and subduction of the Nazca plate beneath South America. Geology 4, 686–692.

Barrionuevo, M., Liu, S., Mescua, J., Yagupsky, D., Quinteros, J., Giambiagi, L., Sobolev, S.V., Rodríguez Piceda, C., Strecker, M.R., 2021. The influence of variations in crustal composition and lithospheric strength on the evolution of deformation processes in the southern Central Andes: insights from geodynamic models. Int. J. Earth Sci. https://doi.org/10.1007/s00531-021-01982-5.

Bayona, B., Baquero, M., Ramírez, C., Tabares, M., Salazar, A.M., Nova, G., Duarte, E., Pardo, A., Plata, A., Jaramillo, C., Rodríguez, G., Caballero, V., Cardona, A., Montes, C., Gómez Marulanda, S., Cárdenas-Rozo, L., 2020. Unravelling the widening of the earliest Andean northern orogen: Maastrichtian to early Eocene intra-basinal deformation in the northern Eastern Cordillera of Colombia. Basin Res. 33, 809–845. https://doi.org/10.1111/bre.12496.

Bayona, G., Cardona, A., Jaramillo, C., Mora, A., Montes, C., Caballero, V., Mahecha, H., Lamus, F., Montenegro, O., Jimenez, G., Mesa, A., Valencia, V., 2013. Onset of fault reactivation in the Eastern Cordillera of Colombia and proximal Llanos basin; response to Caribbean–South American collision in early Palaeogene time. In: Nemčok, M., Mora, A.R., Cosgrove, J.W. (Eds.), Thick-Skin-Dominated Orogens: From Initial Inversion to Full Accretion: Geol. Soc. London Spec. Publ., 377, pp. 285–314. https://doi.org/10.1144/sp377.1.

Beaudoin, N., Lacombe, O., Bellahsen, N., Amrouch, K., Daniel, J.M., 2014. Evolution of pore-fluid pressure during folding and basin contraction in overpressured reservoirs: Insights from the Madison-Phosphoria carbonate formations in the Bighorn Basin (Wyoming, USA). Mar. Pet. Geol. 55, 214–229.

Beaudoin, N.E., Lacombe, O., Koehn, D., David, M.E., Farrell, N., Healy, D., 2020. Vertical stress history and paleoburial in foreland basins unravelled by stylolite roughness paleopiezometry: Insights from bedding-parallel stylolites in the Bighorn Basin, Wyoming, USA. J. Struct. Geol. 136 https://doi.org/10.1016/j.jsg.2020.104061.

Beaumont, C., Nguyen, M.H., Jamieson, R.A., Ellis, S., 2006. Crustal flow modes in large hot orogens. In: Law, R.D., Searle, M.P., Godin, L. (Eds.), Channel Flow, Ductile Extrusion and Exhumation in Continental Collision Zones: Geol. Soc. London Spec. Publ., 268, pp. 91–145.

Beck, R.A., Vondra, C.F., Filkins, J.E., Olander, J.D., 1988. Syntectonic sedimentation and Laramide basement thrusting, Cordilleran foreland: Timing of deformation. In: Schmidt, C.J., Perry Jr., W.J. (Eds.), Interaction of the Rocky Mountain Foreland and the Cordilleran Thrust Belt: Geol. Soc. Am. Memoir, 171, pp. 465–487.

Behr, W.M., Smith, D., 2016. Deformation in the mantle wedge associated with Laramide flat-slab subduction. Geochem. Geophys. Geosyst. 17 https://doi.org/10.1002/2016GC006361.

Bellahsen, N., Sebrier, M., Siame, L., 2016. Crustal shortening at the Sierra Pie de Palo (Sierras Pampeanas, Argentina): near-surface basement folding and thrusting. Geol. Mag. 153, 992–1012.

Bense, F.A., Löbens, S., Dunkl, I., Wemmer, K., Siegesmund, S., 2013. Is the exhumation of the Sierras Pampeanas only related to Neogene flat-slab subduction? Implications from a multi-thermochronological approach. J. S. Am. Earth Sci. 48, 123–144. https://doi.org/10.1016/j.jsames.2013.09.002.

Berg, R.R., 1962. Mountain flank thrusting in Rocky Mountain foreland, Wyoming and Colorado. AAPG Bull. 46, 2019–2032.

Bernard, T., Sinclair, H.D., Gailleton, B., Mudd, S.M., Ford, M., 2019. Lithological control on the post-orogenic topography and erosion history of the Pyrenees. Earth Planet. Sci. Lett. 518, 53–66. https://doi.org/10.1016/j.epsl.2019.04.034.

Bilmes, A., D'Elia, L., Franzese, J.R., Veiga, G.D., Hernández, M., 2013. Miocene block uplift and basin formation in the Patagonian foreland: The Gastre Basin, Argentina. Tectonophysics 601, 98–111. https://doi.org/10.1016/j.tecto.2013.05.001.
Bird, P., 1984. Formation of the Rocky Mountains foreland and Great Plains. Tectonics 3, 741–758.
Bird, P., 1998. Kinematic history of the Laramide orogeny in latitudes 35°-49°N, western United States. Tectonics 17, 780–801.
Bishop, B.T., Beck, S.L., Zandt, G., Wagner, L., Long, M., Antonijevic, S.K., Kumar, A., Tavera, H., 2017. Causes and consequences of flat slab subduction in southern Peru. Geosphere 13, 1392–1407. https://doi.org/10.1130/GES01440.1.
Bishop, B.T., Beck, S.L., Zandt, G., Wagner, L.S., Long, M.D., Tavera, H., 2018. Foreland uplift during flat subduction: Insights from the Peruvian Andes and Fitzcarrald Arch. Tectonophysics 731–732, 73–84.
Blackstone Jr., D.L., 1990. Rocky Mountain foreland structure exemplified by the Owl Creek Mountains, Bridger Range and Casper Arch, central Wyoming. Wyoming Geol. Assoc. Guidebook 41, 151–166.
Blackstone Jr., D.L., 1993a. Precambrian basement map of Wyoming: Outcrop and structural configuration. Geological Survey of Wyoming Map Series MS-43, scale 1: 1,000,000. Geological Survey of Wyoming.
Blackstone Jr., D.L., 1993b. The Wind River Range, Wyoming: An overview. Wyoming Geol. Assoc. Guidebook 44, 121–140.
Bonnet, S., 2009. Shrinking and splitting of drainage basins in orogenic landscapes from the migration of the main drainage divide. Nat. Geosci. 2, 766–771. https://doi.org/10.1038/ngeo666.
Boyer, S., 1995. Sedimentary basin taper as a factor controlling the geometry and advance of thrust belts. Am. J. Sci. 295, 1220–1254.
Bradley, D.C., Kidd, W.S.F., 1991. Flexural extension of the upper continental crust in collisional foredeeps. GSA Bull. 103, 1416–1438.
Bradley, D.C., Kusky, T.M., Haeussler, P., Goldfarb, R., Miller, M., Dumoulin, J., Nelson, S.W., Karl, S., 2003. Geologic signature of early ridge subduction in Alaska. In: Sisson, V.B., et al. (Eds.), Geology of a Transpressional Orogen Developed during Ridge-Trench Interaction along the North Pacific Margin: Geol. Soc. Am. Spec. Paper, 371, pp. 19–49.
Bradley, M.D., Bruhn, R.L., 1988. Structural interactions between the Uinta arch and the overthrust belt, north-central Utah: Implication of strain trajectories and displacement modeling. In: Schmidt, C.J., Perry Jr., W.J. (Eds.), Interaction of the Rocky Mountain Foreland and the Cordilleran Thrust Belt: Geol. Soc. Am. Memoir, 171, pp. 431–445.
Brown, W.G., 1988. Deformation style of Laramide uplifts in the Wyoming foreland. In: Schmidt, C.J., Perry Jr., W.J. (Eds.), Interaction of the Rocky Mountain Foreland and the Cordilleran Thrust Belt: Geol. Soc. Am. Memoir, 171, pp. 1–25.
Bryant, B., Naeser, C.W., Marvin, R.F., Mehnert, H.H., 1989. Upper Cretaceous and Paleogene sedimentary rocks and isotopic ages of Paleogene tuffs, Uinta basin, Utah. U.S. Geological Survey Bull. 1787J, 22 p.
Bryant, B., Nichols, D.J., 1988. Late Mesozoic and early Tertiary reactivation of an ancient crustal boundary along the Uinta trend and its interaction with the Sevier orogenic belt. In: Schmidt, C.J., Perry Jr., W.J. (Eds.), Interaction of the Rocky Mountain Foreland and the Cordilleran Thrust Belt: Geol. Soc. Am. Memoir, 171, pp. 411–429.
Buelow, E., Suriano, J., Mahoney, J.B., Kimbrough, D.L., Mescua, J.F., Giambiagi, L.B., Hoke, G.D., 2018. Sedimentologic and stratigraphic evolution of the Cacheuta basin: Constraints on the development of the Miocene retroarc foreland basin, south-central Andes. Lithosphere 10, 366–391. https://doi.org/10.1130/L709.1.
Buiter, S.J., Govers, R., Wortel, M.J.R., 2002. Two-dimensional simulations of surface deformation caused by slab detachment. Tectonophysics 354, 195–210.
Burov, E., Cloetingh, S., 2009. Controls of mantle plumes and lithospheric folding on modes of intraplate continental tectonics: differences and similarities. Geophys. J. Int. 178, 1691–1722.
Bush, M.A., Horton, B.K., Murphy, M.A., Stockli, D.F., 2016. Detrital record of initial basement exhumation along the Laramide deformation front, southern Rocky Mountains. Tectonics 35, 2117–2130. https://doi.org/10.1002/2016TC004194.
Butler, K.L., Horton, B.K., Echaurren, A., Folguera, A., Fuentes, F., 2020. Cretaceous-Cenozoic growth of the Patagonian broken foreland basin, Argentina: Chronostratigraphic framework and provenance variations during transitions in Andean subduction dynamics. J. S. Am. Earth Sci. 97 https://doi.org/10.1016/j.jsames.2019.102242.
Cahill, T., Isacks, B., 1992. Seismicity and shape of the subducted Nazca plate. J. Geophys. Res. 97, 17503–17529.
Capaldi, T.N., George, S.W.M., Hirtz, J.A., Horton, B.K., Stockli, D.F., 2019. Fluvial and eolian sediment mixing during changing climate conditions recorded in Holocene Andean foreland deposits from Argentina (31–33°S). Frontiers Earth Sci. 7 https://doi.org/10.3389/feart.2019.00298.
Capaldi, T.N., Horton, B.K., McKenzie, N.R., Mackaman-Lofland, C., Stockli, D.F., Ortiz, G., Alvarado, P., 2020. Neogene retroarc foreland basin evolution, sediment provenance, and magmatism in response to flat slab subduction, western Argentina. Tectonics 39. https://doi.org/10.1029/2019TC005958.
Capaldi, T.N., Horton, B.K., McKenzie, N.R., Stockli, D.F., Odlum, M.L., 2017. Sediment provenance in contractional orogens: The detrital zircon record from modern rivers in the Andean fold-thrust belt and foreland basin of western Argentina. Earth Planet. Sci. Lett. 479, 83–97. https://doi.org/10.1016/j.epsl.2017.09.001.
Capaldi, T.N., McKenzie, N.R., Horton, B.K., Mackaman-Lofland, C., Colleps, C.L., Stockli, D.F., 2021. Detrital zircon record of Phanerozoic magmatism in the southern central Andes. Geosphere 17. https://doi.org/10.1130/GES02346.1.
Carlotto, V., 2013. Paleogeographic and tectonic controls on the evolution of Cenozoic basins in the Altiplano and Western Cordillera of southern Peru. Tectonophysics 589, 195–219. https://doi.org/10.1016/j.tecto.2013.01.002.
Carrapa, B., DeCelles, P.G., Romero, M., 2019. Early inception of the Laramide orogeny in southwestern Montana and northern Wyoming: Implications for models of flat-slab subduction. J. Geophys. Res. 124, 2102–2123. https://doi.org/10.1029/2018JB016888.
Carroll, A.R., Chetel, L.M., Smith, M.E., 2006. Feast to famine: Sediment supply control on Laramide basin fill. Geology 34, 197–200.
Carroll, A.R., Graham, S.A., Smith, M.E., 2010. Walled sedimentary basin of China. Basin Res. 22, 17–32. https://doi.org/10.1111/j.1365-2117.2009.00458.x.
Cather, S.M., 2004. Laramide orogeny in central and northern New Mexico and southern Colorado. In: Mack, G.H., Giles, K.A. (Eds.), The Geology of New Mexico: A Geologic History: New Mexico Geol. Soc. Spec. Publ., 11, pp. 203–248.
Cather, S.M., Chapin, C.E., Kelley, S.A., 2012. Diachronous episodes of Cenozoic erosion in southwestern North America and their relationship to surface uplift, paleoclimate, paleodrainage, and paleoaltimetry. Geosphere 8, 1177–1206. https://doi.org/10.1130/GES00801.1.
Cather, S.M., Heizler, M.T., Williamson, T.E., 2019. Laramide fluvial evolution of the San Juan Basin, New Mexico and Colorado: Paleocurrent and detrital-sanidine age constraints from the Paleocene Nacimiento and Animas formations. Geosphere 15, 1641–1664. https://doi.org/10.1130/GES02072.1.
Cawood, P.A., Hawkesworth, C.J., Pisarevsky, S.A., Dhuime, B., Capitanio, F.A., Nebel, O., 2018. Geological archive of the onset of plate tectonics. Philos. Trans. R. Soc. A Math. Phys. Eng. Sci. 376, 20170405. https://doi.org/10.1098/rsta.2017.0405.
Cerveny, P.F., Steidtmann, J.R., 1993. Fission track thermochronology of the Wind River Range, Wyoming: Evidence for timing and magnitude of Laramide exhumation. Tectonics 12, 77–91.
Chapin, C.E., Kelley, S.A., Cather, S.M., 2014. The Rocky Mountain front, southwestern USA. Geosphere 10, 1043–1060. https://doi.org/10.1130/GES01003.1.
Chapin, C.E., Wilks, M., McIntosh, W.C., 2004. Space-time patterns of Late Cretaceous to present magmatism in New Mexico—Comparison with Andean volcanism and potential for future volcanism. In: Chapin, C.E., McIntosh, W.C., Kelley, S.A. (Eds.), Tectonics, Geochronology, and Volcanism in the Southern Rocky Mountains and Rio Grande Rift: New Mexico Bureau of Geology and Mineral Resources Bull. 160, pp. 13–40, 28.
Chapman, J.B., Dafov, M.N., Gehrels, G., Ducea, M.N., Valley, J.W., Ishida, A., 2018. Lithospheric architecture and tectonic evolution of the southwestern U.S. Cordillera: Constraints from zircon Hf and O isotopic data. GSA Bull. https://doi.org/10.1130/B31937.1.
Chase, C.G., Sussman, A.J., Coblentz, D.D., 2009. Curved Andes: Geoid, forebulge, and flexure. Lithosphere 1, 358–363. https://doi.org/10.1130/L67.1.
Chen, H., Zhang, Y., Cheng, X., Lin, X., Deng, H., Shi, X., Li, Y., Wu, H., Li, C., Yang, S., 2022. Using migrating growth strata to confirm a ~230-km-long detachment thrust in the southern Tarim Basin. J. Structural. Geol. 154 https://doi.org/10.1016/j.jsg.2021.104488.
Christiansen, R.O., Gianni, G.M., Ballivián Justiniano, C.A., García, H.P.A., Wohnlich, S., 2022. The role of geotectonic setting on the heat flow distribution of southern South America. Geophys. J. Int. 230, 1911–1927. https://doi.org/10.1093/gji/ggac161.
Ciccioli, P.L., Limarino, C.O., Friedman, R., Marenssi, S.A., 2014. New high precision U-Pb ages for the Vinchina Formation: Implications for the stratigraphy of the Bermejo Andean foreland basin (La Rioja province, western Argentina). J. S. Am. Earth Sci. 56, 200–213. https://doi.org/10.1016/j.jsames.2014.09.005.
Cobbold, P.R., Davy, P., Gapais, D., Rossello, E.A., Sadybakasov, E., Thomas, J.C., Tondji Biyo, J.J., de Urreiztieta, M., 1993. Sedimentary basins and crustal thickening. Sed. Geol. 86, 77–89.
Collo, G., Dávila, F.M., Teixeira, W., Nóbile, J.C., Sant, L.G., Carter, A., 2017. Isotopic and thermochronologic evidence of extremely cold lithosphere associated with a slab flattening in the Central Andes of Argentina. Basin Res. 29, 16–40. https://doi.org/10.1111/bre.12163.
Comínguez, A.H., Ramos, V.A., 1995. Geometry and seismic expression of the Cretaceous Salta rift system, northwestern Argentina. In: Tankard, A.J., Suárez, R., Welsink, H.J. (Eds.), Petroleum Basins of South America: AAPG Memoir, 62, pp. 325–340.
Comeau, M.J., Stein, C., Becken, M., Hansen, U., 2021. Geodynamic modeling of lithospheric removal and surface deformation: Application to intraplate uplift in central Mongolia. J. Geophys. Res. 126 https://doi.org/10.1029/2020JB021304.
Coney, P.J., 1976. Plate tectonics and the Laramide orogeny. In: Woodward, L.A., Northrop, S.A. (Eds.), Tectonics and Mineral Resources of Southwestern North America: Geol. Soc. New Mexico Spec. Publ., 6, pp. 5–10.
Coney, P.J., Reynolds, S.J., 1977. Cordilleran Benioff zones. Nature 270, 403–406.
Constenius, K.N., 1996. Late Paleogene extensional collapse of the Cordilleran foreland fold and thrust belt. GSA Bull. 108, 20–39.
Constenius, K.N., Esser, R.P., Layer, P.W., 2003. Extensional collapse of the Charleston-Nebo salient and its relationship to space-time variations in Cordilleran orogenic belt tectonism and continental stratigraphy. In: Raynolds, R.G., Flores, R.M. (Eds.), Cenozoic Systems of the Rocky Mountain Region: SEPM, Rocky Mountain Section, pp. 303–353.
Copeland, P., Currie, C.A., Lawton, T.F., Murphy, M.A., 2017. Location, location, location: the variable lifespan of the Laramide orogeny. Geology 45, 223–226.
Costa, C., et al., 2020. Hazardous faults of South America; compilation and overview. J. S. Am. Earth Sci. 104 https://doi.org/10.1016/j.jsames.2020.102837.
Coughlin, T.J., O'Sullivan, P.B., Kohn, B.P., Holcombe, R.J., 1998. Apatite fission-track thermochronology of the Sierras Pampeanas, central western Argentina: Implications for the mechanism of plateau uplift in the Andes. Geology 26, 999–1002.
Coutand, I., Barrier, L., Govin, G., Grujic, D., Hoorn, C., Dupont-Nivet, G., Najman, Y., 2016. Late Miocene-Pleistocene evolution of India-Eurasia convergence partitioning between the Bhutan Himalaya and the Shillong Plateau: New evidences from

foreland basin deposits along the Dungsam Chu section, eastern Bhutan. Tectonics 35, 2963–2994. https://doi.org/10.1002/2016TC004258.
Coutand, I., Carrapa, B., Deeken, A., Schmitt, A.K., Sobel, E.R., Strecker, M.R., 2006. Propagation of orographic barriers along an active range front: Insights from sandstone petrography and detrital apatite fission-track thermochronology in the intramontane Angastaco basin, NW Argentina. Basin Res. 18, 1–26.
Cristallini, E.O., Comínguez, A.H., Ramos, V.A., Mercerat, E.D., 2004. Basement double-wedge thrusting in the northern Sierras Pampeanas of Argentina (27°S)—Constraints from deep seismic reflection: In: McClay, K.R. (Ed.), Thrust Tectonics and Hydrocarbon Systems: AAPG Memoir, 82, pp. 65–90.
Cristallini, E.O., Ramos, V.A., 2000. Thick-skinned and thin-skinned thrusting in the La Ramada fold and thrust belt: Crustal evolution of the High Andes of San Juan, Argentina (32°SL). Tectonophysics 317, 205–235.
Cross, T.A., 1986. Tectonic controls of foreland basin subsidence and Laramide style deformation, western United States. In: Allen, P.A., Homewood, P. (Eds.), Foreland Basins: Int. Assoc. Sed. Spec. Publ., 8, pp. 15–40.
Cunningham, D., 2005. Active intracontinental transpressional mountain building in the Mongolian Altai: Defining a new class of orogen. Earth Planet. Sci. Lett. 240, 436–444.
Currie, C.A., Beaumont, C., 2011. Are diamond-bearing Cretaceous kimberlites related to low-angle subduction beneath western North America? Earth Planet. Sci. Lett. 303, 59–70. https://doi.org/10.1016/j.epsl.2010.12.036.
Currie, C.A., Hyndman, R.D., 2006. The thermal structure of subduction zone back arcs. J. Geophys. Res. 111, B08404. https://doi.org/10.1029/2005JB004024.
Damanti, J.F., 1993. Geomorphic and structural controls on facies patterns and sediment composition in a modern foreland basin. In: Marzo, M., Puigdefábregas, C. (Eds.), Alluvial Sedimentation: Int. Assoc. Sed. Spec. Publ., 17, pp. 221–233.
Davis, S.J., Wiegand, B.A., Carroll, A.R., Chamberlain, C.P., 2008. The effect of drainage reorganization on paleoaltimetry studies: An example from the Paleogene Laramide foreland. Earth Planet. Sci. Lett. 275, 258–268. https://doi.org/10.1016/j.epsl.2008.08.009.
DeCelles, P.G., 1986. Sedimentation in a tectonically partitioned, nonmarine foreland basin: The Lower Cretaceous Kootenai Formation, southwestern Montana. GSA Bull. 97, 911–931.
DeCelles, P.G., 2004. Late Jurassic to Eocene evolution of the Cordilleran thrust belt and foreland basin system, western U.S.A. Am. J. Sci. 304, 105–168.
DeCelles, P.G., Giles, K.N., 1996. Foreland basin systems. Basin Res. 8, 105–123.
DeCelles, P.G., Graham, S.A., 2015. Cyclical processes in the North American Cordilleran orogenic system. Geology 43, 499–502. https://doi.org/10.1130/G36482.1.
DeCelles, P.G., Gray, M.B., Ridgway, K.D., Cole, R.B., Pivnik, D.A., Pequera, A., Srivastava, P., 1991a. Controls on synorogenic alluvial-fan architecture, Beartooth Conglomerate (Palaeocene), Wyoming and Montana. Sedimentology 38, 567–590.
DeCelles, P.G., Gray, M.B., Ridgway, K.D., Cole, R.B., Srivastava, P., Pequera, N., Pivnik, D.A., 1991b. Kinematic history of a foreland uplift from Paleocene synorogenic conglomerate, Beartooth Range, Wyoming and Montana. GSA Bull. 103, 1458–1475.
Delgado, A., Mora, A., Reyes-Harker, A., 2012. Deformation partitioning in the Llanos foreland basin during the Cenozoic and its correlation with mountain building in the hinterland. J. S. Am. Earth Sci. 39, 228–244. https://doi.org/10.1016/j.jsames.2012.04.011.
del Papa, C., Hongn, F., Powell, J., Payrola, P., Do Campo, M., Strecker, M.R., Petrinovic, I., Schmitt, A.K., Pereyra, R., 2013. Middle Eocene-Oligocene broken-foreland evolution in the Andean Calchaqui Valley, NW Argentina: insights from stratigraphic, structural and provenance studies. Basin Res. 25, 574–593. https://doi.org/10.1111/bre.12018.
Dewey, J.F., Bird, J.M., 1970. Mountain belts and the new global tectonics. J. Geophys. Res. 75, 2625–2647.
Dickinson, W.R., 1974. Plate tectonics and sedimentation. In: Dickinson, W.R. (Ed.), Tectonics and Sedimentation: SEPM Spec. Publ., 22, pp. 1–27.
Dickinson, W.R., 1976. Plate tectonic evolution of sedimentary basins. In: Dickinson, W. R., Yarborough, H. (Eds.), Plate Tectonics and Hydrocarbon Accumulation: AAPG Continuing Education Course Notes Series, 1, pp. 1–62.
Dickinson, W.R., Snyder, W.S., 1978. Plate tectonics of the Laramide orogeny. In: Matthews III, V. (Ed.), Laramide Folding Associated with Basement Block Faulting in the Western United States: Geol. Soc. Am. Memoir, 151, pp. 355–366.
Dickinson, W.R., 2004. Evolution of the North American Cordillera. Annual Rev. Earth Planet. Sci. 32, 13–44.
Dickinson, W.R., Klute, M.A., Hayes, M.J., Janecke, S.U., Lundin, E.R., McKittrick, M.A., Olivares, M.D., 1988. Paleogeographic and paleotectonic setting of Laramide sedimentary basins in the central Rocky Mountain region. GSA Bull. 124, 1023–1039.
Dorr Jr., J.A., Spearing, D.R., Steidtmann, J.R., 1977. Deformation and deposition between a foreland uplift and an impinging thrust belt: Hoback Basin, Wyoming. Geol. Soc. Am. Spec. Paper 177, 82 p.
Dumitru, T.A., Gans, P.B., Foster, D.A., Miller, E.L., 1991. Refrigeration of the western Cordilleran lithosphere during Laramide shallow-angle subduction. Geology 19, 1145–1148.
Eakin, C.M., Lithgow-Bertelloni, C., Dávila, F.M., 2014. Influence of Peruvian flat-subduction dynamics on the evolution of western Amazonia. Earth Planet. Sci. Lett. 404, 250–260. https://doi.org/10.1016/j.epsl.2014.07.027.
Echaurren, A., Folguera, A., Gianni, G., Orts, D., Tassara, A., Encinas, A., Giménez, M., Valencia, V., 2016. Tectonic evolution of the North Patagonian Andes (41°–44°S) through recognition of syntectonic strata. Tectonophysics 677, 99–114. https://doi.org/10.1016/j.tecto.2016.04.009.
Enriquez St. Pierre, G.A., Johnson, C.L., 2022. Faulty foundations: Early breakup of the southern Utah Cordilleran foreland basin. GSA Bull. 134, 547–566. https://doi.org/10.1130/B35872.1.
Erslev, E.A., 1993. Thrusts, back-thrusts, and detachment of Rocky Mountain foreland arches. In: Schmidt, C.J., Chase, R.B., Erslev, E.A. (Eds.), Laramide Basement Deformation in the Rocky Mountain Foreland of the Western United States: Geol. Soc. Am. Spec. Paper, 280, pp. 339–358.
Erslev, E.A., 2005. 2D Laramide geometries and kinematics of the Rocky Mountains, western U.S.A. In: Karlstrom, K.E., Keller, G.R. (Eds.), The Rocky Mountain Region: An Evolving Lithosphere: Am. Geophys. Union, Geophysical Monographs, 154, pp. 7–20.
Erslev, E.A., Hennings, P.H., Zahm, C.K., 2001. Kinematics and structural closure of basement-involved anticlines in the central Rocky Mountains petroleum province. AAPG Annual Convention 85, A58.
Erslev, E.A., Koenig, N.B., 2009. kinematics of Laramide, basement-involved Rocky Mountain deformation, U.S.A.: Insights from minor faults and GIS-enhanced structure maps. In: Kay, S.M., Ramos, V.A., Dickinson, W.R. (Eds.), Backbone of the Americas: Shallow Subduction, Plateau Uplift, and Ridge and Terrane Collision: Geol. Soc. Am. Memoir, 204, pp. 125–150.
Espurt, N., Brusset, S., Baby, P., Hermoza, W., Bolanõs, R., Uyen, D., Déramond, J., 2008. Paleozoic structural controls on shortening transfer in the Subandean foreland thrust system, Ene and southern Ucayali basins, Peru. Tectonics 27, TC3009. https://doi.org/10.1029/2007TC002238.
Ewing, T.E., 2019. Tectonics of the West Texas (Permian) Basin—Origins, structural geology, subsidence, and later modification. In: Ruppel, S.C. (Ed.), Anatomy of a Paleozoic Basin: The Permian Basin, USA, Volume 1: AAPG Memoir, 118, pp. 63–96.
Fairhurst, B., Ewing, T., Lindsay, B., 2021. West Texas (Permian) super basin, United States. Tectonics, structural development, sedimentation, petroleum systems, and hydrocarbon reserves. AAPG Bull. 105, 1099–1147.
Fan, M.J., Carrapa, B., 2014. Late Cretaceous-early Eocene Laramide uplift, exhumation, and basin subsidence in Wyoming: Crustal responses to flat slab subduction. Tectonics 33, 509–529.
Fan, M., DeCelles, P.G., Gehrels, G.E., Dettman, D.L., Quade, J., Peyton, L., 2011. Sedimentology, detrital zircon geochronology, and stable isotope geochemistry of the lower Eocene strata in the Wind River Basin, central Wyoming. GSA Bull. 123, 979–996.
Fang, X., Wang, J., Zhang, W., Zan, J., Song, C., Yan, M., Appel, E., Zhang, T., Wu, F., Yang, Y., Lu, Y., 2016. Tectonosedimentary evolution model of an intracontinental flexural (foreland) basin for paleoclimatic research. Glob. Planet. Change 145, 78–97.
Fernandes, V.M., Roberts, G.G., White, N., Whittaker, A.C., 2019. Continental-scale landscape evolution: A history of North American topography. J. Geophys. Res. 124, 2689–2722. https://doi.org/10.1029/2018JF004979.
Fernández-Lozano, J., Sokoutis, D., Willingshofer, E., Cloetingh, S., de Vicente, G., 2011. Cenozoic deformation of Iberia: A model for intraplate mountain building and basin development based on analogue modeling. Tectonics 30, TC1001. https://doi.org/10.1029/2010TC002719.
Fielding, E.J., Jordan, T.E., 1988. Active deformation at the boundary between the Precordillera and the Sierras Pampeanas, Argentina and comparison with ancient Rocky Mountain deformation. In: Schmidt, C.J., Perry Jr., W.J. (Eds.), Interaction of the Rocky Mountain Foreland and the Cordilleran Thrust Belt: Geol. Soc. Am. Memoir, 171, pp. 143–163.
Finzel, E.S., Trop, J.M., Ridgway, K.D., Enkelmann, E., 2011. Upper plate proxies for flat-slab subduction processes in southern Alaska. Earth Planet. Sci. Lett. 303, 348–360.
Flemings, P.B., Nelson, S.N., 1991. Paleogeographic evolution of the latest Cretaceous and Paleocene Wind River Basin. Mountain Geologist 28, 37–52.
Flores, R.M., Ethridge, F.G., 1985. Evolution of intermontane fluvial systems of Tertiary Powder River Basin, Montana and Wyoming. In: Flores, R.M., Kaplan, S.S. (Eds.), Cenozoic Paleogeography of the West-Central United States: SEPM, Rocky Mountain Section, pp. 107–126.
Flowers, R.M., Ehlers, T.A., 2018. Rock erodibility and the interpretation of low-temperature thermochronologic data. Earth Planet. Sci. Lett. 482, 312–323. https://doi.org/10.1016/j.epsl.2017.11.018.
Folguera, A., Encinas, A., Alvarez, O., Orts, D., Gianni, G., Echaurren, A., Litvak, V.D., Navarrete, C., Sellés, D., Tobal, J., Ramos, M., Fennell, L., Fernández, L., Giménez, M., Martínez, P., Ruiz, F., Iannelli, S., 2018. Neogene growth of the Patagonian Andes. In: Folguera, A. (Ed.), The Evolution of the Chilean-Argentinean Andes. Springer, Cham, Switzerland, pp. 475–501.
Folguera, A., Gianni, G., Sagripanti, L., Rojas Vera, E., Novara, I., Colavitto, B., Alvarez, O., Orts, D., Tobal, J., Giménez, M., Introcaso, A., Ruiz, F., Martínez, P., Ramos, V.A., 2015. A review about the mechanisms associated with active deformation, regional uplift and subsidence in southern South America. J. S. Am. Earth Sci. 64, 511–529.
Folguera, A., Ramos, V.A., 2011. Repeated eastward shifts of arc magmatism in the southern Andes: A revision to the long-term pattern of Andean uplift and magmatism. J. S. Am. Earth Sci. 32, 531–546.
Fosdick, J.C., Carrapa, B., Ortíz, G., 2015. Faulting and erosion in the Argentine Precordillera during changes in subduction regime: Reconciling bedrock cooling and detrital records. Earth Planet. Sci. Lett. 432, 73–83. https://doi.org/10.1016/j.epsl.2015.09.041.
Fosdick, J.C., Reat, E.J., Carrapa, B., Ortiz, G., Alvarado, P.M., 2017. Retroarc basin reorganization and aridification during Paleogene uplift of the southern central Andes. Tectonics 36, 493–514. https://doi.org/10.1002/2016TC004400.
Fuentes, F., Horton, B.K., Starck, D., Boll, A., 2016. Structure and tectonic evolution of hybrid thick- and thin-skinned systems in the Malargüe fold-thrust belt, Neuquén

basin, Argentina. Geol. Mag. 153, 1066–1084. https://doi.org/10.1017/S0016756816000583.
Fuentes, F., DeCelles, P.G., Constenius, K.N., Gehrels, G.E., 2011. Evolution of the Cordilleran foreland basin system in northwestern Montana, U.S.A. GSA Bull. 123, 507–533. https://doi.org/10.1130/B30204.1.
Gans, C.R., Beck, S.L., Zandt, G., Gilbert, H., Alvarado, P., Anderson, M., Linkimer, L., 2011. Continental and oceanic crustal structure of the Pampean flat slab region, western Argentina, using receiver function analysis: new high-resolution results. Geophys. J. Int. 186, 45–58. https://doi.org/10.1111/j.1365-246X.2011.05023.x.
Gao, M., Fan, M., Moucha, R., 2016. Southwestward weakening of Wyoming lithosphere during the Laramide orogeny. J. Geophys. Res. 121, 6219–6234. https://doi.org/10.1002/2016JB013130.
Gao, Z., Perez, N.D., Miller, B., Pope, M.C., 2020. Competing sediment sources during Paleozoic closure of the Marathon-Ouachita remnant ocean basin. GSA Bull. 132, 3–16. https://doi.org/10.1130/B35201.1.
Garber, K.L., Finzel, E.S., Pearson, D.M., 2020. Provenance of synorogenic foreland basin strata in southwestern Montana requires revision of existing models for Laramide tectonism: North American Cordillera. Tectonics 39. https://doi.org/10.1029/2019TC005944.
Garzanti, E., Capaldi, T., Limonta, M., Sosa, N., Vezzoli, G., 2021. Transcontinental retroarc sediment routing controlled by subduction geometry and climate change (central and southern Andes, Argentina). Basin Res. 33, 3406–3437. https://doi.org/10.1111/bre.12607.
Garzanti, E., Capaldi, T., Tripaldi, A., Zárate, M., Limonta, M., Vezzoli, G., 2022. Andean retroarc-basin dune fields and Pampean Sand Sea (Argentina): Provenance and drainage changes driven by tectonics and climate. Earth Sci. Rev. 231 https://doi.org/10.1016/j.earscirev.2022.104077.
Gautheron, C., Espurt, N., Barbarand, J., Roddaz, M., Baby, P., Brusset, S., Tassan-Got, L., Douville, E., 2013. Direct dating of thick- and thin-skin thrusts in the Peruvian Subandean zone through apatite (U-Th)/He and fission track thermochronometry. Basin Res. 25, 419–435. https://doi.org/10.1111/bre.12012.
Gentry, A., Yonkee, W.A., Wells, M.L., Balgord, E.A., 2018. Resolving the history of early fault slip and foreland basin evolution along the Wyoming salient of the Sevier fold-and-thrust belt: Integrating detrital zircon geochronology, provenance modeling, and subsidence analysis. In: Ingersoll, R.V., Lawton, T.F., Graham, S.A. (Eds.), Tectonics, Sedimentary Basins, and Provenance: A Celebration of William R. Dickinson's Career: Geol. Soc. Am. Spec. Paper, 540, pp. 509–545. https://doi.org/10.1130/2018.2540(23).
Ghiglione, M.C., Ronda, G., Suárez, R.J., Aramendía, I., Barberón, V., Ramos, M.E., Tobal, J., Morabito, E.G., Martinod, J., Sue, C., 2019. Structure and tectonic evolution of the South Patagonian fold and thrust belt: Coupling between subduction dynamics, climate and tectonic deformation. In: Horton, B.K., Folguera, A. (Eds.), Andean Tectonics. Elsevier, pp. 675–697. https://doi.org/10.1016/B978-0-12-816009-1.00024-1.
Ghiglione, M.C., Sue, C., Ramos, M.E., Tobal, J.E., Gallardo, R.E., 2016. The relation between Neogene denudation of the southernmost Andes and sedimentation in the offshore Argentine and Malvinas basins during the opening of the Drake Passage. In: Ghiglione, M. (Ed.), Geodynamic Evolution of the Southernmost Andes: Connections with the Scotia Arc. Springer, pp. 109–135.
Giambiagi, L., et al., 2015. Evolution of shallow and deep structures along the Maipo–Tunuyan transect (33°40'S): from the Pacific coast to the Andean foreland. In: Sepúlveda, S.A., Giambiagi, L.B., Moreiras, S.M., Pinto, L., Tunik, M., Hoke, G.D., Farías, M. (Eds.), Geodynamic Processes in the Andes of Central Chile and Argentina. Geol. Soc. London Spec. Publ., 399, pp. 63–82.
Giambiagi, L., et al., 2022. Crustal anatomy and evolution of a subduction-related orogenic system: Insights from the Southern Central Andes (22–35°S). Earth Sci. Rev. 232, 63–82. https://doi.org/10.1016/j.earscirev.2022.104138.
Giambiagi, L.B., Bechis, F., García, V.H., Clark, A., 2008. Temporal and spatial relationships of thick- and thin-skinned deformation in the Malargüe fold and thrust belt, southern Central Andes. Tectonophysics 459, 123–139.
Giambiagi, L.B., Tunik, M.A., Ghiglione, M., 2001. Cenozoic tectonic evolution of the Alto Tunuyán foreland basin above the transition zone between the flat and normal subduction segments (33°30'–34°S), western Argentina. J. S. Am. Earth Sci. 14, 707–724.
Gianni, G., Navarrete, C., Orts, D., Tobal, J., Folguera, A., Giménez, M., 2015. Patagonian broken foreland and related synorogenic rifting: the origin of the Chubut Group Basin. Tectonophysics 649, 81–99.
Gianni, G.M., Pérez Luján, S., 2021. Geodynamic controls on magmatic arc migration and quiescence. Earth Sci. Rev. 218 https://doi.org/10.1016/j.earscirev.2021.103676.
González Bonorino, F., 1950. Algunos problemas geológicos de las Sierras Pampeanas. Rev. Asoc. Geol. Argent. 5, 81–110.
Graham, S.A., Hendrix, M.S., Wang, L.B., Carroll, A.R., 1993. Collisional successor basins of western China: Impact of tectonic inheritance on sand composition. GSA Bull. 105, 323–344.
Gries, R., 1983. Oil and gas prospecting beneath Precambrian of foreland thrust plates in Rocky Mountains. AAPG Bull. 67, 1–28.
Gunnell, G.F., Murphey, P.C., Stucky, R.K., Townsend, K.E.B., Robinson, P., Zonneveld, J. P., Bartels, W.S., 2009. Biostratigraphy and biochronology of the latest Wasatchian, Bridgerian, and Uintan North American land mammal "ages". In: Albright III, L.B. (Ed.), Papers on Geology, Vertebrate Paleontology, and Biostratigraphy in Honor of Michael O. Woodburne: Museum of Northern Arizona Bull., 65, pp. 279–330.
Gustason, E.R., 1989. Stratigraphy and Sedimentology of the Middle Cretaceous (Albian-Cenomanian) Dakota Formation, Southwestern Utah (Ph.D. thesis). University of Colorado, Boulder, USA, 376 p.
Gutscher, M.A., Spakman, W., Bijwaard, H., Engdahl, E.R., 2000. Geodynamics of flat subduction: Seismicity and tomographic constraints from the Andean margin. Tectonics 19, 814–833.
Gutscher, M.A., 2002. Andean subduction styles and their effect on thermal structure and interplate coupling. J. S. Am. Earth Sci. 15, 3–10.
Hafiz, I., Kellogg, J., Saeid, E., Albesher, Z., 2019. Thin-skinned and thick-skinned structural control on the evolution of a foreland basin petroleum system – Parrando and Guavio anticlines, Eastern Cordillera Llanos foothills, Colombia. J. S. Am. Earth Sci. 96 https://doi.org/10.1016/j.jsames.2019.102373.
Hagen, E.S., Shuster, M.W., Furlong, K.P., 1985. Tectonic loading and subsidence of intermontane basins: Wyoming foreland province. Geology 13, 585–588.
Hain, M.P., Strecker, M.R., Bookhagen, B., Alonso, R.N., Pingel, H., Schmitt, A.K., 2011. Neogene to Quaternary broken foreland formation and sedimentation dynamics in the Andes of NW Argentina (25°S). Tectonics 30, TC2006. https://doi.org/10.1029/2010TC002703.
Hall, M.K., Chase, C.G., 1989. Uplift, unbuckling, and collapse: Flexural history and isostasy of the Wind River Range and Granite Mountains, Wyoming. J. Geophys. Res. 94, 17581–17593.
Heller, P.L., Liu, L., 2016. Dynamic topography and vertical motion of the U.S. Rocky Mountain region prior to and during the Laramide orogeny. GSA Bull. 128, 973–988.
Heller, P.L., McMillan, M.E., Humphrey, N., 2011. Climate-induced formation of a closed basin: Great Divide Basin, Wyoming. GSA Bull. 123, 150–157.
Hendrix, M., 2000. Evolution of Mesozoic sandstone compositions, southern Junggar, northern Tarim, and western Turpan basins, northwest China: A detrital record of the ancestral Tian Shan. J. Sed. Res. 70, 520–532.
Hennings, P.H., Hager, R.C., 1996. Basement backthrusts and thin-skinned detachments in Gooseberry field, western Bighorn Basin, Wyoming. Wyoming Geological Association 47th Annual Field Conference Guidebook, pp. 221–238.
Henry, S.G., Pollack, H.N., 1988. Terrestrial heat flow above the Andean subduction zone in Bolivia and Peru. J. Geophys. Res. 93, 15153–15162.
Hermoza, W., Baby, P., Esurt, N., Martinez, E., Bolaños, R., 2006. The Ucayali Subandean Basin: a complex fold and thrust belt and inverted system. IX Simposio Bolivariano: Exploración Petrolera en las Cuencas Subandinas, September 24–26, 2006, 12 p.
Hilley, G.E., Coutand, I., 2010. Links between topography, erosion, rheological heterogeneity, and deformation in contractional settings: Insights from the central Andes. Tectonophysics 495, 78–92.
Hindle, D., Kley, J., 2021. The Subhercynian Basin: an example of an intraplate foreland basin due to a broken plate. Solid Earth 12, 2425–2438. https://doi.org/10.5194/se-12-2425-2021.
Horton, B.K., 1999. Erosional control on the geometry and kinematics of thrust belt development in the central Andes. Tectonics 18, 1292–1304.
Horton, B.K., 2012. Cenozoic evolution of hinterland basins in the Andes and Tibet. In: Busby, C.J., Azor, A. (Eds.), Tectonics of Sedimentary Basins: Recent Advances: Wiley-Blackwell, pp. 427–444.
Horton, B.K., 2018a. Tectonic regimes of the central and southern Andes: Responses to variations in plate coupling during subduction. Tectonics 37, 402–429. https://doi.org/10.1002/2017TC004624.
Horton, B.K., 2018b. Sedimentary record of Andean mountain building. Earth Sci. Rev. 178, 279–309. https://doi.org/10.1016/j.earscirev.2017.11.025.
Horton, B.K., 2022. Unconformity development in retroarc foreland basins: Implications for the geodynamics of Andean-type margins. J. Geol. Soc. Lond. 179 https://doi.org/10.1144/jgs2020-263.
Horton, B.K., Capaldi, T.N., Perez, N.D., 2022. The role of flat slab subduction, ridge subduction, and tectonic inheritance in Andean deformation. Geology 50. https://doi.org/10.1130/G50094.1.
Horton, B.K., DeCelles, P.G., 1997. The modern foreland basin system adjacent to the Central Andes. Geology 25, 895–898.
Horton, B.K., DeCelles, P.G., 2001. Modern and ancient fluvial megafans in the foreland basin system of the central Andes, southern Bolivia: Implications for drainage network evolution in fold-thrust belts. Basin Res. 13, 43–63.
Horton, B.K., Folguera, A., 2022. Tectonic inheritance and structural styles in the Andean fold-thrust belt and foreland basin. In: Zamora, G., Mora, A. (Eds.), Andean Structural Styles: A Seismic Atlas: Elsevier, 3–28. https://doi.org/10.1016/B978-0-323-85175-6.00001-8.
Horton, B.K., Fuentes, F., 2016. Sedimentary record of plate coupling and decoupling during growth of the Andes. Geology 44, 647–650. https://doi.org/10.1130/G37918.1.
Horton, B.K., Parra, M., Mora, A., 2020. Construction of the Eastern Cordillera of Colombia: Insights from the sedimentary record. In: Gómez, J., Mateus-Zabala, D. (Eds.), The Geology of Colombia: Servicio Geológico Colombiano, Publicaciones Geológicas Especiales, 37, pp. 67–88. https://doi.org/10.32685/pub.esp.37.2019.03.
Howell, L., Besly, B., Sooriyathasan, S., Egan, S., Leslie, G., 2020. Seismic and borehole-based mapping of the late Carboniferous succession in the Canonbie Coalfield, SW Scotland: evidence for a 'broken' Variscan foreland? Scottish J. Geol. 57 https://doi.org/10.1144/sjg2020-007.
Hoy, R.G., Ridgway, K.D., 1997. Structural and sedimentological development of footwall growth synclines along an intraforeland uplift, east-central Bighorn Mountains, Wyoming. GSA Bull. 109, 915–935.
Hu, J., Liu, L., Gurnis, M., 2021. Southward expanding plate coupling due to variation in sediment subduction as a cause of Andean growth. Nat. Comm. 12 (7271) https://doi.org/10.1038/s41467-021-27518-8.
Humphreys, E., 2009. Relation of flat subduction to magmatism and deformation in the western United States. In: Kay, S.M., Ramos, V.A., Dickinson, W.R. (Eds.), Backbone of the Americas: Shallow Subduction, Plateau Uplift, and Ridge and Terrane Collision: Geol. Soc. Am. Memoir, 204, pp. 85–98.

Humphreys, E., Hessler, E., Dueker, K., Erslev, E., Farmer, G.L., Atwater, T., 2003. How Laramide-age hydration of North America by the Farallon slab controlled subsequent activity in the western U.S. Int. Geol. Rev. 45, 575–595.
Hyndman, R.D., Currie, C.A., Mazzotti, S.P., 2005. Subduction zone backarcs, mobile belts, and orogenic heat. GSA Today 15, 4–10. https://doi.org/10.1130/1052-5173(2005)015<4:SZBMBA>2.0.co;2.
Ibarra, F., Prezzi, C.B., Bott, J., Scheck-Wenderoth, M., Strecker, M.R., 2021. Distribution of temperature and strength in the Central Andean lithosphere and its relationship to seismicity and active deformation. J. Geophys. Res. 126 https://doi.org/10.1029/2020JB021231.
Ingersoll, R.V., 2012. Tectonics of sedimentary basins, with revised nomenclature. In: Busby, C., Azor, A. (Eds.), Tectonics of Sedimentary Basins: Recent Advances: Wiley-Blackwell, pp. 3–43.
Ingersoll, R.V., 2019. Subduction-related sedimentary basins of the US Cordillera. In: Miall, A.D. (Ed.), Sedimentary Basins of the United States and Canada, pp. 477–510. https://doi.org/10.1016/B978-0-444-63895-3.00011-5.
Irigoyen, M.V., Buchan, K.L., Brown, R.L., 2000. Magnetostratigraphy of Neogene Andean foreland-basin strata, lat 33°S, Mendoza Province, Argentina. GSA Bull. 112, 803–816.
Iriondo, M., 1999. Climatic changes in the South American plains: Records of a continent-scale oscillation. Quaternary Int. 57, 93–112.
Isacks, B.L., 1988. Uplift of the central Andean plateau and bending of the Bolivian orocline. J. Geophys. Res. 93, 3211–3231.
Jacques, J.M., 2003. A tectonostratigraphic synthesis of the Sub-Andean basins: implications for the geotectonic segmentation of the Andean Belt. J. Geol. Soc. Lond. 160, 687–701.
James, D.E., Sacks, I.S., 1999. Cenozoic formation of the central Andes: A geophysical perspective. Soc. Econ. Geol. Spec. Publ. 7, 1–25.
Jones, C.H., Farmer, G.L., Sageman, B., Zhong, S., 2011. Hydrodynamic mechanism for the Laramide orogeny. Geosphere 7, 183–201.
Jordan, T.E., 1995. Retroarc foreland and related basins. In: Busby, C.J., Ingersoll, R.V. (Eds.), Tectonics of Sedimentary Basins. Blackwell Science, pp. 331–362.
Jordan, T.E., Allmendinger, R.W., 1986. The Sierras Pampeanas of Argentina: A modern analogue of Rocky Mountain foreland deformation. Am. J. Sci. 286, 737–764.
Jordan, T.E., Allmendinger, R.W., Damanti, J.F., Drake, R.E., 1993. Chronology of motion in a complete thrust belt: The Precordillera, 30–31°S, Andes Mountains. J. Geol. 101, 135–156.
Jordan, T.E., Isacks, B.L., Allmendinger, R.W., Brewer, J.A., Ramos, V.A., Ando, C.J., 1983. Andean tectonics related to geometry of subducted Nazca plate. GSA Bull. 94, 341–361.
Jordan, T.E., Schlunegger, F., Cardozo, N., 2001. Unsteady and spatially variable evolution of the Neogene Andean Bermejo foreland basin, Argentina. J. S. Am. Earth Sci. 14, 775–798.
Jordan, T.E., Tamm, V., Figueroa, G., Flemings, P.B., Richards, D., Tabbutt, K., Cheatham, T., 1996. Development of the Miocene Manantiales foreland basin, Principal Cordillera, San Juan, Argentina. Andean Geol. 23, 43–79.
Kauffman, E.G., Caldwell, W.G.E., 1993. The Western Interior Basin in space and time. In: Caldwell, W.G.E., Kauffman, E.G. (Eds.), Evolution of the Western Interior Basin. Geol. Assoc. Canada Spec. Paper, 39, pp. 1–30.
Kay, S.M., Coira, B.L., 2009. Shallowing and steepening subduction zones, continental lithospheric loss, magmatism, and crustal flow under the Central Andean Altiplano-Puna Plateau. In: Kay, S.M., Ramos, V.A., Dickinson, W.R. (Eds.), Backbone of the Americas: Shallow Subduction, Plateau Uplift, and Ridge and Terrane Collision: Geol. Soc. Am. Memoir, 204, pp. 229–259.
Kay, S., Maksaev, V., Moscoso, R., Mpodozis, C., Nasi, C., Gordillo, C.E., 1988. Tertiary Andean magmatism in Chile and Argentina between 28°S and 33°S: Correlation of magmatic chemistry with a changing Benioff zone. J. S. Am. Earth Sci. 1, 21–38.
Kay, S.M., Godoy, E., Kurtz, A., 2005. Episodic arc migration, crustal thickening, subduction erosion, and magmatism in the south-central Andes. Geol. Soc. Am. Bull. 117, 67–88.
Kay, S.M., Mpodozis, C., 2002. Magmatism as a probe to the Neogene shallowing of the Nazca plate beneath the modern Chilean flat-slab. J. S. Am. Earth Sci. 15, 39–57.
Kelley, S.A., Chapin, C.E., 2004. Denudation history and internal structure of the Front Range and Wet Mountains, Colorado, based on apatite fission-track thermochronology. In: Cather, S.M., McIntosh, W., Kelley, S.A. (Eds.), Tectonics, Geochronology and Volcanism in the Southern Rocky Mountains and Rio Grande Rift: New Mexico Bureau of Geology and Mineral Resources Bull. 160, pp. 41–77.
Kelley, V.C., 1955. Monoclines of the Colorado Plateau. GSA Bull. 66, 789–804.
Kley, J., Voigt, T., 2008. Late Cretaceous intraplate thrusting in central Europe: Effect of Africa-Iberia-Europe convergence, not Alpine collision. Geology 36, 839–842.
Kley, J., Monaldi, C.R., Salfity, J.A., 1999. Along-strike segmentation of the Andean foreland: Causes and consequences. Tectonophysics 301, 75–94.
Kluth, C.F., Coney, P.J., 1981. Plate tectonics of the Ancestral Rocky Mountains. Geology 9, 10–15.
Kraig, D.H., Wiltschko, D., Spang, J.H., 1987. Interaction of basement uplift and thin-skinned thrusting, Moxa arch and the western overthrust belt, Wyoming: A hypothesis. Geol. Soc. Am. Bull. 99, 654–662.
Krzywiec, P., 2001. Contrasting tectonic and sedimentary history of the central and eastern parts of the Polish Carpathian foredeep basin — results of seismic data interpretation. Mar. Pet. Geol. 18, 13–38.
Kuhlemann, J., Kempf, O., 2002. Post-Eocene evolution of the North Alpine foreland basin and its response to Alpine tectonics. Sed. Geol. 152, 45–78.
Kusky, M.T., Windley, F.B., Wang, L., Wang, Z.S., Li, X.Y., Zhu, P.M., 2014. Flat slab subduction, trench suction, and craton destruction: Comparison of the North China, Wyoming, and Brazilian cratons. Tectonophysics 630, 208–221.
Kusky, T.M., Polat, A., Windley, B.F., Burke, K.C., Dewey, J.F., Kidd, W.S.F., Maruyama, S., Wang, J.P., Deng, H., Wang, Z.S., Wang, C., Fu, D., Li, X.W., Peng, H. T., 2016. Insights into the tectonic evolution of the North China Craton through comparative tectonic analysis: A record of outward growth of Precambrian continents. Earth Sci. Rev. 162, 387–432. https://doi.org/10.1016/j.earscirev.2016.09.002.
Lacombe, O., Bellahsen, N., 2016. Thick-skinned tectonics and basement-involved fold–thrust belts: Insights from selected Cenozoic orogens. Geol. Mag. 152, 763–810. https://doi.org/10.1017/S0016756816000078.
Lacombe, O., Mouthereau, F., 2002. Basement-involved shortening and deep detachment tectonics in forelands of orogens: Insights from recent collision belts (Taiwan, Western Alps, Pyrenees). Tectonics 21, 1030. https://doi.org/10.1029/2001TC901018.
Lacombe, O., Parlangeau, C., Beaudoin, N.E., Amrouch, K., 2021. Calcite twin formation, measurement and use as stress-strain indicators: A review of progress over the last decade. Geosciences 11. https://doi.org/10.3390/geosciences11110445.
Lageson, D.R., Schmitt, J.G., 1994. The Sevier orogenic belt of the western United States: Recent advances in understanding its structural and sedimentologic framework. In: Caputo, M.V., Peterson, J.A., Franczyk, K.J. (Eds.), Mesozoic Systems of the Rocky Mountain Region. SEPM Spec. Publ, pp. 27–64.
Lalami, H.R.K., Hajialibeigi, H., Sherkati, S., Adabi, M.H., 2020. Tectonic evolution of the Zagros foreland basin since Early Cretaceous, SW Iran: Regional tectonic implications from subsidence analysis. J. Asian Earth Sci. 204 https://doi.org/10.1016/j.jseaes.2020.104550.
Lamb, S., Davis, P., 2003. Cenozoic climate change as a possible cause for the rise of the Andes. Nature 425, 792–797. https://doi.org/10.1038/nature02049.
Laskowski, A.K., DeCelles, P.G., Gehrels, G.E., 2013. Detrital zircon geochronology of Cordilleran retroarc foreland basin strata, western North America. Tectonics 32, 1027–1048. https://doi.org/10.1002/tect.20065.
Lawton, T.F., 1986. Fluvial systems of the Upper Cretaceous Mesaverde Group and Paleocene North Horn Formation, central Utah: A record of transition from thin-skinned to thick-skinned deformation in the foreland region. In: Peterson, J.A. (Ed.), Paleotectonics and Sedimentation in the Rocky Mountain Region, United States: AAPG Memoir, 41, pp. 423–442.
Lawton, T.F., 2019. Laramide sedimentary basins and sediment-dispersal system. In: Miall, A.D. (Ed.), The Sedimentary Basins of the United States and. Elsevier, Canada, pp. 529–557. https://doi.org/10.1016/B978-0-444-63895-3.00013-9.
Lawton, T.F., Blakey, R.C., Stockli, D.F., Liu, L., 2021. Late Paleozoic (Late Mississippian-Middle Permian) sediment provenance and dispersal in western equatorial Pangea. Palaeogeogr. Palaeoclimatol. Palaeoecol. 572 https://doi.org/10.1016/j.palaeo.2021.110386.
Leary, R.J., Umhoefer, P., Smith, M.E., Riggs, N., 2017. A three-sided orogen: A new tectonic model for Ancestral Rocky Mountain uplift and basin development. Geology 45, 735–738. https://doi.org/10.1130/G39041.1.
Leary, R.J., Umhoefer, P., Smith, M.E., Smith, T.M., Saylor, J.E., Riggs, N., Burr, G., Lodes, E., Foley, D., Licht, A., Mueller, M.A., Baird, C., 2020. Provenance of Pennsylvanian-Permian sedimentary rocks associated with the Ancestral Rocky Mountains orogeny in southwestern Laurentia: Implications for continental-scale Laurentian sediment transport systems. Lithosphere 12, 88–121.
Leva López, J.L., Steel, R.J., 2015. Laramide signals and architecture of a widespread fluvial sand sheet: Canyon Creek Member, southern Wyoming, U.S.A. J. Sed. Res. 85, 1102–1122. https://doi.org/10.2110/jsr.2015.67.
Levina, M., Horton, B.K., Fuentes, F., Stockli, D.F., 2014. Cenozoic sedimentation and exhumation of the foreland basin system preserved in the Precordillera thrust belt (31–32°S), southern central Andes, Argentina. Tectonics 33, 1659–1680. https://doi.org/10.1002/2013tc003424.
Li, C., Wang, S., Naylor, M., Sinclair, H., Wang, L., 2020. Evolution of the Cenozoic Tarim Basin by flexural subsidence and sediment ponding: Insights from quantitative basin modelling. Marine Petrol. Geol. 112 https://doi.org/10.1016/j.marpetgeo.2019.104047.
Li, Z., Aschoff, J., 2022. Constraining the effects of dynamic topography on the development of Late Cretaceous Cordilleran foreland basin, western United States. GSA Bull. 134, 446–462. https://doi.org/10.1130/B35838.1.
Li, Z.X., Li, X.H., 2007. Formation of the 1300-km-wide intracontinental orogen and postorogenic magmatic province in Mesozoic South China: A flat-slab subduction model. Geology 35, 179–182.
Lillegraven, J.A., 1993. Correlation of Paleogene strata across Wyoming—a users' guide. In: Snoke, A.W., Steidtmann, J.R., Roberts, S.M. (Eds.), Geology of Wyoming: Geological Survey of Wyoming Memoir, 5, pp. 414–477.
Lillegraven, J.A., 2015. Late Laramide tectonic fragmentation of the eastern greater Green River Basin, Wyoming. Rocky Mountain Geology 50, 30–118. https://doi.org/10.2113/gsrocky.50.1.30.
Lillegraven, J.A., Ostresh Jr., L.M., 1988. Evolution of Wyoming's early Cenozoic topography and drainage patterns. Natl. Geog. Res. 4, 303–327.
Lindsey, D.A., 1998. Laramide structure of the central Sangre de Cristo Mountains and adjacent Raton Basin, southern Colorado. Mountain Geologist 35, 55–70.
Liu, S., Zhang, J., Hong, S., Ritts, B.D., 2007. Early Mesozoic basin development and its response to thrusting in the Yanshan fold-and-thrust belt, China. Int. Geol. Rev. 49, 1025–1049.
Liu, L., Spasojevic, S., Gurnis, M., 2008. Reconstructing Farallon plate subduction beneath North America back to the Late Cretaceous. Science 322 (5903), 934–938.
Liu, S., Nummedal, D., Gurnis, M., 2014. Dynamic versus flexural controls of Late Cretaceous Western Interior Basin, USA. Earth Planet. Sci. Lett. 389, 221–229.
Liu, S., Currie, C.A., 2016. Farallon plate dynamics prior to the Laramide orogeny: Numerical models of flat subduction. Tectonophysics 666, 33–47. https://doi.org/10.1016/j.tecto.2015.10.010.

Liu, X., Currie, C.A., Wagner, L.S., 2021. Cooling of the continental plate during flat-slab subduction. Geosphere 18, 49–68. https://doi.org/10.1130/GES02402.1.
Löbens, S., Sobel, E.R., Bense, F.A., Wemmer, K., Dunkl, I., Siegesmund, S., 2013. Refined exhumation history of the northern Sierras Pampeanas, Argentina. Tectonics 32, 453–472. https://doi.org/10.1002/tect.20038.
Lossada, A.C., Giambiagi, L., Hoke, G.D., Fitzgerald, P.G., Creixell, C., Murillo, I., Mardonez, D., Velásquez, R., Suriano, J., 2017. Thermochronologic evidence for late Eocene Andean mountain building at 30°S. Tectonics 36, 2693–2713. https://doi.org/10.1002/2017TC004674.
Love, J.D., 1970. Cenozoic geology of the Granite Mountains area, central Wyoming. U.S. Geological Survey Professional Paper 495-C, 154 p.
Love, J.D., Christiansen, A.C., 1985. Geologic map of Wyoming, USA. U.S. Geological Survey scale 1:500,000.
Lynds, R.M., Slattery, J.S., 2017. Correlation of Upper Cretaceous strata of Wyoming. Wyoming State Geological Survey Open File Report, 2017-3, one sheet.
Macellari, C., Hermoza, W., 2009. Subandean segmentation and its impact on hydrocarbon exploration in the Central/Northern Andes. X Simposio Bolivariano: Exploración Petrolera en las Cuencas Subandinas, Associatión Colombiana de Geólogos y Geofisicos del Petróleo, July 26–29, 2009, 13 p.
Mackaman-Lofland, C., Horton, B.K., Fuentes, F., Constenius, K.N., Stockli, D.F., 2019. Mesozoic to Cenozoic retroarc basin evolution during changes in tectonic regime, southern Central Andes (31–33°S): Insights from zircon U-Pb geochronology. J. S. Am. Earth Sci. 89, 299–318. https://doi.org/10.1016/j.jsames.2018.10.004.
Mackaman-Lofland, C., Horton, B.K., Fuentes, F., Constenius, K.N., Ketcham, R.A., Capaldi, T.N., Stockli, D.F., Ammirati, J.B., Alvarado, P., Orozco, P., 2020. Andean mountain building and foreland basin evolution during thin- and thick-skinned Neogene deformation (32–33°S). Tectonics 39. https://doi.org/10.1029/2019TC005838.
Mackaman-Lofland, C., Horton, B.K., Ketcham, R.A., McQuarrie, N., Fosdick, J.C., Fuentes, F., Constenius, K.N., Capaldi, T.N., Stockli, D.F., Alvarado, P., 2022. Causes of variable shortening and tectonic subsidence during changes in subduction: Insights from flexural thermokinematic modeling of the Neogene southern central Andes (28–30°S). Tectonics 41. https://doi.org/10.1029/2022TC007334.
Mackey, G.N., Horton, B.K., Milliken, K.L., 2012. Provenance of the Paleocene-Eocene Wilcox Group, western Gulf of Mexico basin: Evidence for integrated drainage of the southern Laramide Rocky Mountains and Cordilleran arc. GSA Bull. 124, 1007–1024. https://doi.org/10.1130/B30458.1.
Madritsch, H., Schmid, S.M., Fabbri, O., 2008. Interactions between thin- and thick-skinned tectonics at the northwestern front of the Jura fold-and-thrust belt (eastern France). Tectonics 27, TC5005. https://doi.org/10.1029/2008TC002282.
Manea, V.C., Manea, M., 2011. Flat-slab thermal structure and evolution beneath central Mexico. Pure Applied Geophys. 168, 1475–1487.
Marshak, S., Karlstrom, K., Timmons, J.M., 2000. Inversion of Proterozoic extensional faults: An explanation for the pattern of Laramide and Ancestral Rockies intracratonic deformation, United States. Geology 28, 735–738.
Martín-González, F., Heredia, N., 2011. Complex tectonic and tectonostratigraphic evolution of an Alpine foreland basin: The western Duero Basin and the related Tertiary depressions of the NW Iberian Peninsula. Tectonophysics 502, 75–89.
Martino, R.D., Guereschi, A.B., Montero, A.C., 2016. Reactivation, inversion and basement faulting and thrusting in the Sierras Pampeanas of Córdoba (Argentina) during Andean flat-slab deformation. Geol. Mag. 153, 962–991. https://doi.org/10.1017/S0016756816000339.
Martinod, J., Gérault, M., Husson, L., Regard, V., 2020. Widening of the Andes: An interplay between subduction dynamics and crustal wedge tectonics. Earth Sci. Rev. 204 https://doi.org/10.1016/j.earscirev.2020.103170.
Martinod, J., Husson, L., Roperch, P., Guillaume, B., Espurt, N., 2010. Horizontal subduction zones, convergence velocity and the building of the Andes. Earth Planet. Sci. Lett. 299, 299–309.
May, S.R., Gray, G.G., Summa, L.L., Stewart, N.R., Gehrels, G.E., Pecha, M.E., 2013. Detrital zircon geochronology from the Bighorn Basin, Wyoming, USA: Implications for tectonostratigraphic evolution and paleogeography. GSA Bull. 125, 1403–1422. https://doi.org/10.1130/B30824.1.
McClay, K., Mora Bohorquez, A., Tamara, J., Hammerstein, J., Zamora, G., Uzkeda, H., 2018. Sub-Andean thick and thin-skinned thrust systems of southeastern Peru and Bolivia—A review. In: Zamora, G., McClay, K.R., Ramos, V.A. (Eds.), Petroleum Basins and Hydrocarbon Potential of the Andes of Peru and Bolivia: AAPG Memoir, 117, pp. 35–62.
McGroder, M.F., Lease, R.O., Pearson, D.M., 2015. Along-strike variation in structural styles and hydrocarbon occurrences, Subandean fold-and-thrust belt and inner foreland, Colombia to Argentina. In: DeCelles, P.G., Ducea, M.N., Carrapa, B., Kapp, P.A. (Eds.), Geodynamics of a Cordilleran Orogenic System: The Central Andes of Argentina and Northern Chile: Geol. Soc. Am. Memoir, 212, pp. 79–113. https://doi.org/10.1130/2015.1212(05).
McMillan, M.E., Heller, P.L., Wing, S.L., 2006. History and causes of post-Laramide relief in the Rocky Mountain orogenic plateau. GSA Bull. 118, 393–405.
McQuarrie, N., 2002. Initial plate geometry, shortening variations, and evolution of the Bolivian orocline. Geology 30, 867–870.
McQuarrie, N., Chase, C.G., 2000. Raising the Colorado Plateau. Geology 28, 91–94.
McQueen, H.W.S., Beaumont, C., 1989. Mechanical models of tilted block basins. In: Price, R.A. (Ed.), Origin and Evolution of Sedimentary Basins and Their Energy and Mineral Resources: Am. Geophys. Union, Geophys. Monograph, 48, pp. 65–71.
Meigs, A., Krugh, W.C., Schiffman, C., Vergés, J., Ramos, V.A., 2006. Refolding of thin-skinned thrust sheets by active basement-involved thrust faults in the Eastern Precordillera of western Argentina. Rev. Asoc. Geol. Argent. 61, 589–603.
Métivier, F., Gaudemer, Y., Tapponnier, P., Meyer, B., 1998. Northeastward growth of the Tibet plateau deduced from balanced reconstruction of two depositional areas: The Qaidam and Hexi Corridor basins, China. Tectonics 17, 823–842.
Meyer, B., Tapponnier, P., Bourjot, L., Métivier, F., Gaudemer, Y., Peltzer, G., Shunmin, G., Zhitai, C., 1998. Crustal thickening in Gansu-Qinghai, lithospheric mantle subduction, and oblique, strike-slip controlled growth of the Tibet Plateau. Geophys. J. Int. 135, 1–47.
Miall, A.D., Arush, M., 2001. The Castlegate Sandstone of the Book Cliffs, Utah: Sequence stratigraphy, paleogeography, and tectonic controls. J. Sed. Res. 71, 537–548.
Milana, J.P., 2000. Characterization of alluvial bajada facies distribution using TM imagery. Sedimentology 47, 741–760.
Milana, J.P., Bercowski, F., Jordan, T.E., 2003. Paleoambientes y magnetoestrigrafía del Neógeno de la Sierra de Mogna, y su relación con la Cuenca de Antepaís Andina. Revista de la Associatión Geológica Argentina 38, 447–473.
Minor, K.P., Steel, R.J., Olariu, C., 2022. Tectonic and eustatic control of Mesaverde Group (Campanian–Maastrichtian) architecture, Wyoming-Utah-Colorado region, USA. GSA Bull. 134, 419–445. https://doi.org/10.1130/B36032.1.
Mitrovica, J.X., Beaumont, C., Jarvis, G.T., 1989. Tilting of continental interiors by the dynamical effects of subduction. Tectonics 8, 1079–1094.
Montagne, J., 1991. Cenozoic history of the Saratoga Valley area, Wyoming and Colorado. University of Wyoming. Contrib. Geol 29, 13–70.
Montero-López, C., del Papa, C., Hongn, F., Strecker, M., Aramayo, A., 2018. Synsedimentary broken-foreland tectonics during the Paleogene in the Andes of NW Argentine: New evidence from regional to centimeter-scale deformation features. Basin Res. 30, 142–159. https://doi.org/10.1111/bre.12212.
Montgomery, D.R., Balco, G., Willett, S.D., 2001. Climate, tectonics, and the morphology of the Andes. Geology 29, 579–582.
Mora, A., Tesón, E., Martínez, J., Parra, M., Lasso, Á., Horton, B.K., Ketcham, R.A., Velásquez, A., Arias-Martínez, J.P., 2020. The Eastern Foothills of Colombia. In: Gómez, J., Mateus-Zabala, D. (Eds.), The Geology of Colombia: Servicio Geológico Colombiano, Publicaciones Geológicas Especiales, 37, pp. 123–142. https://doi.org/10.32685/pub.esp.37.2019.05.
Mouthereau, F., Watts, A.B., Burov, E., 2013. Structure of orogenic belts controlled by lithosphere age. Nat. Geosci. 6, 785–789. https://doi.org/10.1038/ngeo1902.
Mpodozis, C., Ramos, V.A., 1990. The Andes of Chile and Argentina. In: Ericksen, G.E., Cañas Pinochet, M.T., Reinemund, J.A. (Eds.), Geology of the Andes and its Relation to Hydrocarbon and Mineral Resources: Circum-Pacific Council for Energy and Mineral Resources, Earth Science Series, 11, pp. 59–90.
Naylor, M., Sinclair, H.D., 2008. Pro- vs. Retro-foreland basins. Basin Res. 20, 285–303.
Neely, T.G., Erslev, E.A., 2009. The interplay of fold mechanisms and basement weaknesses at the transition between Laramide basement-involved arches, north-central Wyoming, USA. J. Structural Geol. 31, 1012–1027.
Nelson, W.J., 1993. Structural geology of the Cat Creek anticline and related features, central Montana: Montana Bureau of Mines and Geology. Memoir 64, 44 p.
Norton, K., Schlunegger, F., 2011. Migrating deformation in the Central Andes from enhanced orographic rainfall. Nat. Commun. 2, 584. https://doi.org/10.1038/ncomms1590.
Oldow, J.S., Bally, A.W., Avé Lallemant, H.G., Leeman, W.P., 1989. Phanerozoic evolution of the North American Cordillera; United States and Canada. In: Bally, A. W., Palmer, A.R. (Eds.), The Geology of North America—An Overview: Geol. Soc. Am., The Geology of North America, A, pp. 139–232.
Oliveira, C.M.M., Zalán, P.V., Alkmin, F.F., 1997. Tectonic evolution of the Acre Basin, Brasil. VI Simpósio Bolivariano, Exploracion Petrolera en las Cuencas Subandinas, Memórias, Tomo 1. Cartagena, Colombia, pp. 46–65.
Omar, G.I., Lutz, T.M., Giegengack, R., 1994. Apatite fission-track evidence for Laramide and post-Laramide uplift and anomalous thermal regime at the Beartooth overthrust, Montana-Wyoming. GSA Bull. 106, 74–85.
Orme, D.A., 2020. New timing constraints for the onset of Laramide deformation in southwest Montana challenge our understanding of the development of a thick-skinned structural style during flat-slab subduction. Tectonics 39. https://doi.org/10.1029/2020TC006193.
Ortiz, G., Goddard, A.L.S., Fosdick, J.C., Alvarado, P., Carrapa, B., Cristofolini, E., 2021. Fault reactivation in the Sierras Pampeanas resolved across Andean extensional and compressional regimes using thermochronologic modeling. J. S. Am. Earth Sci. 112 https://doi.org/10.1016/j.jsames.2021.103533.
Orts, D., Folguera, A., Encinas, A., Ramos, M., Tobal, J., Ramos, V.A., 2012. Tectonic development of the North Patagonian Andes and their related Miocene foreland basin (41°30′-43°S). Tectonics 31. https://doi.org/10.1029/2011TC003084.
Orts, D., Folguera, A., Giménez, M., Ruiz, F., Rojas Vera, E., Lince Klinger, F., 2015. Cenozoic building and deformational processes in the North Patagonian Andes. J. Geodyn. 86, 26–41.
Parker, S.D., Pearson, D.M., 2021. Pre-thrusting stratigraphic control on the transition from a thin-skinned to thick-skinned structural style: An example from the double-decker Idaho-Montana fold-thrust belt. Tectonics 40. https://doi.org/10.1029/2020TC006429.
Parra, M., Mora, A., Lopez, C., Rojas, L.E., Horton, B.K., 2012. Detecting earliest shortening and deformation advance in thrust belt hinterlands: Example from the Colombian Andes. Geology 40, 175–178. https://doi.org/10.1130/G32519.1.
Pearson, D.M., Kapp, P., DeCelles, P.G., Reiners, P.W., Gehrels, G.E., Ducea, M.N., Pullen, A., 2013. Influence of pre-Andean crustal structure on Cenozoic thrust belt kinematics and shortening magnitude: Northwestern Argentina. Geosphere 9, 1766–1782. https://doi.org/10.1130/GES00923.1.
Pecha, M.E., Gehrels, G.E., Karlstrom, K.E., Dickinson, W.R., Donahue, M.S., Gonzales, D. A., Blum, M.D., 2018. Provenance of Cretaceous through Eocene strata of the Four Corners region: Insights from detrital zircons in the San Juan Basin, New Mexico and Colorado. Geosphere 14, 785–811. https://doi.org/10.1130/GES01485.1.

Perez, N.D., Horton, B.K., 2014. Oligocene-Miocene deformational and depositional history of the Andean hinterland basin in the northern Altiplano plateau, southern Peru. Tectonics 33, 1819–1847. https://doi.org/10.1002/2014TC003647.

Perez, N.D., Levine, K.G., 2020. Diagnosing an ancient shallow-angle subduction event from Cenozoic depositional and deformational records in the central Andes of southern Peru. Earth Planet. Sci. Lett. v. 541 https://doi.org/10.1016/j.epsl.2020.116263.

Perez, N.D., Horton, B.K., Carlotto, V., 2016. Structural inheritance and selective reactivation in the central Andes: Cenozoic deformation guided by pre-Andean structures in southern Peru. Tectonophysics 671, 264–280. https://doi.org/10.1016/j.tecto.2015.12.031.

Peyton, S.L., Carrapa, B., 2013. An overview of low-temperature thermochronology in the Rocky Mountains and its application to petroleum system analysis. In: Knight, C., Cuzella, J. (Eds.), Application of Structural Methods to Rocky Mountain Hydrocarbon Exploration and Development. AAPG Studies in Geology, 65, pp. 37–70.

Pfiffner, O.A., 2017. Thick-skinned and thin-skinned tectonics: A global perspective. Geosciences 7, 71. https://doi.org/10.3390/geosciences7030071.

Pilger Jr., R.H., 1981. Plate reconstructions, aseismic ridges and low-angle subduction beneath the Andes. GSA Bull. 92, 448–456.

Pinto, L., Alarcón, P., Morton, A., Naipauer, M., 2018. Geochemistry of heavy minerals and U-Pb detrital zircon geochronology in the Manantiales Basin: Implications for Frontal Cordillera uplift and foreland basin connectivity in the Andes of central Argentina. Palaeogeogr. Palaeoclimat. Palaeoecol. 492, 104–125. https://doi.org/10.1016/j.palaeo.2017.12.017.

Portner, D.E., Rodríguez, E.E., Beck, S., Zandt, G., Scire, A., Rocha, M.P., Bianchi, M.B., Ruiz, M., França, G.S., Condori, C., Alvarado, P., 2020. Detailed structure of the subducted Nazca slab into the lower mantle derived from continent-scale teleseismic P-wave tomography. J. Geophys. Res. 125 https://doi.org/10.1029/2019JB017884.

Proyecto Multinacional Andino, 2009. Atlas de deformaciones cuaternarias de los Andes; Servicio Nacional de Geológia y Minería. Publicacion Geológica Multinacional 7, 311 p.

Quiroga, R., Peña, M., Poblete, F., Giambiagi, L., Mescua, J., Gómez, I., Echaurren, A., Perroud, S., Suriano, J., Martínez, F., Espinoza, D., 2021. Spatio-temporal variation of the strain field in the southern Central Andes broken-foreland (27°30'S) during the late Cenozoic. J. S. Am. Earth Sci. 106 https://doi.org/10.1016/j.jsames.2020.102981.

Raimondo, T., Hand, M., Collins, W.J., 2014. Compressional intracontinental orogens: Ancient and modern perspectives. Earth Sci. Rev. 130, 128–153.

Ramos, M.E., Tobal, J.E., Sagripanti, L., Folguera, A., Orts, D.L., Giménez, M., Ramos, V.A., 2015. The North Patagonian orogenic front and related foreland evolution during the Miocene, analyzed from synorogenic sedimentation and U/Pb dating (~42°S). J. S. Am. Earth Sci. 64, 467–485.

Ramos, V.A., 1999. Los depósitos sinorogénicos de la region andina. In: Caminos, R. (Ed.), Geología Argentina. Instituto de Geología y Recursos Naturales, Anales, 29, pp. 651–682.

Ramos, V.A., 1999b. Plate tectonic setting of the Andean Cordillera. Episodes 22, 183–190.

Ramos, V.A., 2005. Seismic ridge subduction and topography: Foreland deformation in the Patagonian Andes. Tectonophysics 399, 73–86.

Ramos, V.A., 2009. Anatomy and global context of the Andes: Main geologic features and the Andean orogenic cycle. In: Kay, S.M., Ramos, V.A., Dickinson, W.R. (Eds.), Backbone of the Americas: Shallow Subduction, Plateau Uplift, and Ridge and Terrane Collision: Geol. Soc. Am. Memoir, 204, pp. 31–65.

Ramos, V.A., Cristallini, E.O., Perez, D.J., 2002. The Pampean flat-slab of the Central Andes. J. S. Am. Earth Sci. 15, 59–78.

Ramos, V.A., Folguera, A., 2009. Andean flat-slab subduction through time. In: Murphy, J.B., Keppie, J.D., Hynes, A.J. (Eds.), Ancient Orogens and Modern Analogues: Geol. Soc. London Spec. Publ., 327, pp. 31–54.

Reynolds, J.H., Jordan, T.E., Johnson, N.M., Damanti, J.F., Tabbutt, K.D., 1990. Neogene deformation of the flat-subduction segment of the Argentine-Chilean Andes: Magnetostratigraphic constraints from Las Juntas, La Rioja province, Argentina. GSA Bull. 102, 1607–1622.

Rodgers, J., 1987. Chains of basement uplifts within cratons marginal to orogenic belts. Am. J. Sci. 287, 661–692.

Rodríguez, E.E., Portner, D.E., Beck, S.L., Rocha, M.P., Bianchi, M.B., Assumpção, M., Ruiz, M., Alvarado, P., Condori, C., Lynner, C., 2021. Mantle dynamics of the Andean subduction zone from continent-scale teleseismic S-wave tomography. Geophys. J. Int. 224 https://doi.org/10.1093/gji/ggaa536.

Rodriguez Piceda, C., Scheck-Wenderoth, M., Cacace, M., Bott, J., Strecker, M.R., 2022. Long-term lithospheric strength and upper-plate seismicity in the southern Central Andes, 29°–39°S. Geochem. Geophys. Geosyst. 23 https://doi.org/10.1029/2021GC010171.

Rodríguez Tribaldos, V., White, N.J., Roberts, G.G., Hoggard, M.J., 2017. Spatial and temporal uplift history of South America from calibrated drainage analysis. Geochem. Geophys. Geosyst. 18, 2321–2353. https://doi.org/10.1002/2017GC006909.

Rosenblume, J.A., Finzel, E.S., Pearson, D.M., 2021. Early Cretaceous provenance, sediment dispersal, and foreland basin development in southwestern Montana, North American Cordillera. Tectonics 40. https://doi.org/10.1029/2020TC006561.

Royse Jr., F., Warner, M.A., Reese, D.L., 1975. Thrust belt structural geometry and related stratigraphic problems, Wyoming-Idaho-northern Utah. In: Bolyard, D.W. (Ed.), Symposium on Deep Drilling in the Central Rocky Mountains. Rocky Mountain Association of Geologists, pp. 41–54.

Rudolph, K.W., Devlin, W.J., Carabaugh, J.P., 2015. Upper Cretaceous sequence stratigraphy of the Rock Springs Uplift, Wyoming. Mountain Geologist 52, 13–157.

Runyon, B., Saylor, J.E., Horton, B.K., Reynolds, J.H., Hampton, B., 2022. Basin evolution in response to flat subduction in the Altiplano. J. Geol. Soc. Lond. 179 https://doi.org/10.1144/jgs2021-003.

Ruppel, E.T., Lopez, D.A., 1984. The thrust belt in southwest Montana and east-central Idaho. U.S. Geol. Survey Prof. Paper, 1278, 41 p.

Sacek, V., 2014. Drainage reversal of the Amazon River due to the coupling of surface and lithospheric processes. Earth Planet. Sci. Lett. 401, 301–312.

Saleeby, J., 2003. Segmentation of the Laramide slab—evidence from the southern Sierra Nevada region. GSA Bull. 115, 655–668.

Sandeman, H.A., Clark, A.H., Farrar, E., 1995. An integrated tectonomagmatic model for the evolution of the southern Peruvian Andes (13–20°S) since 55 Ma. Int. Geol. Rev. 37, 1039–1073. https://doi.org/10.1080/00206819509465439.

Saylor, J.E., Horton, B.K., Nie, J., Corredor, J., Mora, A., 2011. Evaluating foreland basin partitioning in the northern Andes using Cenozoic fill of the Floresta basin, Eastern Cordillera, Colombia. Basin Res. 23, 377–402. https://doi.org/10.1111/j.1365-2117.2010.00493.x.

Saylor, J.E., Jordan, J.C., Sundell, K.E., Wang, X., Wang, S., Deng, T., 2017. Topographic growth of the Jishi Shan and its impact on basin and hydrology evolution, NE Tibetan Plateau. Basin Res. 30, 544–563. https://doi.org/10.1111/bre.12264.

Saylor, J.E., Rudolph, K.W., Sundell, K.E., van Wijk, J., 2020. Laramide orogenesis driven by Late Cretaceous weakening of the North American lithosphere. J. Geophys. Res. 125 https://doi.org/10.1029/2020JB019570.

Schmidt, C.J., O'Neill, J.M., Brandon, W.C., 1988. Influence of Rocky Mountain foreland uplifts on the development of the frontal fold and thrust belt, southwestern Montana. In: Schmidt, C.J., Perry Jr., W.J. (Eds.), Interaction of the Rocky Mountain Foreland and the Cordilleran Thrust Belt: Geol. Soc. Am. Memoir, 171, pp. 171–201.

Schmidt, C.J., Astini, R.A., Costa, C.H., Gardini, C.E., Kraemer, P.E., 1995. Cretaceous rifting, alluvial fan sedimentation, and Neogene inversion, southern Sierras Pampeanas, Argentina. In: Tankard, A.J., Suárez, R., Welsink, H.J. (Eds.), Petroleum Basins of South America: AAPG Memoir, 62, pp. 341–358.

Schwartz, R.K., 1982. Broken Early Cretaceous foreland basin in southwestern Montana: Sedimentation related to tectonism. In: Powers, R.B. (Ed.), Geologic Studies of the Cordilleran Thrust Belt. Rocky Mountain Association of Geologists, pp. 159–183.

Seggiaro, R., Caffe, P., Galli, C., Arnosio, M., Da Poian, G., 2014. Evolución tectónica andina entre las Sierras de Hualfín, Capillitas y extremo sur de Aconquija, provincia de Catamarca. Rev. Asoc. Geol. Argent. 71, 500–512.

Shephard, G.E., Müller, R.D., Liu, L., Gurnis, M., 2010. Miocene drainage reversal of the Amazon River driven by plate-mantle interaction. Nat. Geosci. 3, 870–875.

Sherkati, S., Letouzey, J., 2004. Variation of structural style and basin evolution in the Zagros (Izeh zone and Dezful Embayment), Iran. Mar. Pet. Geol. 21, 535–554.

Silva, D., Piazolo, S., Daczko, N.R., Houseman, G., Raimondo, T., Evans, L., 2018. Intracontinental orogeny enhanced by far-field extension and local weak crust. Tectonics 37, 4421–4443. https://doi.org/10.1029/2018TC005106.

Simpson, G., 2014. Decoupling of foreland basin subsidence from topography linked to faulting and erosion. Geology 42, 775–778. https://doi.org/10.1130/G35749.1.

Smalley Jr., R.F., Pujol, J., Regnier, M., Chiu, J.M., Chatelain, J.L., Isacks, B.L., Araujo, M., Puebla, N., 1993. Basement seismicity beneath the Andean Precordillera thin-skinned thrust belt and implications for crustal and lithospheric behavior. Tectonics 12, 63–76.

Smith, M.E., Carroll, A.R., Jicha, B.R., Cassel, E.J., Scott, J.J., 2014. Paleogeographic record of Eocene Farallon slab rollback beneath western North America. Geology 42, 1039–1042.

Smith, M.E., Singer, B., Carroll, A., 2003. $^{40}Ar/^{39}Ar$ geochronology of the Eocene Green River Formation, Wyoming. GSA Bull. 115, 549–565.

Smith, T.M., Sundell, K.E., Johnston, S., Guilherme Andrade, C., Andrea, R., Dickinson, J., Liu, Y., Murphy, M.A., Lapen, T.J., Saylor, J.E., 2020. Drainage reorganization and Laramide tectonics in north-central New Mexico and their downstream effects in the Gulf of Mexico. Basin Res. 32, 419–452. https://doi.org/10.1111/bre.12373.

Smithies, R.H., Champion, D.C., Cassidy, K.F., 2003. Formation of Earth's early Archaean continental crust. Precambrian Res. 127, 89–101.

Smithson, S.B., Brewer, J., Kaufman, S., Oliver, J., 1979. Structure of the Laramide Wind River uplift, Wyoming, from COCORP deep reflection data and from gravity data. J. Geophys. Res. 84, 5955–5972.

Snedden, J.W., Galloway, W.E., 2019. The Gulf of Mexico Sedimentary Basin. In: Cambridge University Press, 326 p.

Snyder, W.S., Dickinson, W.R., Silberman, M.L., 1976. Tectonic implications of space-time patterns of Cenozoic magmatism in the western United States. Earth Planet. Sci. Lett. 32, 91–106.

Sobel, E.R., Hilley, G.E., Strecker, M.R., 2003. Formation of internally drained contractional basins by aridity-limited bedrock incision. J. Geophys. Res. 108, 2344. https://doi.org/10.1029/2002JB001883.

Steidtmann, J.R., Middleton, L.T., 1991. Fault chronology and uplift history of the southern Wind River Range, Wyoming: Implications for Laramide and post-Laramide deformation in the Rocky Mountain foreland. GSA Bull. 103, 472–485.

Stephenson, R., Schiffer, C., Peace, A., Nielsen, S.B., Jesse, S., 2020. Late Cretaceous-Cenozoic basin inversion and palaeostress fields in the North Atlantic-western Alpine-Tethys realm: Implications for intraplate tectonics. Earth Sci. Rev. 222 https://doi.org/10.1016/j.earscirev.2020.103252.

Stevens, A.L., Balgord, E.A., Carrapa, B., 2016. Revised exhumation history of the Wind River Range, WY, and implications for Laramide tectonics. Tectonics 35, 1121–1136. https://doi.org/10.1002/2016TC004126.

Stevens Goddard, A.L., Carrapa, B., 2018. Using basin thermal history to evaluate the role of Miocene-Pliocene flat-slab subduction in the southern Central Andes (27° S–30° S). Basin Res. 30, 564–585. https://doi.org/10.1111/bre.12265.

Stevens Goddard, A., Carrapa, B., Aciar, R.H., 2020. Recognizing drainage reorganization in the stratigraphic record of the Neogene foreland basin of the Central Andes. Sed. Geology 405. https://doi.org/10.1016/j.sedgeo.2020.105704.
Stewart, M.G., Mazur, S., Pimiento, A.M.M., Hermoza, W., Olaiz, A.J., 2018. Integrated geophysical investigations of the pre-Andean basins in Peru and Bolivia—A search for depocenters concealed beneath a foreland basin. In: Zamora, G., McClay, K.R., Ramos, V.A. (Eds.), Petroleum Basins and Hydrocarbon Potential of the Andes of Peru and Bolivia: AAPG Memoir, 117, pp. 63–90.
Stone, D.S., 1993. Basement-involved thrust-generated folds as seismically imaged in the subsurface of the central Rocky Mountain foreland. In: Schmidt, C.J., Chase, R.B., Erslev, E.A. (Eds.), Laramide Basement Deformation in the Rocky Mountain Foreland of the Western United States: Geol. Soc. Am. Spec. Paper, 280, pp. 271–318.
Stone, D.S., 2002. Morphology of the Casper Mountain uplift and related subsidiary structures, central Wyoming: Implications for Laramide kinematics, dynamics, and crustal inheritance. AAPG Bull. 86, 1417–1440.
Strecker, M.R., Hilley, G.E., Bookhagen, B., Sobel, E.R., 2012. Structural, geomorphic and depositional characteristics of contiguous and broken foreland basins: Examples from the eastern flanks of the central Andes in Bolivia and NW Argentina. In: Busby, C.J., Azor, A. (Eds.), Tectonics of Sedimentary Basins: Recent Advances. Wiley-Blackwell, pp. 508–521.
Struble, W.T., Roering, J.J., Dorsey, R.J., Bendick, R., 2021. Characteristic scales of drainage reorganization in Cascadia. Geophys. Res. Lett. 48 https://doi.org/10.1029/2020GL091413.
Styron, R., Pagani, M., 2020. The GEM global active faults database. Earthquake Spectra 36 (S1), 160–180.
Sun, J.P., Dong, Y.P., 2020. Ordovician tectonic shift in the western North China Craton constrained by stratigraphic and geochronological analyses. Basin Res. 32, 1413–1440. https://doi.org/10.1111/bre.12435.
Suppe, J., Wang, X., Wei, X., 2019. The giant SW Tarim foreland basin: New constraints on timing and rates of deformation and sedimentation at the edge of NW Tibet. AGU Fall Meeting, abstract T53A-05.
Suttner, L.J., Schwartz, R.K., James, W.C., 1981. Late Mesozoic to early Cenozoic foreland sedimentation in southwest Montana. In: Tucker, T.E. (Ed.), Montana Geological Society Field Conference and Symposium Guidebook to Southwest Montana: Billings, Montana, pp. 93–103.
Tapponnier, P., Meyer, B., Avouac, J.P., Peltzer, G., Guademer, Y., Guo, S., Xiang, H., Yin, K., Chen, Z., Cai, S., Dai, H., 1990. Active thrusting and folding in the Qilian Shan, and decoupling between upper crust and mantle in northeastern Tibet. Earth Planet. Sci. Lett. 97, 382–403. https://doi.org/10.1016/0012-821X(90)90053-Z.
Tavani, S., Granada, P., Caradetti, A., Camanni, G., Vignaroli, G., Manatschal, G., Mazzoli, S., Muñoz, J.A., Parente, M., 2021. Rift inheritance controls the switch from thin- to thick-skinned thrusting and basal décollement re-localization at the subduction-to-collision transition. GSA Bull. 133, 2157–2170. https://doi.org/10.1130/B35800.1.
Tavani, S., Storti, F., Lacombe, O., Corradetti, A., Muñoz, J.A., Mazzoli, S., 2015. A review of deformation pattern templates in foreland basin systems and fold-and-thrust belts: Implications for the state of stress in the frontal regions of thrust wedges. Earth Sci. Rev. 141, 82–104. https://doi.org/10.1016/j.earscirev.2014.11.013.
Thacker, J.O., Karlstrom, K.E., Kelley, S.A., Crow, R.S., Kendall, J.J., 2022. Late Cretaceous time-transgressive onset of Laramide arch exhumation and basin subsidence across northern Arizona-New Mexico, USA, and the role of a dehydrating Farallon flat slab. GSA Bull. 134 https://doi.org/10.1130/B36245.1.
Thomas, W.A., Gehrels, G.E., Greb, S.F., Nadon, G.C., Satkoski, A.M., Romero, M.C., 2017. Detrital zircons and sediment dispersal in the Appalachian foreland. Geosphere 13, 2206–2230.
Tripaldi, A., Forman, S.L., 2016. Eolian depositional phases during the past 50 ka and inferred climate variability for the Pampean Sand Sea, western Pampas, Argentina. Quaternary Sci. Rev. 139, 77–93. https://doi.org/10.1016/j.quascirev.2016.03.007.
Tweto, O., 1975. Laramide (Late Cretaceous-early Tertiary) orogeny in the southern Rocky Mountains. In: Curtis, B.F. (Ed.), Cenozoic History of the Southern Rocky Mountains. Geol. Soc. Am. Memoir, 144, pp. 1–44.
Tweto, O., 1979. Geologic map of Colorado, USA, U.S. Geological Survey, scale 1: 500,000.
Uba, E.J., Heubeck, C., Hulka, C., 2006. Evolution of the late Cenozoic Chaco foreland basin, southern Bolivia. Basin Res. 18, 145–170.
Van Keken, P.E., Hacker, B.R., Syracuse, E.M., Abers, G.A., 2011. Subduction factory: 4. Depth-dependent flux of H_2O from subducting slabs worldwide. J. Geophys. Res. 116, B01401. https://doi.org/10.1029/2010JB007922.
Veloza, G., Styron, R., Taylor, M., Mora, A., 2012. Open-source archive of active faults for northwest South America. GSA Today 22. https://doi.org/10.1130/GSAT-G156A.1.
Venerdini, A., Alvarado, P., Ammirati, J.B., Podesta, M., López, L., Fuentes, F., Linkimer, L., Beck, S., 2020. Crustal seismicity in the Andean Precordillera of Argentina using seismic broadband data. Tectonophysics 786, 228450. https://doi.org/10.1016/j.tecto.2020.228450.
Vergés, J., Ramos, V., Meigs, A., Cristallini, E., Bettini, F., Cortés, J., 2007. Crustal wedging triggering recent deformation in the Andean thrust front between 31°S and 33°S: Sierras Pampeanas-Precordillera interaction. J. Geophys. Res. 112, B03S15. https://doi.org/10.1029/2006JB004287.
Vergés, J., Ramos, E., Seward, D., Busquets, P., Colombo, F., 2001. Miocene sedimentary and tectonic evolution of the Andean Precordillera at 31°S, Argentina. J. S. Am. Earth Sci. 14, 735–750. https://doi.org/10.1016/S0895-9811(01)00070-0.
Viaplana-Muzas, M., Babault, J., Dominguez, S., Van Den Driessche, J., Legrand, X., 2018. Modelling of drainage dynamics influence on sediment routing system in a fold-and-thrust belt. Basin Res. 31, 290–310. https://doi.org/10.1111/bre.12321.
von Gosen, W., 1992. Structural evolution of the Argentine Precordillera: the Rio San Juan section. J. Structural Geol. 6, 643–667.
Vuke, S.M., 2020. Synorogenic basin deposits and associated Laramide uplifts in the Montana part of the Cordilleran foreland basin system. In: Metesh, J.J., Vuke, S.M. (Eds.), Geology of Montana—Geologic History. Montana Bureau of Mines and Geology Spec. Publ., 122, 39 p.
Wagner, L.S., Beck, S., Zandt, G., 2005. Upper mantle structure in the south central Chilean subduction zone (30° to 36°S). J. Geophys. Res. 110, B01308. https://doi.org/10.1029/2004JB003238.
Wagner, L.S., Jaramillo, J.S., Ramírez-Hoyos, L.F., Monsalve, G., Cardona, A., Becker, T. W., 2017. Transient slab flattening beneath Colombia. Geophys. Res. Lett. 44 https://doi.org/10.1002/2017GL073981.
Wanderley-Filho, J.R., Eiras, J.F., Cunha, P.R.C., van der Ven, P.H., 2010. The Paleozoic Solimões and Amazonas basins and the Acre foreland basin of Brazil. In: Hoorn, C., Wesselingh, F.P. (Eds.), Amazonia: Landscape and Species Evolution: A Look into the Past: Wiley-Blackwell, pp. 29–37. https://doi.org/10.1002/9781444306408.ch3.
Wang, H., Currie, C.A., 2017. Crustal deformation induced by mantle dynamics: Insights from models of gravitational lithosphere removal. Geophys. J. Int. 210, 1070–1091. https://doi.org/10.1093/gji/ggx209.
Wang, C., Dai, J., Zhao, X., Li, Y., Graham, S.A., He, D., Ran, B., Meng, J., 2014. Outward-growth of the Tibetan Plateau during the Cenozoic: A review. Tectonophysics 621, 1–43.
Whipple, K.X., Forte, A.M., DiBiase, R.A., Gasparini, N.M., Ouimet, W.B., 2017. Timescales of landscape response to divide migration and drainage capture: Implications for the role of divide mobility in landscape evolution. J. Geophys. Res. 122, 248–273.
Whitman, D., Isacks, B.L., Kay, S.M., 1996. Lithospheric structure and along-strike segmentation of the Central Andean Plateau: Seismic Q, magmatism, flexure, topography and tectonics. Tectonophysics 259, 29–40.
Willett, S.D., McCoy, S.W., Perron, J.T., Goren, L., Chen, C.Y., 2014. Dynamic reorganization of river basins. Science 343 (6175). https://doi.org/10.1126/science.1248765.
Willett, S.D., Schlunegger, F., 2010. The last phase of deposition in the Swiss Molasse Basin: from foredeep to negative-alpha basin. Basin Res. 22, 623–639. https://doi.org/10.1111/j.1365-2117.2009.00435.x.
Wimpenny, S., 2022. Weak, seismogenic faults inherited from Mesozoic rifts control mountain building in the Andean foreland. Geochem. Geophys. Geosyst. 23 https://doi.org/10.1029/2021GC010270.
Wolf, S.G., Huismans, R.S., Muñoz, J.A., Curry, M.E., van der Beek, P., 2021. Growth of collisional orogens from small and cold to large and hot—Inferences from geodynamic models. J. Geophys. Res. 126 https://doi.org/10.1029/2020JB021168.
Worthington, L.L., Miller, K.C., Erslev, E.A., Anderson, M.L., Chamberlain, K.R., Sheehan, A.F., Yeck, W.L., Harder, S.H., Siddoway, C.S., 2016. Crustal structure of the Bighorn Mountains region: Precambrian influence on Laramide shortening and uplift in north-central Wyoming. Tectonics 35, 208–236.
Wu, F.Y., Yang, J.H., Xu, Y.G., Wilde, A.S., Walker, R.J., 2019. Destruction of the North China Craton in the Mesozoic. Annual Rev. Earth Planet. Sci. 47, 173–195.
Yáñez, G.A., Ranero, C.R., von Huene, R., Díaz, J., 2001. Magnetic anomaly interpretation across the southern central Andes (32°-34°S): The role of the Juan Fernández Ridge in the late Tertiary evolution of the margin. J. Geophys. Res. 106, 6325–6345.
Yang, K.M., Dorobek, S.L., 1995. The Permian Basin of west Texas and New Mexico: Tectonic history of a "composite" foreland basin and its effects on stratigraphic development. In: Dorobek, S.L., Ross, G.M. (Eds.), Stratigraphic Evolution of Foreland Basins: SEPM Spec. Publ., 52, pp. 149–174.
Yin, A., Dubey, C.S., Webb, A.A.G., Kelty, T.K., Grove, M., Gehrels, G.E., Burgess, W.P., 2010. Geologic correlation of the Himalayan orogen and Indian craton: Part 1. Structural geology, U-Pb zircon geochronology, and tectonic evolution of the Shillong Plateau and its neighboring regions in NE India. GSA Bull. 122, 336–359.
Yin, A., Ingersoll, R.V., 1997. A model for evolution of Laramide axial basins in the southern Rocky Mountains, U.S.A. Int. Geol. Rev. 39, 1113–1123.
Yonkee, W.A., Weil, A.B., 2011. Evolution of the Wyoming salient of the Sevier fold-thrust belt, northern Utah to western Wyoming. In: Sprinkel, D.A., Yonkee, W.A., Chidsey Jr., T.C. (Eds.), Sevier Thrust Belt: Northern and Central Utah and Adjacent Areas: Utah Geol. Assoc. Publ. 40, pp. 1–56.
Yonkee, W.A., Weil, A.B., 2015. Tectonic evolution of the Sevier and Laramide belts within the North American Cordillera orogenic system. Earth Sci. Rev. 150, 531–593.
Zapata, T.R., 1998. Crustal structure of the Andean thrust front at 30° latitude from shallow and deep seismic reflection profiles, Argentina. J. S. Am. Earth Sci. 11, 131–151.
Zapata, T.R., Allmendinger, R.W., 1996a. Growth stratal records of instantaneous and progressive limb rotation in the Precordillera thrust belt and Bermejo basin, Argentina. Tectonics 15, 1065–1083.
Zapata, T.R., Allmendinger, R.W., 1996b. Thrust-front zone of the Precordillera, Argentina: A thick-skinned triangle zone. AAPG Bull. 80, 359–381.
Zapata, S., Sobel, E.R., Del Papa, C., Glodny, J., 2020. Upper plate controls on the formation of broken foreland basins in the Andean retroarc between 26°S and 28°S: From Cretaceous rifting to Paleogene and Miocene broken foreland basins. Geochem. Geophys. Geosyst. 21 https://doi.org/10.1029/2019GC008876.
Ziegler, P.A., Cloetingh, S., van Wees, J.D., 1995. Dynamics of intra-plate compressional deformation: the Alpine foreland and other examples. Tectonophysics 252, 7–59.
Ziegler, P.A., Bertotti, G., Cloetingh, S., 2002. Dynamic processes controlling foreland development – the role of mechanical (de)coupling of orogenic wedges and forelands. European Geosciences Union. Stephan Mueller Spec. Publ. Series 1, 17–56.